

Hanford Tank Farms Vadose Zone

**Enhancements, Validations, and Applications of
Spectrum Shape-Analysis Techniques Applied to
Hanford Tank Farms Spectral Gamma Logs**

January 1998

Prepared by
Robert D. Wilson
MACTEC Environmental Restoration Services

Prepared for
U.S. Department of Energy
Albuquerque Operations Office
Grand Junction Office

Contents

| | Page |
|---|------|
| Executive Summary | vi |
| 1.0 Overview | 1 |
| 2.0 Spectrum Shape Analysis for the Gamma-Emitter ⁶⁰Co | 1 |
| 2.1 Simulated ⁶⁰ Co Spectra and Shape Factors | 1 |
| 2.2 Comparison of Simulated and Measured Point-Source ⁶⁰ Co Spectra | 6 |
| 2.3 ⁶⁰ Co Shape Factor Log Analysis Methodology | 11 |
| 2.4 Application of ⁶⁰ Co Shape Factor Log Analysis to Tank Farms Logs | 11 |
| 2.4.1 Borehole 22-06-05 | 11 |
| 2.4.2 Borehole 22-08-01 | 17 |
| 2.4.3 Borehole 22-08-02 | 17 |
| 2.4.4 Borehole 51-03-11 | 20 |
| 2.4.5 Borehole 22-08-12 | 23 |
| 2.5 SGLS Tool Depth Response to Thin Zones of Contamination | 26 |
| 2.6 Summary | 28 |
| 2.7 Recommendations | 29 |
| 3.0 Benchmark Experiments for Validation of Simulated Spectral Shape Factors | 29 |
| 3.1 Potassium Sleeve Experiment | 30 |
| 3.2 ¹³⁷ Cs Point Source in Sand Experiment | 37 |
| 3.3 ¹³⁷ Cs Point Source Experiments With Scattering Materials Removed | 48 |
| 3.4 ⁶⁰ Co Point Source Experiments With Scattering Materials Removed | 53 |
| 3.5 Distributed Potassium Source Benchmark Comparisons | 53 |
| 3.6 Summary and Recommendations | 53 |
| 4.0 Identification of the Bremsstrahlung-Producing Beta-Emitting Contaminant ⁹⁰Sr .. | 54 |
| 4.1 Shape Factor Analysis of Spectral Logs From Crib Borehole 299-E25-191 | 54 |
| 4.2 Measured Spectra for a Prepared ⁹⁰ Sr Source in a Sand Tank | 60 |
| 4.3 Summary | 63 |
| 4.4 Recommendations | 63 |
| 5.0 Spectral Shape Factor Analysis for Expert Panel Borehole 41-12-01 Near Tank SX-112 | 63 |
| 5.1 Shape Factor Logs | 64 |
| 5.2 Conclusions | 79 |
| 6.0 Spectral Shape Factor Analysis for Expert Panel Borehole 41-09-39 Near Tank SX-109 | 79 |

Contents (continued)

| | Page |
|--|-------------|
| 6.1 Shape Factor Logs and Analysis | 81 |
| 6.2 Dead-Time Effect on Spectral Shape | 83 |
| 7.0 Summary and Recommendations | 87 |
| 8.0 Acknowledgments | 89 |
| 9.0 References | 89 |

Tables

| | |
|--|----|
| Table 1. Simulated ⁶⁰ Co Shape Factors for Several Source Distributions | 6 |
| 2. Potassium Sleeve Spectral Window Count Rates for the SGLS Tool | 34 |
| 3. Comparison of Simulated and Measured Potassium Sleeve Response | 35 |
| 4. SGLS Tool Response to Point Sources of ¹³⁷ Cs in a Sand Matrix, 4.6-FCi Source Strength (Randall data of September 1996) | 38 |
| 5. Processed ¹³⁷ Cs Point Source in Sand Measurements, 4.6-FCi Source Strength (Randall data of September 1996) | 40 |
| 6. ¹³⁷ Cs Point Source in Sand Measurements Taken by Mr. Meisner With a 10.3-FCi Source to Provide Overlap of Randall Data | 40 |
| 7. Complete Set of ¹³⁷ Cs Point Source Data Normalized to 4.6-FCi Source | 41 |
| 8. Comparison of Simulated and Measured Shape Factors for a ¹³⁷ Cs Point Source at Various Radial Positions in a Sand Matrix With Cased Borehole | 46 |
| 9. Measured Count Rates for a ¹³⁷ Cs Point Source at Several Axial and Midplane Positions Relative to Detector With Housing Removed and Tool Suspended in Air | 48 |
| 10. Comparison of Simulated and Measured Shape Factors for a ¹³⁷ Cs Point Source at Various Radial and Axial Positions From Detector With Tool in Air and Housing Removed | 50 |
| 11. ¹³⁷ Cs Spectral Shape Factors for 0.5-in.-Thick Steel Casing | 64 |

Figures

| | |
|---|---|
| Figure 1. Simulated SGLS Spectra for Contaminant ⁶⁰ Co | 3 |
| 2. Simulated SF1 and SF2 in Relation to Radial Extent of ⁶⁰ Co | 4 |
| 3. Spectral Shape Factors SF1 and SF2 Values for Several Radial Extents of Formation ¹³⁷ Cs (Wilson 1997) | 5 |
| 4. Simulated SGLS Spectra for Ring-Shaped Remote Sources of ⁶⁰ Co | 7 |
| 5. Simulated SF1 and SF2 for Radially Remote Ring Sources of ⁶⁰ Co | 8 |

Figures (continued)

| | Page |
|--|------|
| Figure 6. Comparison of Measured and Simulated ^{60}Co Spectra for Point Source at Front Face of Detector | 10 |
| 7. Combination Log Plot for Borehole 22-06-05 at Tank BY-106 | 12 |
| 8. Spectrum Measured at 65-ft Depth in Borehole 22-06-05 | 14 |
| 9. ^{60}Co and ^{137}Cs Shape Factor Logs for Borehole 22-06-05 | 15 |
| 10. ^{60}Co Shape Factor Logs for Borehole 22-08-01 | 18 |
| 11. ^{60}Co Shape Factor Logs for Borehole 22-08-02 | 19 |
| 12. Spectrum Measured at 55-ft Depth in Borehole 51-03-11 | 21 |
| 13. ^{60}Co Shape Factor Logs for Borehole 51-03-11 | 22 |
| 14. ^{60}Co Shape Factor Cross Plot for Borehole 51-03-11 | 24 |
| 15. ^{60}Co Shape Factor Logs for Borehole 22-08-12 | 25 |
| 16. ^{137}Cs Shape Factor Logs for Thin Zones in Borehole 41-00-08 | 27 |
| 17. Potassium Sleeve | 31 |
| 18. Arrangement for Potassium Sleeve Experiment | 32 |
| 19. SGLS Spectra Measured Within Potassium Sleeve in Moisture Model | 33 |
| 20. Comparison of Simulated and Measured Potassium Sleeve Spectra | 36 |
| 21. Sand Tank for Point-Source Spectrum Measurements | 39 |
| 22. Measured and Simulated Spectra for 1-in. Tube Position | 42 |
| 23. Measured and Simulated Spectra for 7-in. Tube Position | 43 |
| 24. Measured Spectrum for Point Source in 17-in. Tube Position | 44 |
| 25. Measured and Simulated SF1 and SF2 Dependence on Radial Source Position .. | 45 |
| 26. Simulated Spectra at 4-in. Tube Position and for Uniformly Distributed ^{137}Cs Contamination | 47 |
| 27. Measured Spectrum for ^{137}Cs Source at Front Face of Detector | 49 |
| 28. MCNP Simulation Geometry for Source at Front Face of Detector | 51 |
| 29. Comparison of Simulated and Measured Spectra for ^{137}Cs Source at Front Face of Detector | 52 |
| 30. RLS Spectra at the 14.5-ft Depth in Crib Borehole 299-E25-191 | 56 |
| 31. Background-Corrected Spectrum at 14.5 ft in Borehole 299-E25-191 | 57 |
| 32. Shape Factor SF2 and Continuum Logs for Borehole 299-E25-191 | 58 |
| 33. Linear Shape Factor Log SF2 for Borehole 299-E25-191 | 59 |
| 34. Comparison of Continuum Spectra From Borehole 299-E25-191 and Bremsstrahlung Spectrum From ^{90}Sr Source in Sand Tank | 61 |
| 35. Comparison of Simulated and Measured Bremsstrahlung Spectra From ^{90}Sr Source in Sand Tank | 62 |
| 36. ^{137}Cs Logs for Expert Panel Borehole 41-12-01 | 65 |
| 37. Shape Factor Logs for Run 6, Borehole 41-12-01 | 67 |
| 38. SF1 and SF2 Cross Plot for Run 6, Borehole 41-12-01 | 68 |
| 39. Shape Factor Logs for Run 9, Borehole 41-12-01 | 69 |

Figures (continued)

| | Page |
|--|-------------|
| Figure 40. SF1 and SF2 Cross Plot for Run 9, Borehole 41-12-01 | 70 |
| 41. Shape Factor Logs for Run 10, Borehole 41-12-01 | 71 |
| 42. SF1 and SF2 Cross Plot for Run 10, Borehole 41-12-01 | 72 |
| 43. Shape Factor Logs for Run 11, Borehole 41-12-01 | 73 |
| 44. SF1 and SF2 Cross Plot for Run 11, Borehole 41-12-01 | 74 |
| 45. Shape Factor Logs for Run 13, Borehole 41-12-01 | 75 |
| 46. SF1 and SF2 Cross Plot for Run 13, Borehole 41-12-01 | 76 |
| 47. Shape Factor Logs for Run 15, Borehole 41-12-01 | 77 |
| 48. SF1 and SF2 Cross Plot for Run 15, Borehole 41-12-01 | 78 |
| 49. ¹³⁷ Cs Logs for Expert Panel Borehole 41-09-39 | 80 |
| 50. Shape Factor Logs for Runs 9&15, Borehole 41-09-39 | 82 |
| 51. SF1 and SF2 Cross Plot for Depth Interval 113 to 129 ft, Borehole 41-09-39 ... | 84 |
| 52. Gamma Spectrum at 126-ft Depth in Borehole 41-09-39 | 85 |
| 53. Gamma Spectrum at 122-ft Depth in Borehole 41-09-39 | 86 |
| 54. SF1 and SF2 Compared With Dead Time for Borehole 41-09-39 | 88 |

Executive Summary

This report describes enhancements and benchmark tests of spectral shape methodology for determining the location of gamma-ray-emitting contaminants in the formation around boreholes. This method uses the changes in spectral shape that are caused by the variation in gamma-ray scattering with contaminant distribution in the formation. In many cases, contaminants located near the borehole can be distinguished from contaminants uniformly distributed in the formation or remote from the borehole. The method has been extended so that it includes ^{60}Co , as well as ^{137}Cs and ^{90}Sr . The method has been applied to data obtained from several boreholes in the Tank Farm areas of Hanford, including newly constructed boreholes in the SX Tank Farm.

The spectral shape observed in borehole spectra from gamma-emitting contaminants can be used to identify the localization of contamination to the borehole region and the presence of the bremsstrahlung-producer ^{90}Sr (Wilson 1997). An initial version of shape factor log analysis software (DOE 1997b) is being used by analysts to process the spectral gamma logs obtained at the U.S. Department of Energy Hanford Site Tank Farms near Richland, Washington. The shape factor logs are helping the analyst to determine when the gamma-ray-emitting contaminant measured in the borehole is associated with a subsurface plume, when the contaminant is remote from the borehole, and when the contamination is associated with the borehole, either during drilling or later during migration behind the casing.

Experimental benchmarks have shown that computer simulations of the spectral shapes measured by the Spectral Gamma Logging Systems are sufficiently accurate for use in distinguishing the various contaminant source distributions. An important enhancement has been the addition of the gamma-emitting contaminant ^{60}Co to the shape factor analysis methodology.

1.0 Overview

This report documents results of studies conducted to enhance, improve, and verify the spectral shape factor analysis methods documented in *Spectrum Shape Analysis Techniques Applied to the Hanford Tank Farms Spectral Gamma Logs* (Wilson 1997), which provides the background and serves as a foundation document to this report. Specifically, shape factor analysis methods were determined for the contaminant ^{60}Co , and the computer models used to develop spectral shape parameters for a range of gamma sources, distributions, and borehole conditions were verified with experiments. Improvements include the experimental determination of the spectral shape produced by the bremsstrahlung-producer ^{90}Sr and refinements to shape factor log interpretation. Shape factor analysis methods were applied to logs of the newly “pushed” boreholes near a high-contamination zone beneath tank SX-112 at the SX Tank Farm at the Hanford Site near Richland, Washington. Logs from the BY and TX Tank Farms illustrate the use of ^{60}Co shape factor analysis.

2.0 Spectrum Shape Analysis for the Gamma-Emitter ^{60}Co

The shape factor log analysis methodology developed for the gamma-emitter ^{137}Cs and the bremsstrahlung-producer ^{90}Sr was extended for use with the contaminant ^{60}Co encountered at the Hanford Tank Farms. Monte Carlo simulations were used to produce Spectral Gamma Logging System (SGLS) spectra for the various source distributions of interest: ^{60}Co localized to the outer surface of the casing, ^{60}Co uniformly distributed in the sediment, and ^{60}Co located remotely from the borehole. Simulations were also performed for ^{60}Co distributed in the sediment to various radial extents. These spectra, in particular, quantify how the spectral shape depends on the radial extent of a contaminant and provide the investigation depth for the passive measurement of ^{60}Co gamma rays. Most of the simulated spectra correspond to source material with a large vertical extent. Various shape factor values were derived from these simulations for use in the identification of ^{60}Co source distributions.

The contaminant spectral shape-factor log analysis software implemented at Richland, Washington, for the Hanford Tank Farms Vadose Zone Project now accommodates gamma spectra from both ^{60}Co and ^{137}Cs and from the bremsstrahlung-producer ^{90}Sr . When spectra contain both ^{60}Co and ^{137}Cs components, application of the shape factor analysis methodology requires knowledge of the spatial distribution (or a presumed distribution) for one of these gamma emitters. When ^{60}Co contamination is detected without the presence of ^{137}Cs , the shape factor analysis requires no assumptions and proceeds in analogy with the methods developed for ^{137}Cs (Wilson 1997).

2.1 Simulated ^{60}Co Spectra and Shape Factors

The Monte Carlo model developed for the SGLS tool and reported in Wilson (1997) was used to produce pulse-height spectra for various radial distributions of ^{60}Co localized to the borehole, uniform in the formation around the borehole, and remote from the borehole. The gamma signature from ^{60}Co differs from the ^{137}Cs signature because ^{60}Co emits two gammas of near equal intensity, rather than the one gamma emitted from ^{137}Cs , with energies of 1173 and 1332 kilo-electron-volts (keV). Because of their slightly different energies and resultant small differences in gamma attenuation, the relative intensity of these two gamma peaks is somewhat sensitive to source distribution. However, the conventional shape factor analysis method, which uses the peak counts and the counts in continuum windows, is expected to prove most sensitive to source distribution.

Figure 1 presents simulated spectra for two of the source distributions of greatest interest in Hanford Tank Farms logs. One spectrum is for ^{60}Co coating the outside wall of the casing and the other spectrum is for ^{60}Co distributed uniformly in the sediment. The spectrum for the source on the outer casing wall is normalized to the spectrum for the uniform sediment distribution at the 1173-keV peak energy. The counts in the scattered continuum portion of the spectra for the two source distributions differ similar to those simulated for ^{137}Cs (Wilson 1997). The formation-distributed source has more continuum counts relative to the pair of photo peaks than does the casing-localized source. A small difference is apparent in the relative magnitude of the two photo peaks: the 1332-keV peak is slightly more intense relative to the 1173-keV peak for the formation-distributed source. This difference is not large enough to exploit for the purpose of inferring source distribution.

Simulations were also conducted for ^{60}Co distributed in the sediment for a range of radial extents of 2, 4, 6, 10, 15, 20, 30, and 50 centimeters (cm) from the casing wall. In all cases, the source effectively extends indefinitely in the axial direction. These spectra not only show how the value of the spectral shape makes the transition from local to the casing to uniform in the sediment, but they also provide a measure of the radial investigation depth of the passive measurement.

Figure 2 presents a plot of the ^{60}Co spectral shape factor SF1, defined as the ratio of counts from 60 to 650 keV to the sum of the counts in the 1173-keV and 1332-keV peaks as a function of contaminant radial extent. The shape approaches an asymptotic limit of about 14.6, which is characteristic of the uniform sediment distribution with indefinite radial extent. The shape factor reaches 90 percent of the difference between this value and the value of 7.4 for contamination on the casing wall for a radial extent of about 20 cm (about 8 inches [in.]). This value is a measure of the radial investigation depth of the passive ^{60}Co SF1 measurement. A similar examination of the change in SF1 with radial extent of ^{137}Cs in the sediment, shown on Figure 3, gives an investigation depth of about 16 cm (about 7 in.) for the passive ^{137}Cs spectral measurement. A scattered continuum shape factor SF2 is defined in analogy with the definition for ^{137}Cs in Wilson (1997) as the ratio of counts from 60 to 350 keV to the counts from 350 to 650 keV. As with the contaminant ^{137}Cs , the SF2 value for ^{60}Co does not vary strongly with source distribution but is useful in identifying the presence of the bremsstrahlung-emitter ^{90}Sr . Figure 2 also

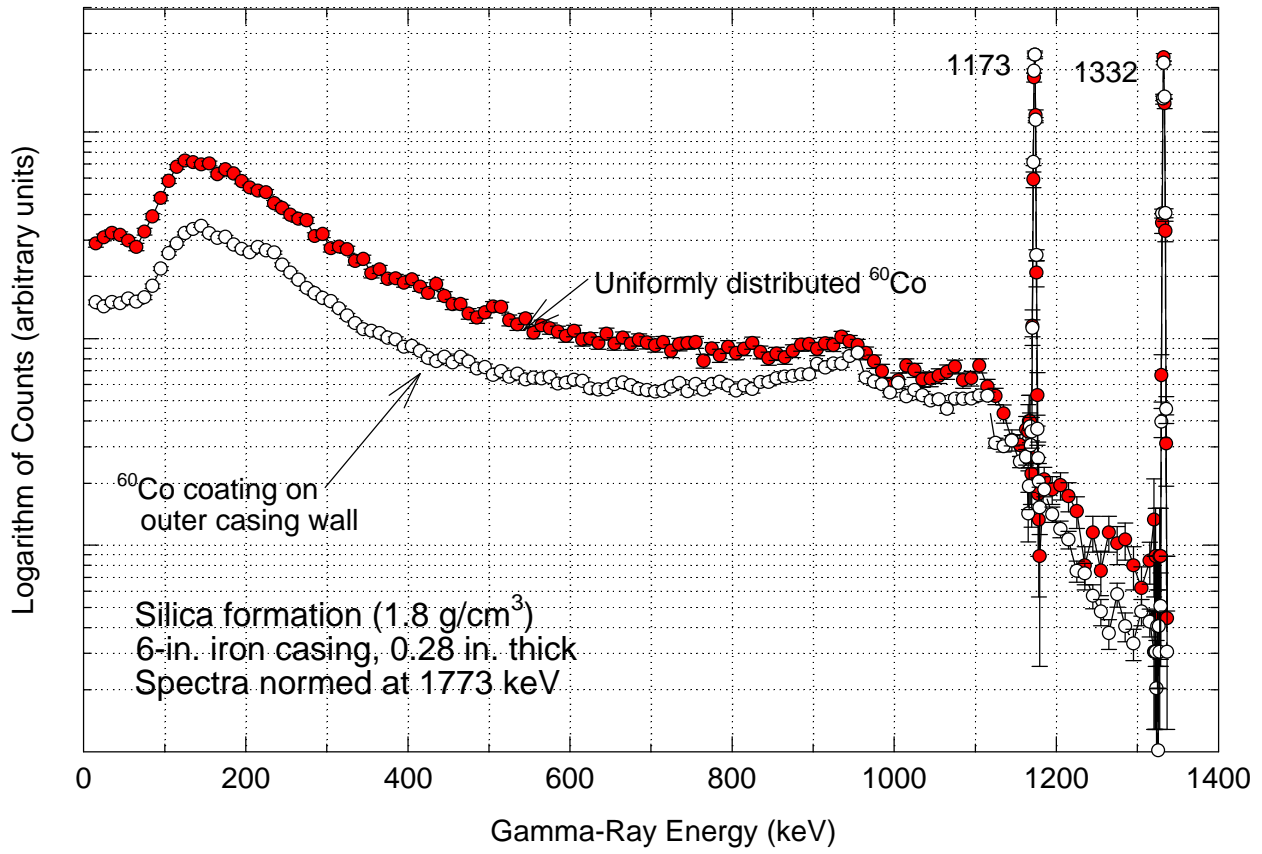


Figure 1. Simulated SGLS Spectra for Contaminant ^{60}Co

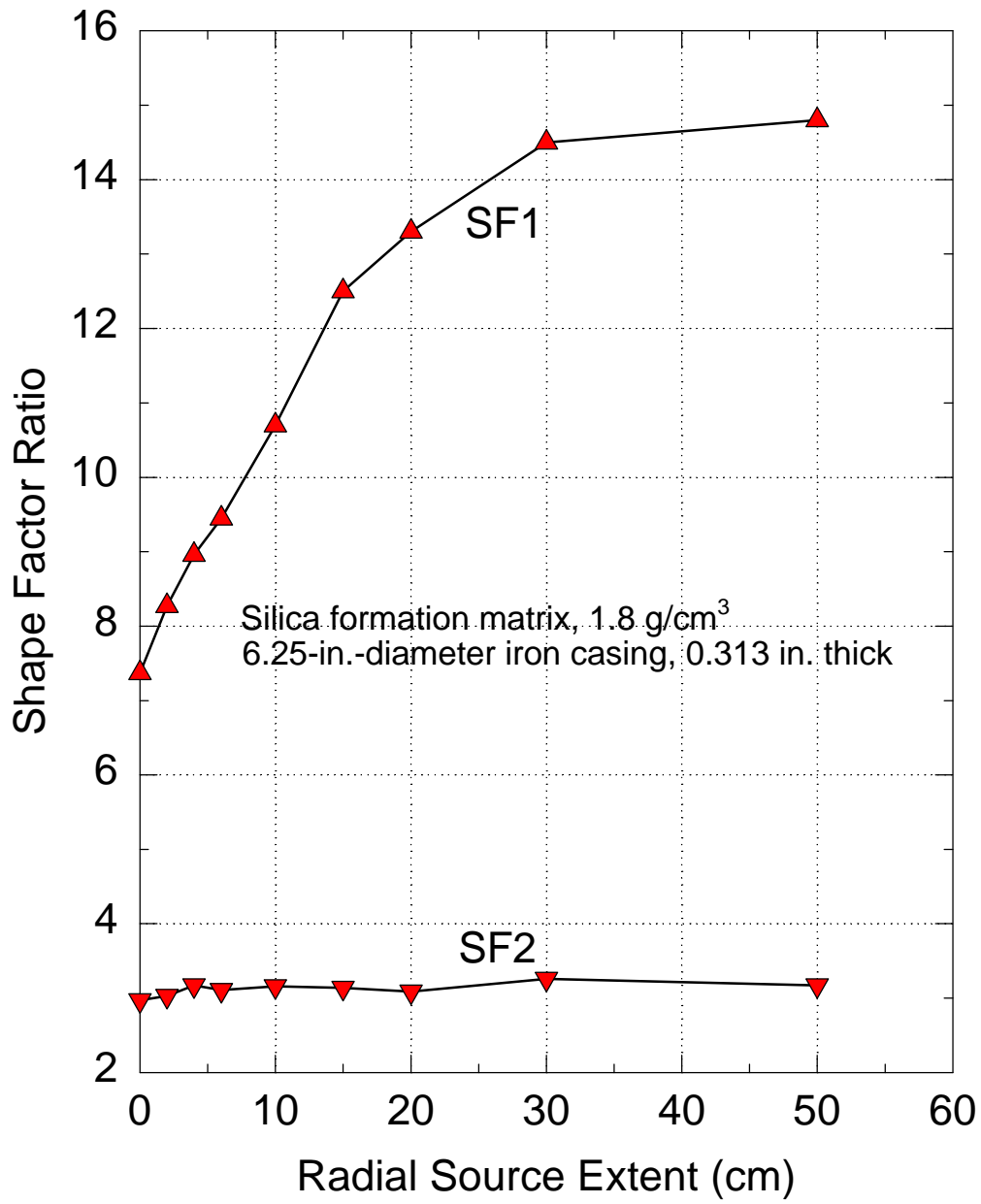


Figure 2. Simulated SF1 and SF2 in Relation to Radial Extent of ⁶⁰Co

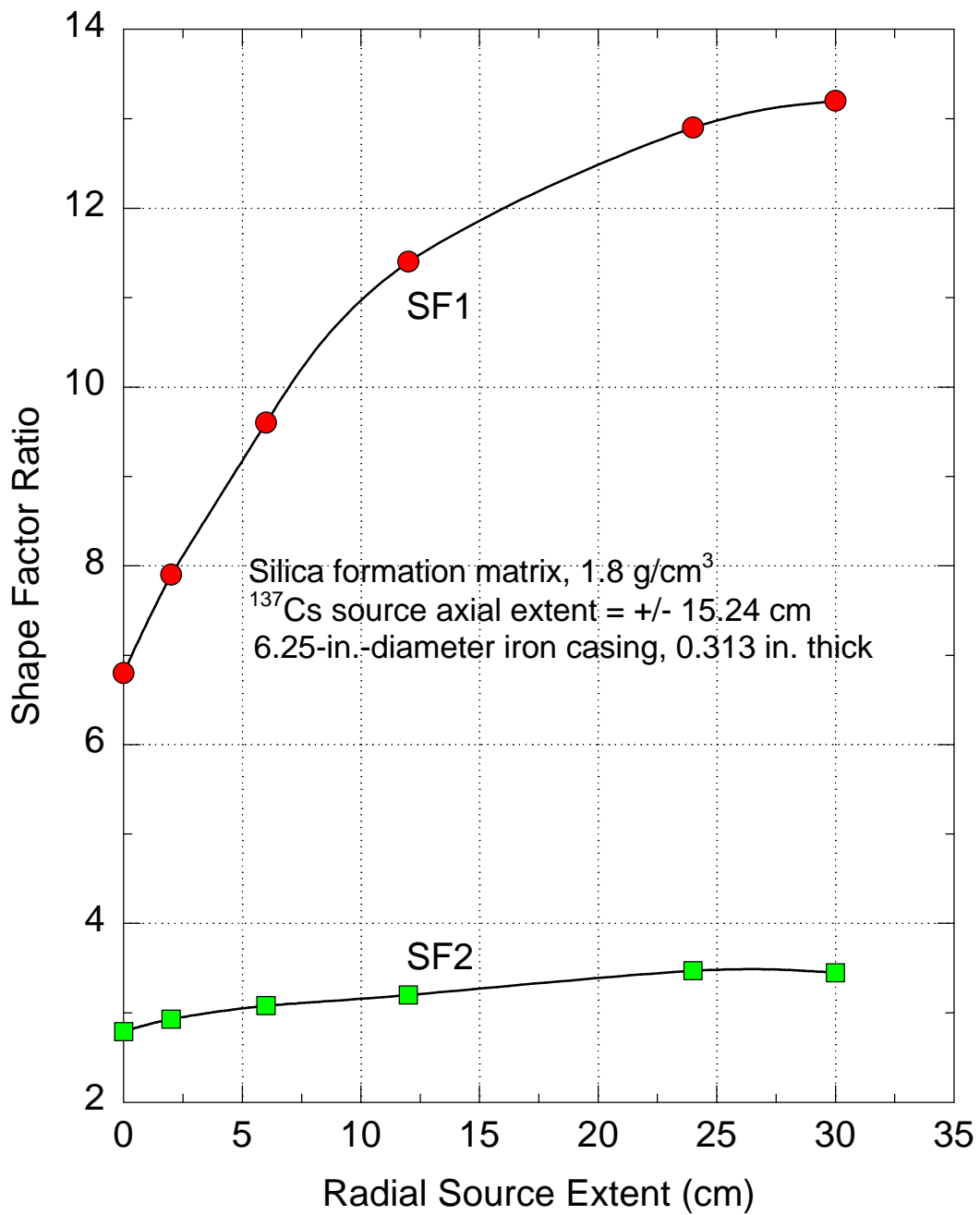


Figure 3. Spectral Shape Factors SF1 and SF2 Values for Several Radial Extents of Formation ¹³⁷Cs (Wilson 1997)

presents a plot of SF2 as a function of radial source extent and shows a variation from 2.97 to 3.20 as ^{60}Co contamination varies from localized to the outer casing wall to uniform distribution in the sediment. Spectral shapes for radially remote ^{60}Co sources were also simulated. Figure 4 presents simulated spectra, all normalized to the 1173-keV peak intensity, for ring-shaped ^{60}Co sources imbedded in the formation at radial depths of 0, 10, and 50 cm. As reported with similar simulations for radially remote ^{137}Cs (Wilson 1997), the Monte Carlo simulation statistics limit the radii that can be simulated to those less than about 50 cm. Figure 5 shows plots of SF1 and SF2 values in relation to radial formation depth of the remote ring source. SF1 monotonically increases to a value of about 70 at the remote source radius of 50 cm, while SF2 increases to about 3.3 at the 10-cm depth and seems to be constant at this value for larger depths in the formation. It is not possible to estimate the remote source asymptotic limit for the ^{60}Co spectral shape factor SF1 from these results, but clearly it must be in excess of 70.

Table 1 presents the simulated ^{60}Co shape factor results for several source distributions. The continuum windows are identical to those developed for ^{137}Cs (Wilson 1997). An upper continuum window extending from 350 to 1100 keV was also investigated, but this window suffers more from uncertainties in the background correction than the 350- to 650-keV window and will not be used in ^{60}Co shape factor analyses of logging data.

Table 1. Simulated ^{60}Co Shape Factors for Several Source Distributions

| Source Distribution | SF1 (60 to 650 keV) / 1173 + 1332 keV peaks | SF2 (60 to 350 keV) / (350 to 650 keV) |
|---|---|--|
| ^{60}Co Radially Uniform in Formation | 14.6 | 3.2 |
| ^{60}Co on Outside Surface of Casing | 7.4 | 2.97 |
| ^{60}Co on Inside Surface of Casing | 5.45 | 2.67 |
| 1-cm-Thick ^{60}Co Ring with 10-cm Radius | 15 | 3.3 |
| 1-cm-Thick ^{60}Co Ring with 30-cm Radius | 38 | 3.3 |
| 1-cm-Thick ^{60}Co Ring with 50-cm Radius | 68 | 3.1 |

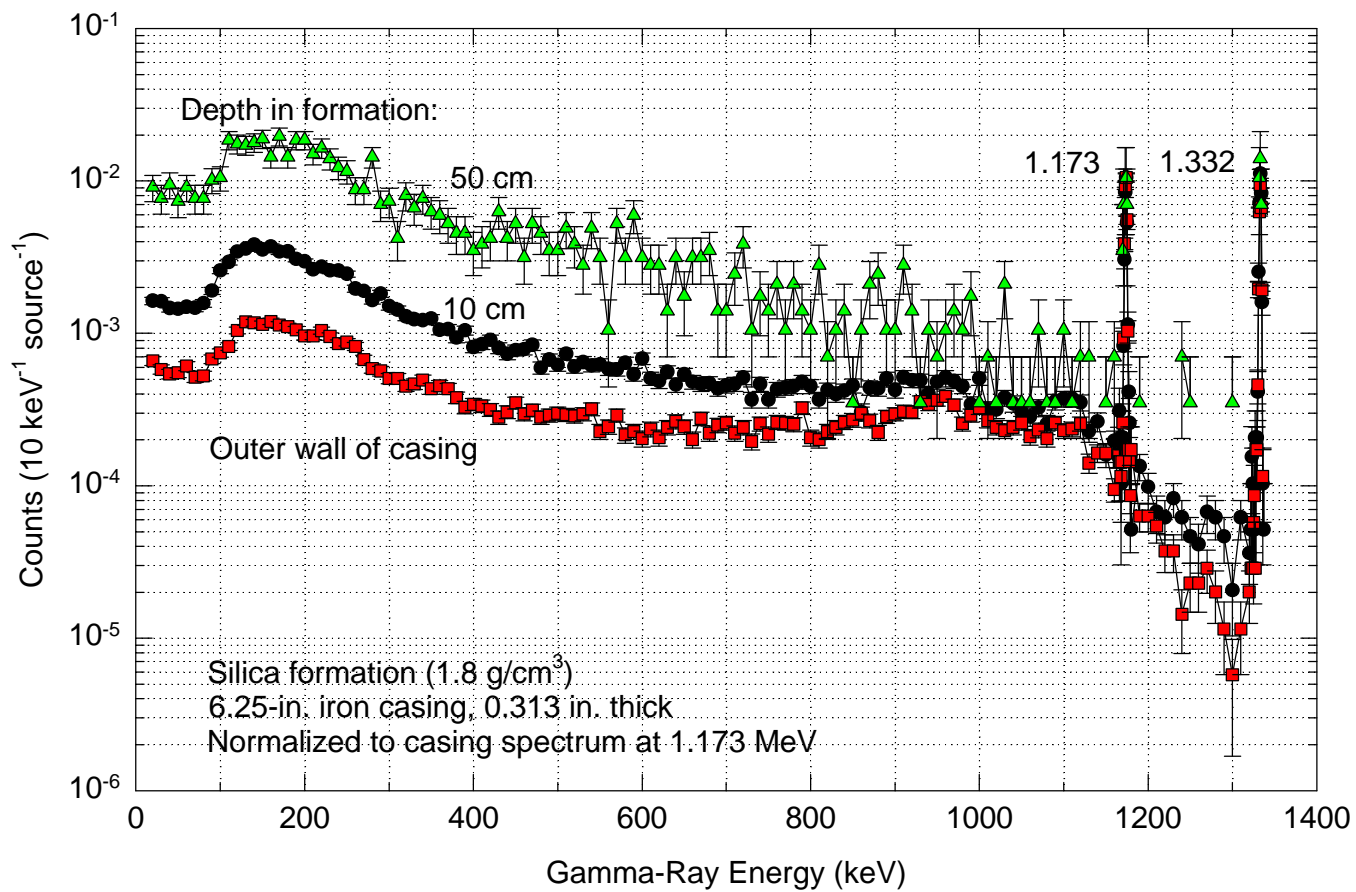


Figure 4. Simulated SGLS Spectra for Ring-Shaped Remote Sources of ^{60}Co

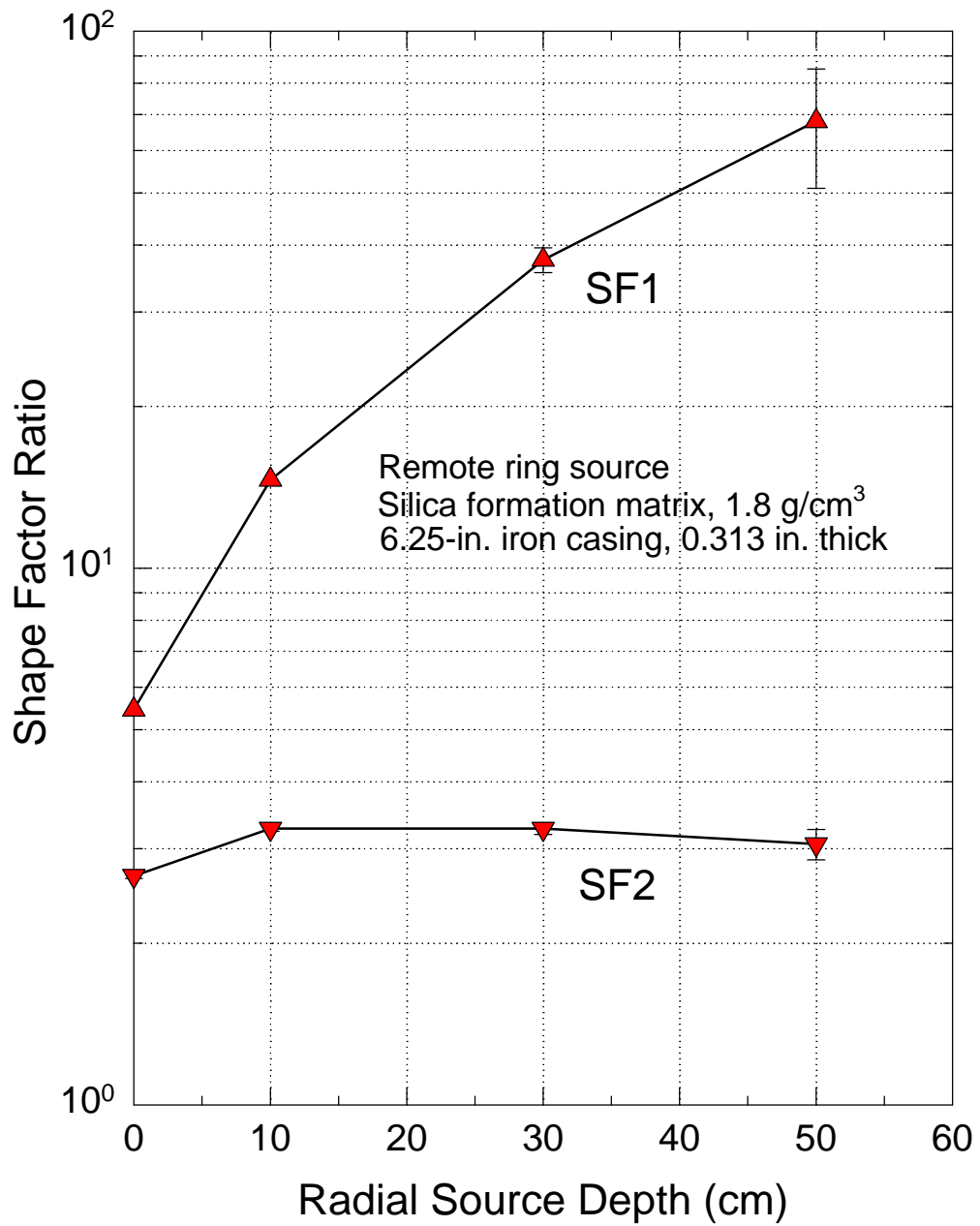


Figure 5. Simulated SF1 and SF2 for Radially Remote Ring Sources of ⁶⁰Co

2.2 Comparison of Simulated and Measured Point-Source ^{60}Co Spectra

Spectra were measured with a point ^{60}Co source as part of a benchmarking process for the simulation models. ^{60}Co spectra were obtained for the source at various positions near the detector with the SGLS tool housing removed. Section 3.0, "Benchmark Experiments for Validation of Simulated Spectral Shape Factors," contains descriptions of the benchmark experiments. A phenomenon observed in the experiments cannot be included in the current simulation models for ^{60}Co spectra: a true coincidence component to the measured spectra exists for all count rates. The true coincidence component is caused by the emission of the two gammas simultaneously, in cascade, as ^{60}Co decays. Sometimes both gammas are detected from the same decay, producing a peak with effective energy of $1173 + 1332 = 2505$ keV, along with a scattered continuum to low energies. The magnitude of this true coincidence spectrum relative to the primary or principal spectral components from the 1173-keV and 1332-keV gammas detected separately depends primarily on the solid angle for detection of the source gammas and on the angular distribution of emission for one gamma relative to the other (Knoll 1987).

Figure 6 shows a comparison of the measured and simulated spectra for the source at the front face of the detector with the tool housing removed. The coincidence component of the spectrum, with its so-called "sum" peak at 2505 keV, is clearly evident. Because the solid angle of detection is greater for this geometry than it will be for formation contaminant sources, this comparison illustrates the worst case for the discrepancy between simulation and experiment. It is not presently known how important the true coincidence component is to the computation of the spectral shape factors SF1 and SF2 for ^{60}Co . However, the large difference between the measured and simulated values of SF1 for the point source at the detector face are much larger than the difference obtained for the same geometry with a source, such as ^{137}Cs , for which there is no true coincidence spectral component. This larger difference is evidence that the true coincidence effect on SF1 is important for a point source of ^{60}Co close to the detector. Figure 6 shows the large difference between the simulated and measured counts in the energy range between the photo peaks at 1173 and 1332 keV. This disparity is probably due to a filling in of this region by the scattered continuum part of the coincidence component and means that a shape factor based on the high-energy portion of the scattered continuum is less feasible for ^{60}Co than for ^{137}Cs contamination.

The effective solid angle of detection is dependent on source distribution. When ^{60}Co contamination is close to the logging tool (borehole localized), the solid angle is greater and, therefore, the true coincidence component is larger in magnitude relative to the primary spectrum than if the source is uniformly distributed. This behavior was verified in the experiments by recording data for several source-detector spacings. Measured ^{60}Co spectra show a larger coincidence component for the source close to the detector where the solid angle for detection is larger, but this effect is not due to pulse pileup because the count rates were not large enough for a significant random coincidence effect. This true coincidence effect is expected to increase the spectral shape factor SF1, mainly because of the loss in counts in the 1173-keV and 1332-keV peaks. Because this effect is present regardless of count rate, depending only on changes in effective detection solid angle, the measured values of SF1

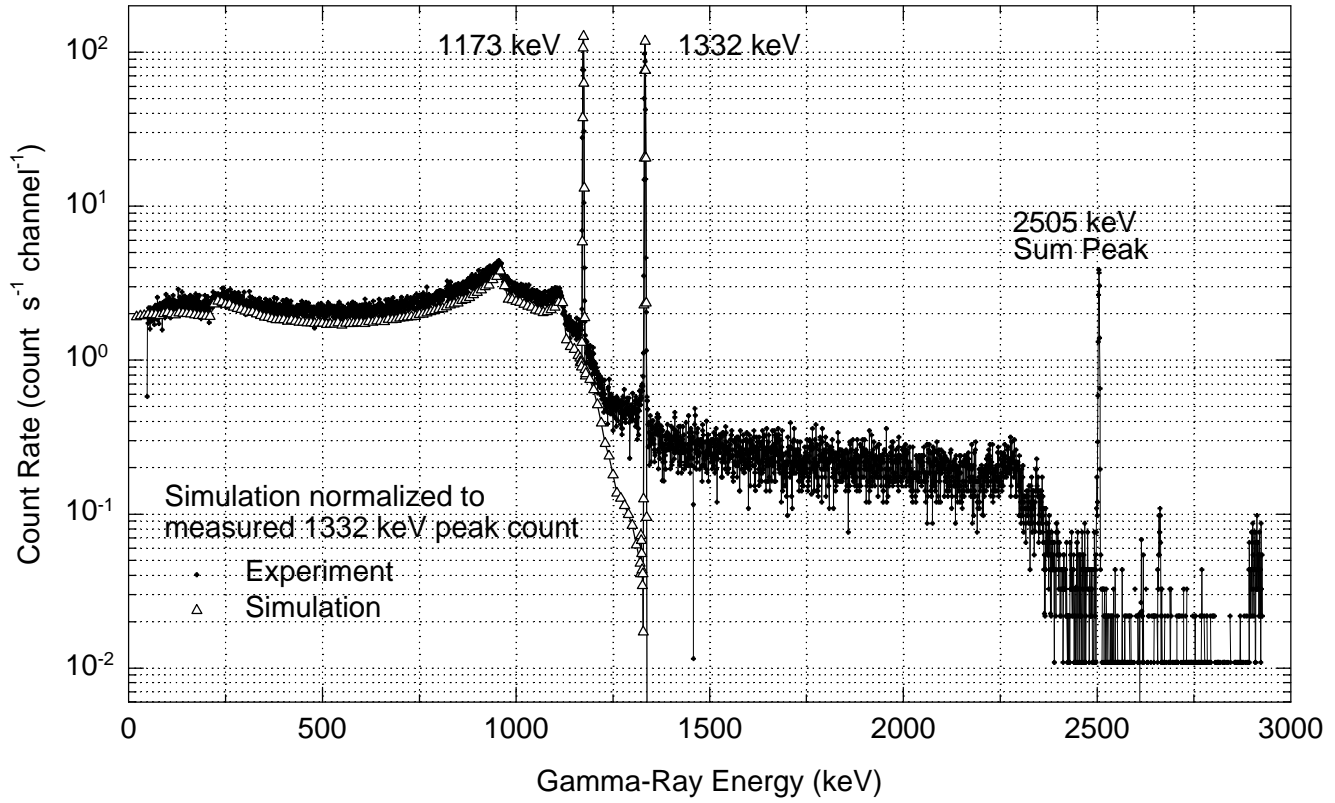


Figure 6. Comparisons of Measured and Simulated ^{60}Co Spectra for Point Source at Front Face of Detector

will always be larger than those simulated with the MCNP code. Furthermore, as the source distribution changes from being local to the borehole to being uniformly distributed in the formation, the coincidence component will become a smaller part of the primary spectrum from which the shape factor information is obtained. Therefore, the coincidence effect is expected to act in opposition to the increase in spectral shape that occurs because of increased scattering as the source becomes uniformly distributed in the formation. The overall sensitivity of spectral shape to source distribution is expected to be less than in the absence of the coincidence effect. The coincidence component for ^{60}Co spectra measured in borehole logs is difficult to detect and is seen only for the most active ^{60}Co zones. It is not clear at this point if true coincidences are a significant effect in the shape factor log interpretation problem for ^{60}Co .

2.3 ^{60}Co Shape Factor Log Analysis Methodology

A method for processing ^{60}Co spectra acquired by the SGLS in the monitoring boreholes at the Hanford Tank Farms has been developed. It is analogous to the methods developed previously for ^{137}Cs (Wilson 1997). Shape factors SF1 and SF2 are defined

$$\begin{aligned} \text{SF1} &= [(CL + CH) - (BL + BH)_{\text{AVG}}] / (Co1 + Co2) \\ \text{SF2} &= (CL - BL_{\text{AVG}}) / (CU - BH_{\text{AVG}}) \end{aligned} \quad (1)$$

where

- CL = counts in 60- to 350-keV continuum window,
- CH = counts in 350- to 650-keV continuum window,
- BL = KUT background for 60- to 350-keV continuum window,
- BH = KUT background for 350- to 650-keV continuum window,
- $Co1$ = net counts in 1173-keV peak, and
- $Co2$ = net counts in 1332-keV peak.

The background counts BL and BH are from the natural radioelements of potassium, uranium, and thorium and are estimated using a procedure introduced for the ^{137}Cs shape factor analysis methodology in Wilson (1997). The gamma peak counts measured from K (1461 keV), U1(609 keV) or U2(1765 keV), and Th (2614 keV) are multiplied by the stripping factors developed for the ^{137}Cs shape factor analysis. The background counts are given by the equations

$$BL = 12.9(K) + [40(U1) \text{ or } 117(U2)] + 90(\text{Th}) \quad (2)$$

$$BH = 4.1(K) + [10(U1) \text{ or } 29(U2)] + 21(\text{Th}) \quad (3)$$

$$BL + BH = 17(K) + [50(U1) \text{ or } 146(U2)] + 111(\text{Th}) \quad (4)$$

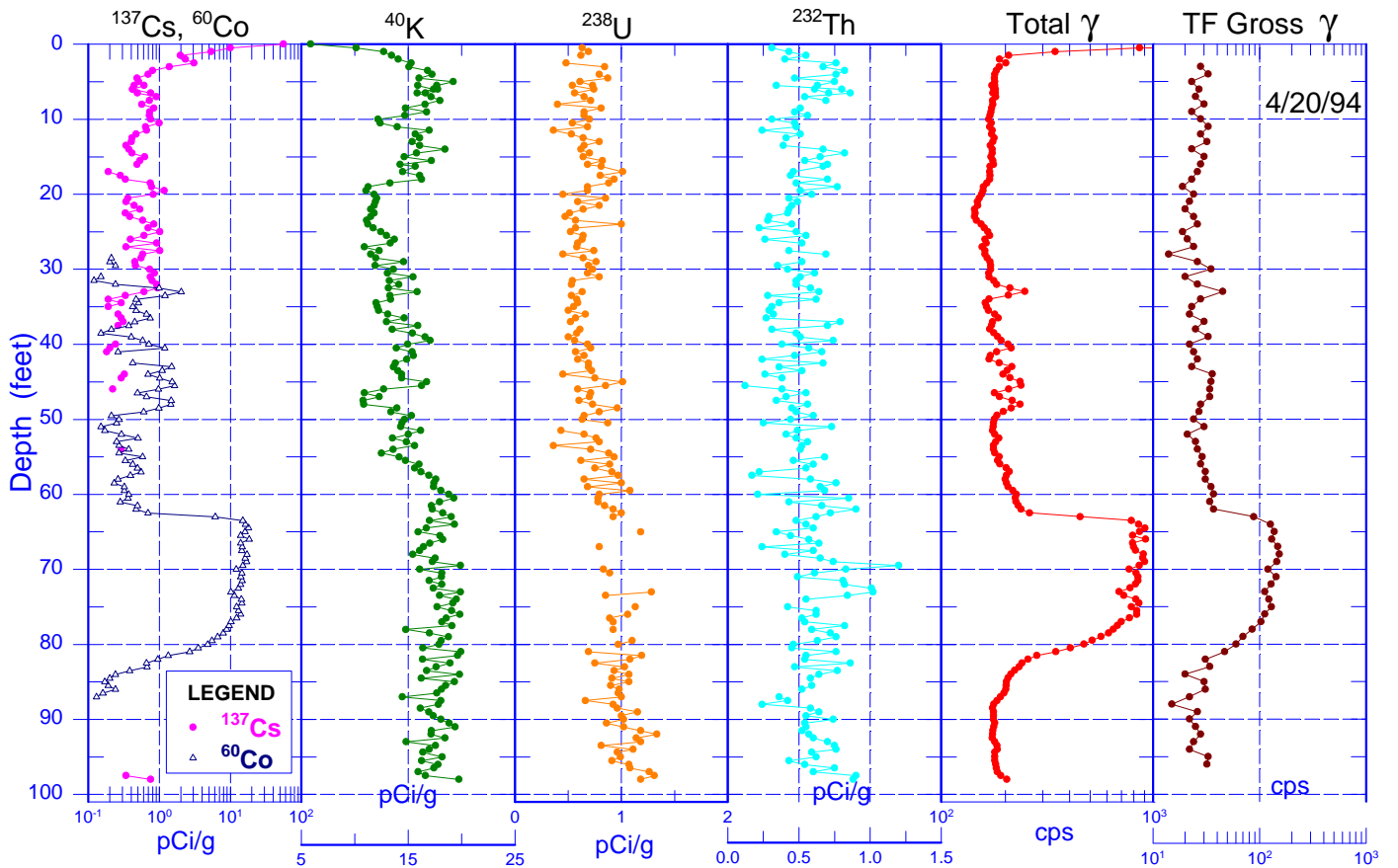


Figure 7. Combination Log Plot for Borehole 22-06-05 at Tank BY-106

As described in Wilson (1997), the stripping factors were derived from a combination of SGLS calibration data, simulated spectra, and testing with field data. The U contribution is estimated with either the 609-keV or 1765-keV net peak count, depending on which has better statistical precision.

2.4 Application of ^{60}Co Shape Factor Log Analysis to Tank Farms Logs

2.4.1 Borehole 22–06–05

The SGLS logs reported in the Tank Summary Data Report for tank BY–106 (DOE 1996a) show a strong ^{60}Co presence in the lower portion of borehole 22–06–05. Figure 7 is the combination log plot for this borehole (DOE 1996a). ^{60}Co contamination is detected from about 30 to 90 feet (ft), with a relatively high and constant activity of about 15 picocuries per gram (pCi/g) from 62 to 80 ft. ^{137}Cs is present at low activity in the upper portion of the borehole, from the surface to about 40 ft. A weak ^{60}Co presence is detected from 32 to 60 ft. This borehole will be used to test the ^{60}Co shape factor analysis method and to determine how this analysis might proceed even in the presence of ^{137}Cs . In the 62 to 80 ft interval where ^{60}Co activity is nearly independent of depth, the spectral shape should be determined solely by the radial distribution of the gamma emitter and by the scattering properties of the various materials of the tool, borehole, and sediment.

Figure 8 is a plot of the SGLS pulse-height spectrum measured at 65 ft. The standard continuum shape factor energy windows are shown with their energy ranges of 60 to 350 keV and 350 to 650 keV. A third window, from 650 to 1100 keV, was initially added to the 350- to 650-keV window to test the effect of widening this continuum window for ^{60}Co shape-factor analysis. The photo peaks at 1173 and 1332 keV are also identified. Background corrections were made to the continuum windows using the K, U, and Th peak intensities and Equations (2), (3), and (4). Shape factors SF1 and SF2 were computed and plotted with depth using one of two upper continuum window (*CH*) settings: either 350 to 650 keV or 350 to 1100 keV. The background stripping factors for the latter window are not given in Equations (2), (3), and (4). SF1 and SF2 values are more stable, especially at low values of ^{60}Co activity, if the 350- to 650-keV range is used for the upper continuum energy window *CH*. Therefore, the continuum windows *CL* and *CH* preferred for ^{60}Co shape factor analyses are identical to those used for ^{137}Cs .

Figure 9 shows a shape factor log presentation for borehole 22–06–05. The three-track format contains SF1 logs in track 1, the SF2 log in track 2, and contaminant count rate logs and one or more quality indicator logs in track 3. The ^{60}Co peak count rates are labeled *Co1* and *Co2* for the 1173 and 1332 keV gammas, respectively. The 662 keV ^{137}Cs peak count rate is labeled *Cs*. The quality indicator (QI) log is the count rate in a high-energy window from 1350 to 1450 keV. This QI is meant to detect pulse pileup but is influenced slightly by the ^{60}Co activity, probably by some counts from the scattered continuum part of the true coincidence component of the ^{60}Co spectrum. Another quality indicator, the percent dead time, will be included in a production version of the log analysis software. Vertical lines on tracks 1 and 2 of Figure 9 represent expected shape factors for the contaminant ^{60}Co , either uniform in the formation or local to the outer wall of the iron casing. The corresponding shape

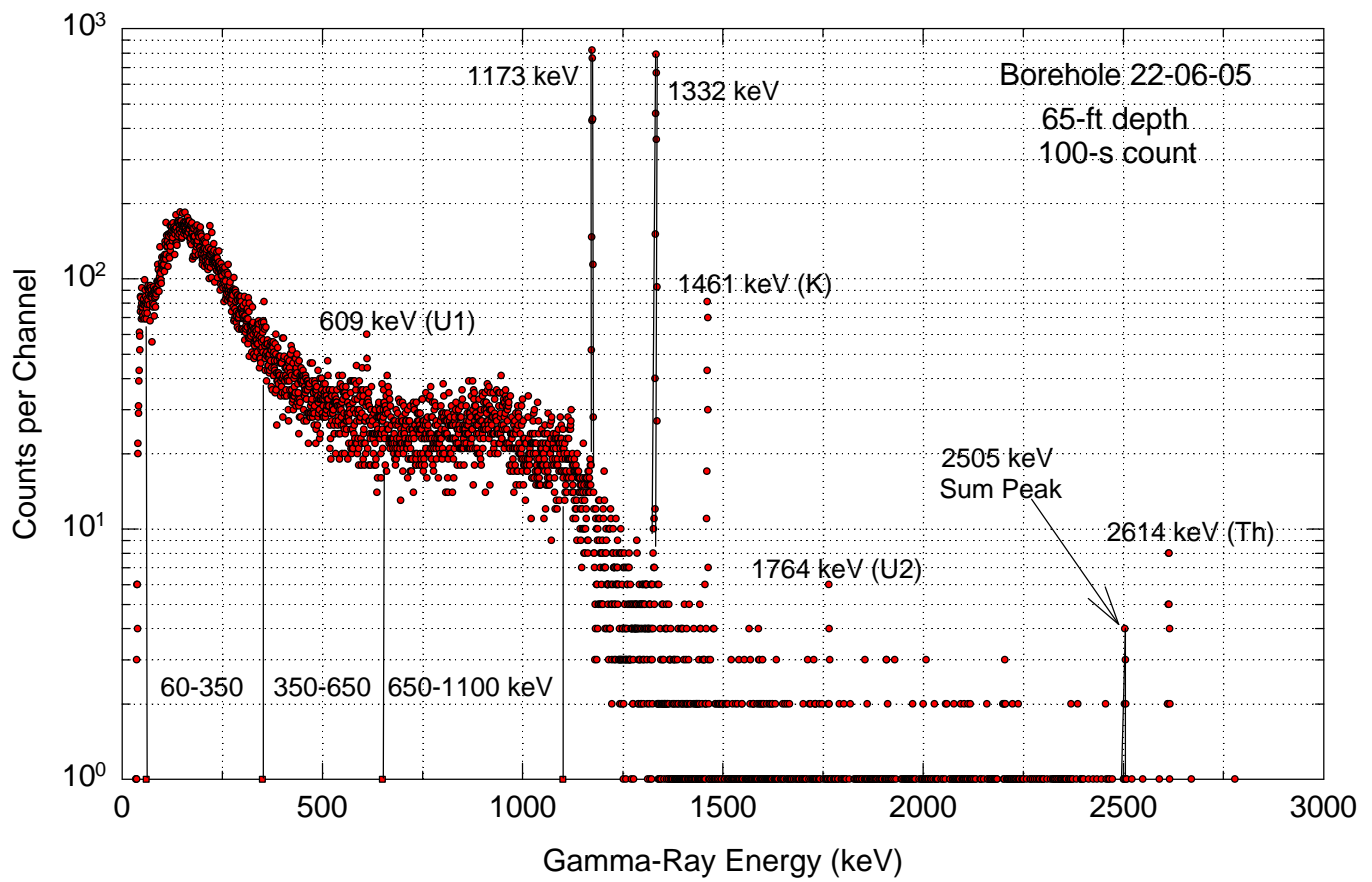


Figure 8. Spectrum Measured at 65-ft Depth in Borehole 22-06-05

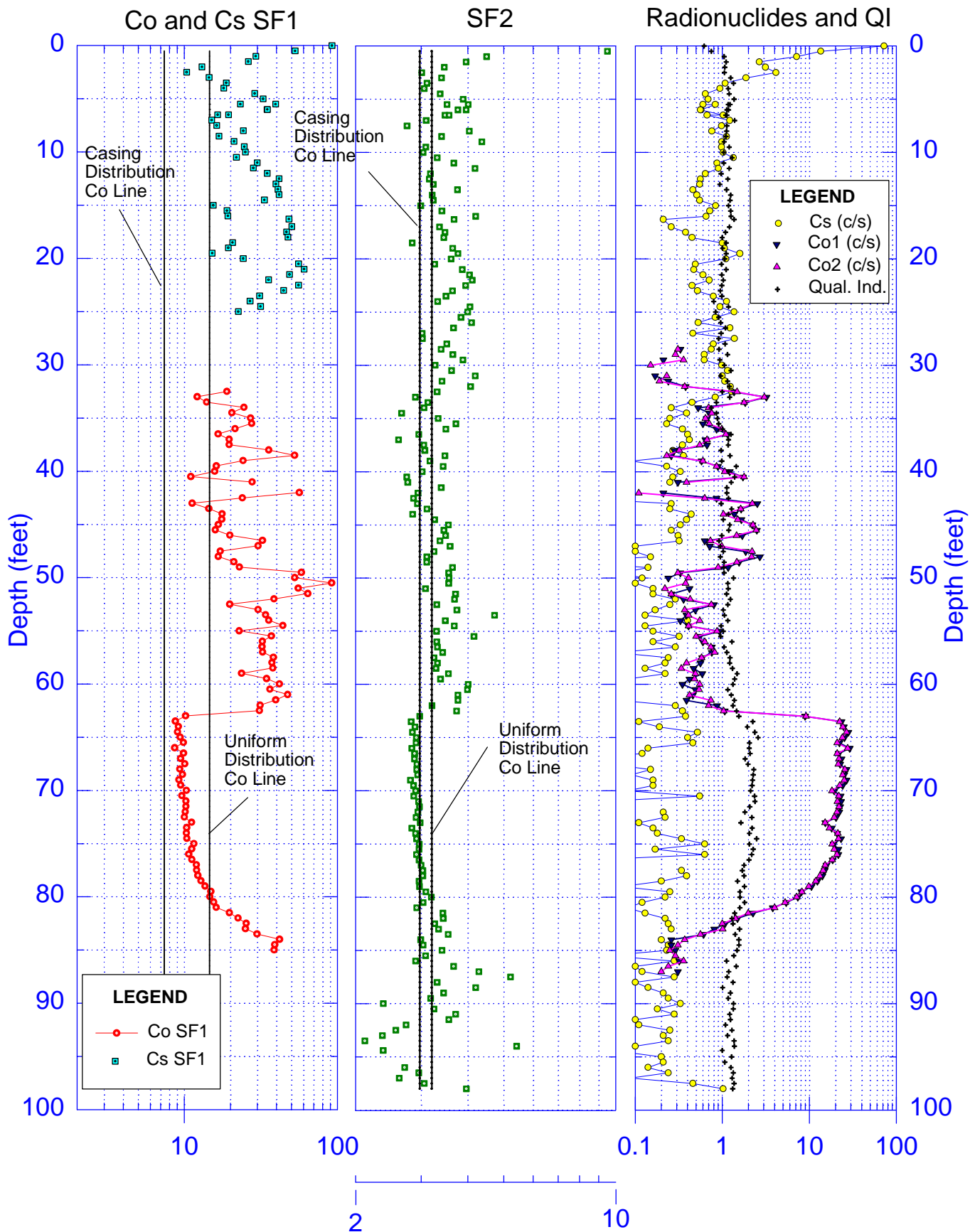


Figure 9. ^{60}Co and ^{137}Cs Shape Factor Logs for Borehole 22-06-05

factors for ^{137}Cs are only slightly different from these values. The magnitude of the background correction was “tuned” by requiring that the net continuum counts be nearly zero in the interval from about 92 to 95 ft where there is no indication of ^{60}Co contamination and only a small indication of the presence of ^{137}Cs . This adjustment required a 3- to 5-percent increase in the nominal stripping values given in Equations (2), (3), and (4) for the continuum energy windows. The interval from the surface to 25 ft was processed for the ^{137}Cs shape factor SF1, while the interval from 32 to 85 ft was processed for the ^{60}Co shape factor SF1.

A strong negative correlation with the ^{60}Co peak count rates $Co1$ and $Co2$ is immediately apparent from the ^{60}Co SF1 log (depth interval from 32 to 85 ft). Such a correlation has been observed previously with ^{137}Cs SF1 logs, although it has been less pronounced. For ^{137}Cs contamination, the negative correlation has been attributed to strong variations in contaminant concentration with depth, or to imperfect background correction of the continuum energy window counts when contaminant count rates are low. For ^{60}Co this behavior would be expected if the background correction were grossly underestimated or if there were a significant contribution to the continuum counts from ^{137}Cs . Neither is the case for depths where the values of $Co1$ and $Co2$ exceed about 1 count per second (c/s), yet the negative correlation is quite pronounced for these depths. The ^{137}Cs SF1 values from the surface to 25 ft show large statistical fluctuations because the ^{137}Cs count rate is below the value of 1 c/s considered necessary for stable SF1 results, as is the ^{60}Co count rate log for certain depths from 32 to 60 ft. When shape factor log analysis software is developed for ^{60}Co it will have to include tests to suppress the shape factor presentation for such intervals. The SF1 log was suppressed for certain depths where both ^{137}Cs and ^{60}Co count rates are negligible (25 to 32 ft and below 85 ft). The resulting SF1 for ^{137}Cs (0 to 25 ft interval) is somewhat elevated from what is expected for a uniform formation distribution, but the peak count rate is too low to conclude that the ^{137}Cs is remote.

The cause of the negative correlation between SF1 and the ^{60}Co peak count rates is not completely understood. In the absence of this negative correlation, the increases in SF1 values for certain depths from 32 to about 62 ft would be evidence of remote ^{60}Co contamination, while the intense activity from 63 to 80 ft, with SF1 values between the values expected for a borehole with a localized and uniform formation source, would be evidence for a somewhat borehole-localized source. However, the negative correlation with peak intensity makes this shape factor interpretation uncertain.

Certain features of the negative correlation may be explained by the possibility that the ^{60}Co peak count rate persists to greater depths relative to the depth of the source location than has been observed previously with ^{137}Cs . Computer simulations (Wilson 1997) and measurements with point sources (Randall 1996) showed that the spectral shape factors increase with increasing vertical distance from a thin layered source of ^{137}Cs . Under certain conditions, this effect manifests itself in ^{137}Cs shape factor logs as a similar negative correlation between SF1 values and the activity (peak count rate) log. The effect would be enhanced for ^{60}Co shape factor logs if the thin zone response is found to persist to greater depths than for ^{137}Cs , but this explanation only applies to depth intervals where the contaminant activity is changing rapidly with depth. This effect may explain the large change in SF1 near 63 ft where the ^{60}Co source activity changes by a factor of about 40, but it does not explain why SF1 persists at high values from 63 ft upward to about 50 ft. The same explanation may apply to the rise in SF1 values

from 75 to 84 ft because the ^{60}Co count rates are decreasing in this depth range at a constantly increasing rate with increasing depth. When the ^{60}Co peak count rate is low and ^{137}Cs contamination is present (33 to 63 ft), the negative correlation can be explained by the continuum contributed by the presence of ^{137}Cs , if this component is relatively constant with depth.

In spite of the interfering effects from ^{137}Cs , ^{60}Co contamination from 33 to 63 ft is probably a combination of uniformly and remotely distributed ^{60}Co . ^{60}Co concentrations from 63 to 80 ft are more local to the borehole casing region. When ^{60}Co count rates are greater than about 2 c/s, the SF1 values seem to be relatively stable and unaffected by the small ^{137}Cs component that also is present. When ^{60}Co count rates are less than about 2 c/s, SF1 values tend to be inflated, probably because of a continuum contribution from the ^{137}Cs component. The attempt to produce a SF1 shape factor log for the zones containing ^{60}Co contamination in borehole 22-06-05 has been problematic, but instructive.

The SF2 shape factor log appears to be less erratic. SF2 shows little variation with depth for the ^{60}Co contamination zones. This uniformity in values is predicted by the simulations, as illustrated by the slight separation in the vertical lines, one for borehole-localized ^{60}Co contamination and one for ^{60}Co contamination uniform in the formation. However, SF2 values do increase at depths above 30 ft. This increase may be caused by the dominance of ^{137}Cs with an SF2 value predicted to be slightly higher. The SF2 log can be interpreted to indicate there is no bremsstrahlung component to these spectra from the presence of ^{90}Sr .

2.4.2 Borehole 22-08-01

Significant ^{60}Co activity was measured in borehole 22-08-01 from about 30 to 95 ft. The reported activity (DOE 1996b) exhibits considerable variation with depth, from the minimum detection level of about 0.1 pCi/g to about 30 pCi/g. Figure 10 presents the shape factor logs for this borehole. The nominal background correction has been applied to the continuum energy windows. The shape factor SF1 seems to be reasonably stable above the ^{60}Co peak count rate of about 3 c/s. There is a pronounced negative correlation between peak count rate and the value of SF1 as observed previously with the shape factor logs from borehole 22-06-05. When ^{60}Co peak count rates are below about 1 c/s, some of this negative correlation is probably explained by the continuum associated with the relatively small ^{137}Cs signal present. The QI log is relatively constant at about 1 c/s and indicates good spectral quality throughout the depth range. At ^{60}Co count rates of about 3 c/s, rapid changes in ^{60}Co activity with depth cause the negative correlation effect. No attempt was made to correct the continuum counts for a ^{137}Cs contribution; therefore, SF1 values computed for ^{60}Co will be too high where ^{60}Co peak count rates are less than about 1 c/s. For the high ^{60}Co count rate intervals, SF1 values fall in a tight range from 10 to 11, below the value of 14.6 predicted by simulations for uniformly distributed ^{60}Co . SF2 values are quite stable with no indication of the bremsstrahlung-producing contaminant ^{90}Sr .

The SF1 log result suggests that the ^{60}Co distribution is intermediate between localized to the casing and uniform in the sediment.

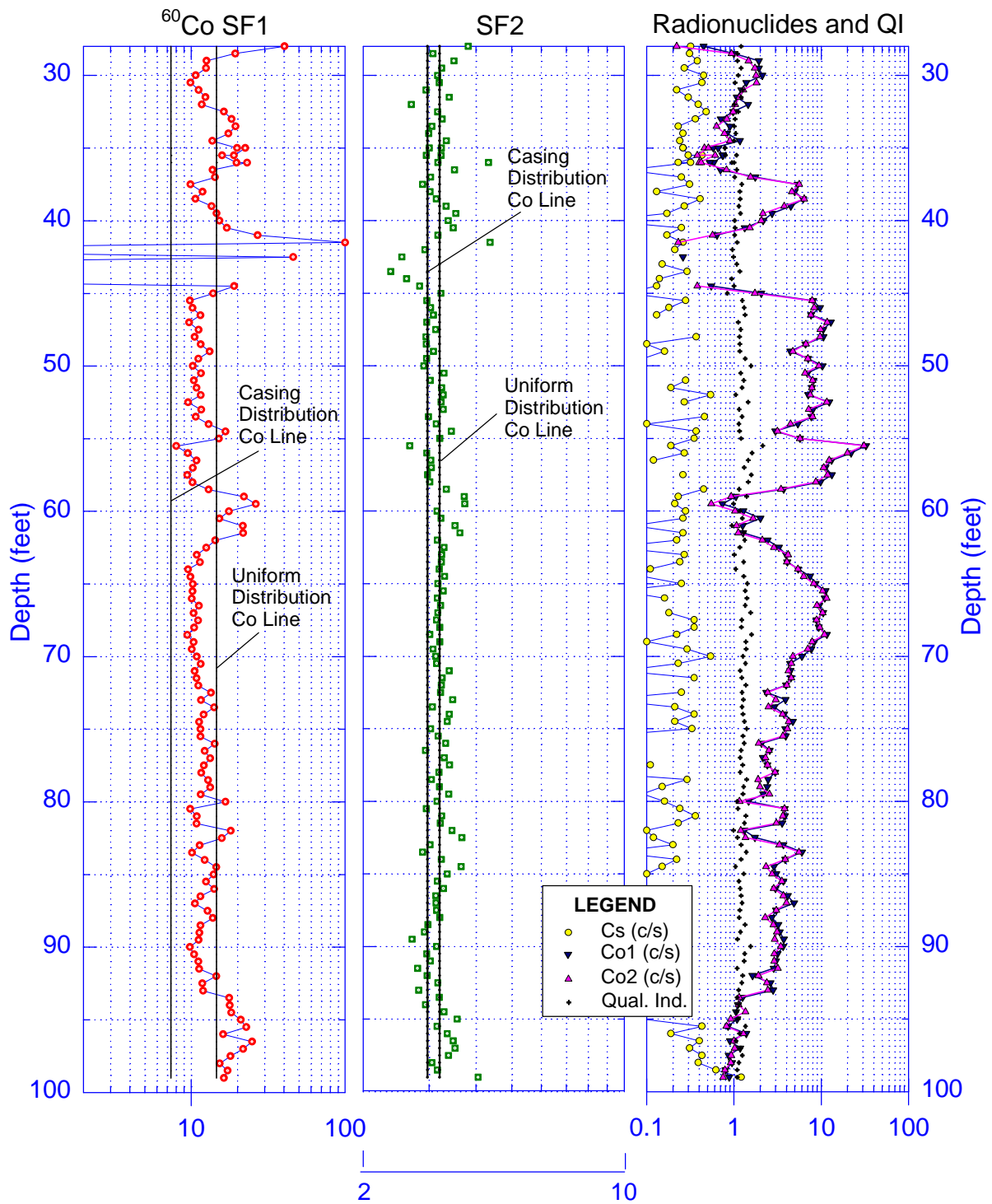


Figure 10. ^{60}Co Shape Factor Logs for Borehole 22-08-01

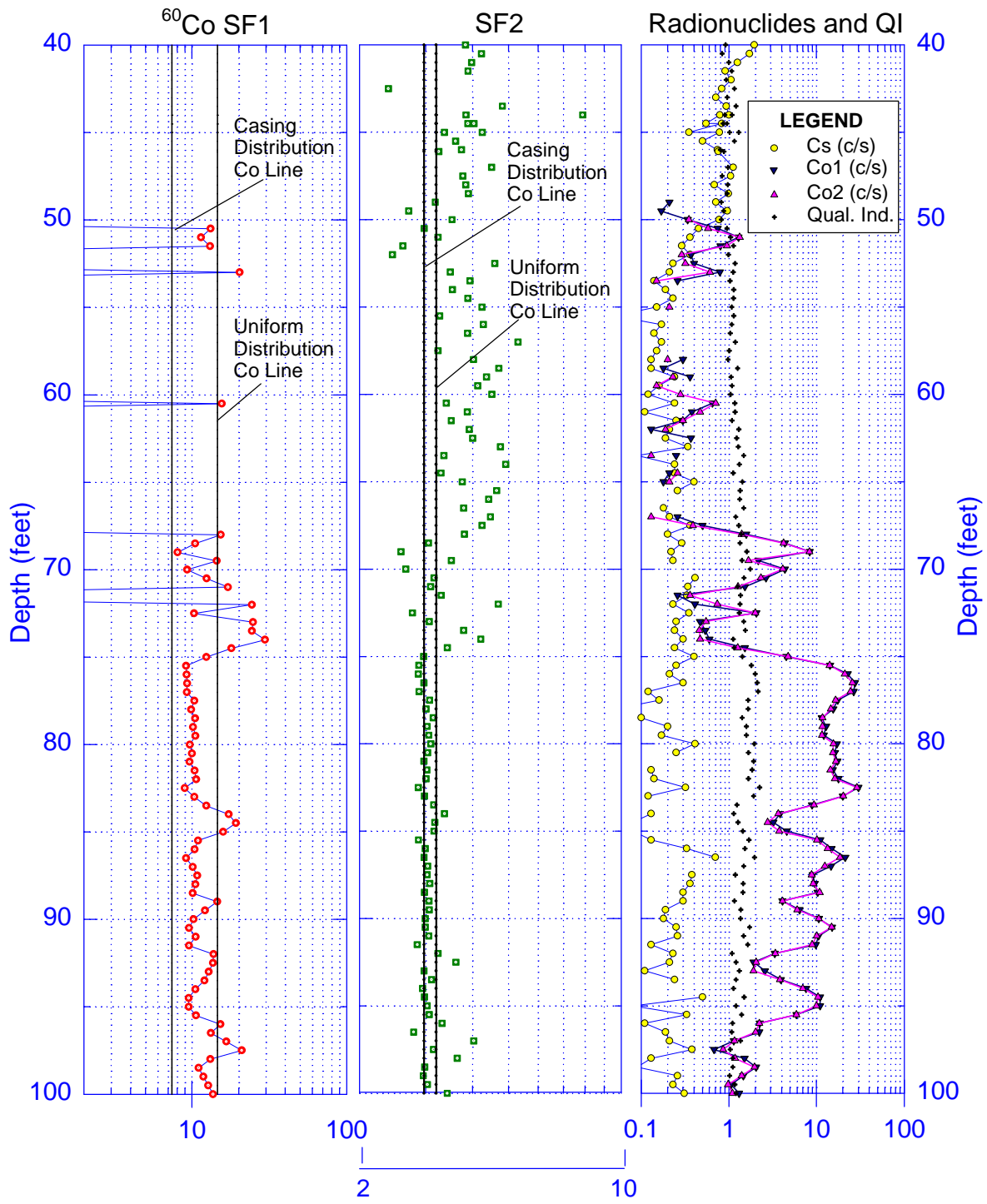


Figure 11. ^{60}Co Shape Factor Logs for Borehole 22-08-02

2.4.3 Borehole 22–08–02

Significant ^{60}Co activity was detected in borehole 22–08–02 from about 65 to 95 ft (DOE 1996b). Only a few isolated occurrences of ^{137}Cs were measured in this depth range, but amounts of ^{137}Cs contamination are too small to affect the shape factor analysis for ^{60}Co count rates above about 2 c/s. Figure 11 presents the shape factor logs for this borehole. SF1 and SF2 values seem to be reasonably well behaved for this depth range. Above 65 ft, the minor ^{60}Co concentration detected does not permit computation of meaningful shape factors and the background-corrected spectra are dominated by the presence of ^{137}Cs contamination from 50 ft to the surface.

In the area shown on Figure 11 where the ^{60}Co concentration is most intense, the SF1 values seem to be stable at a value of about 10, intermediate between the values simulated for a borehole-localized source and a uniformly distributed formation source. Although there is a negative correlation of SF1 with ^{60}Co peak intensity, the correlation is not as strong as that observed for borehole 22–06–05. The negative correlation is similar to that observed with ^{137}Cs contamination (Wilson 1997) and is probably caused by the depth variation in ^{60}Co concentration intensity. The ^{60}Co SF1 values for depths above 65 ft are suppressed because the ^{60}Co count rates are too low and are influenced by the presence of ^{137}Cs , producing inflated values that falsely indicate the presence of remote ^{60}Co . Production analysis software should suppress such occurrences because of excessive inaccuracy in the shape factor analysis for depth intervals like those above 50 ft (DOE 1996b) where there is significant ^{137}Cs contamination in the absence of ^{60}Co contamination, as done in the analysis presented on Figure 9.

The ^{60}Co shape factor analysis for borehole 22–08–02 is stable (except for the negative correlation effect) for the intervals where ^{60}Co count rates are above about 2 c/s. These values are indicative of ^{60}Co contamination somewhat local to the borehole region. This interpretation, and those interpretations given previously for ^{60}Co distributions, are somewhat uncertain because of the unknown effect of true coincidence detections on the shape factors, an effect that is not included in the simulation models. There is no indication of ^{90}Sr contamination on the basis of the stability of SF2 at values in the range expected for borehole-localized and uniformly distributed ^{60}Co or ^{137}Cs contamination. The somewhat high SF2 values above 70 ft are probably an artifact of incomplete background compensation to the continuum portion of the spectra.

2.4.4 Borehole 51–03–11

Borehole 51–03–11 is near tank TX–103 in the TX Tank Farm. The analysis of this borehole for gamma-emitting contaminants (DOE 1996c) shows the usual occurrence of ^{137}Cs near the surface but none at depths below 25 ft. A strong ^{60}Co occurrence begins at 52 ft with a sharp rise in activity at this depth. The high activity persists to 68 ft, where a sharp drop to about 1 pCi/g occurs. The peak analysis also identified the presence of the contaminant ^{154}Eu from 52 to 56 ft with an activity of about 10 pCi/g. Figure 12 presents a typical spectrum from this depth interval. Examination of this spectrum suggests that the ^{154}Eu response in the continuum windows used for the ^{60}Co shape factor analysis (60 to 350 keV and 350 to 650 keV) is

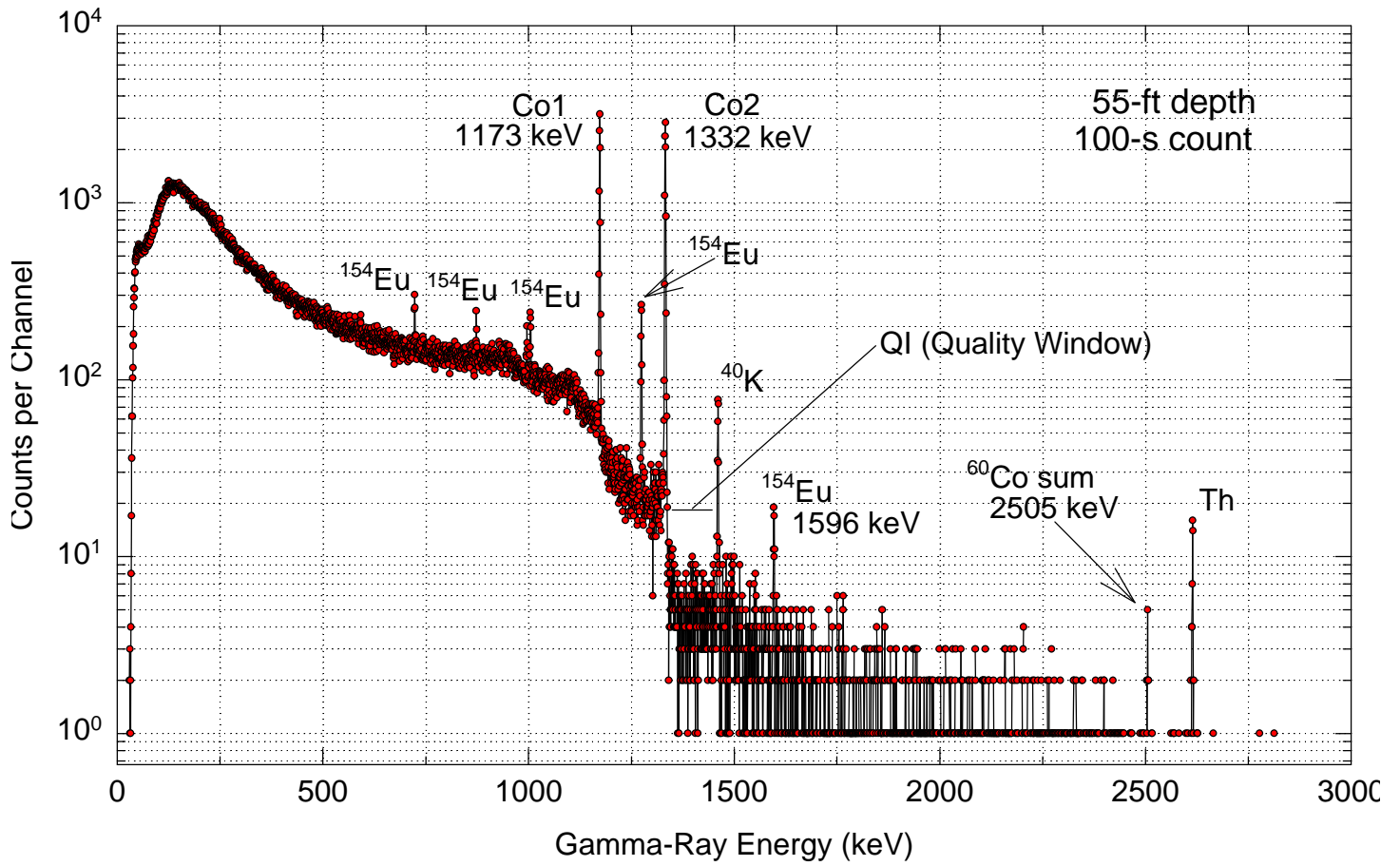


Figure 12. Spectrum Measured at 55-ft Depth in Borehole 51-03-11

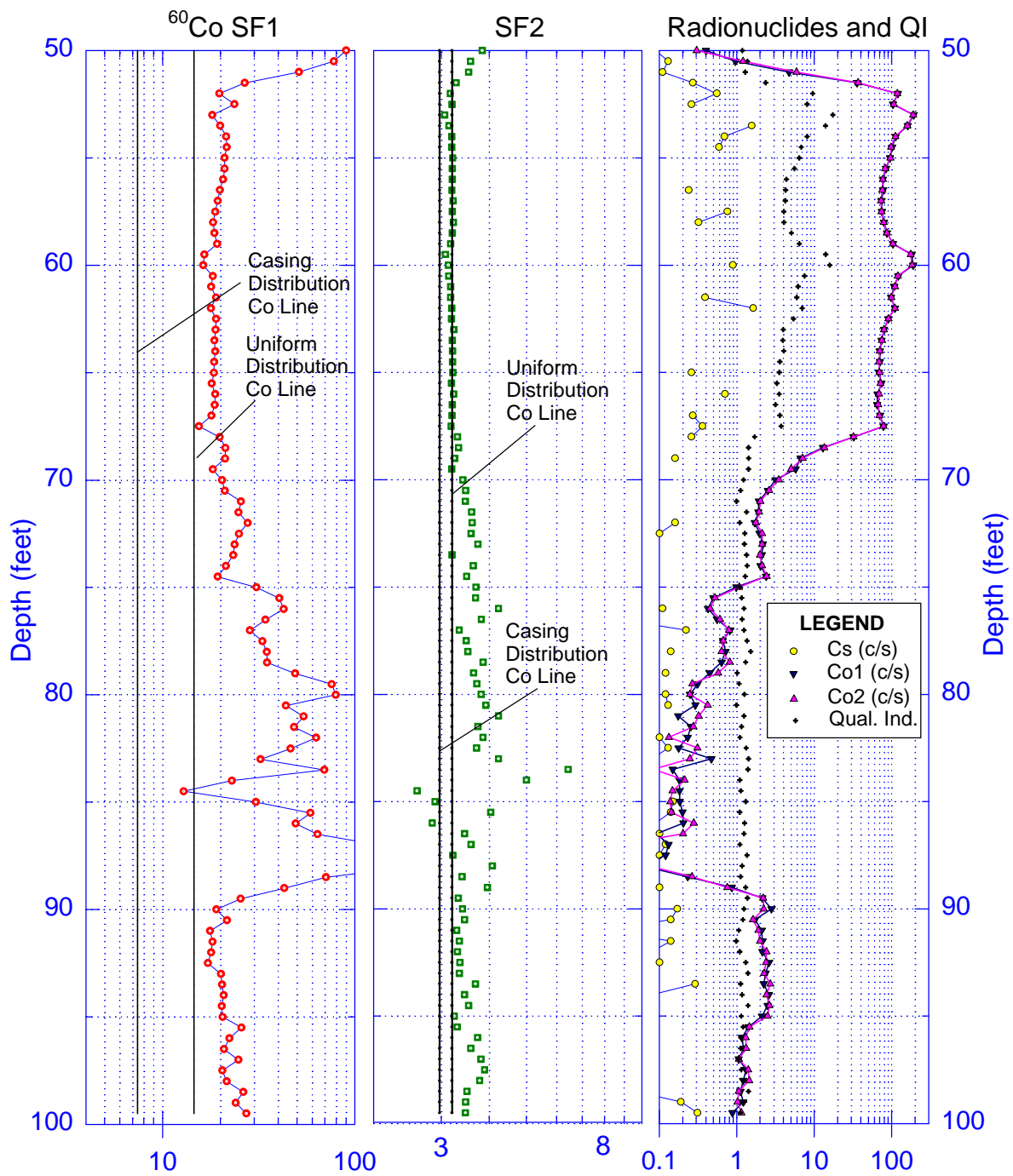


Figure 13. ^{60}Co Shape Factor Logs for Borehole 51-03-11

significant. The 1596-keV gamma from ^{154}Eu is above the QI window from 1350 to 1450 keV; a few of these gammas may produce counts in this window by Compton scattering. Figure 13 presents the shape factor analysis for the depth interval from 50 to 100 ft in borehole 51–03–11. The increase in the QI counts from 52 to 68 ft mirrors the shape of the log of the ^{60}Co peak counts $Co1$ and $Co2$ and results from pulse pileup that is becoming significant for the dead times of 4 to 10 percent that are typical of this ^{60}Co contamination zone. Judging by the small intensity of the true coincidence sum peak at 2505 keV (Figure 12), there is little contribution from this effect to the QI window. Although there is some pulse pileup in these spectra, the shape factor does not seem to be affected significantly.

SF1 values are somewhat elevated from 52 to 56 ft, where the ^{154}Eu contamination is measured, compared to values from 60 to 68 ft where no ^{154}Eu is detected. However, the effect of ^{154}Eu on the SF1 values for ^{60}Co is not large. The SF1 value for this zone averages about 19 or 20, well above the value of 14.6 expected for uniformly distributed ^{60}Co contamination. Because the SF2 values are stable throughout, this anomalously high SF1 occurrence is evidence that at least a portion of the detected ^{60}Co is remote from the borehole. This is the first such instance documented thus far in this application of the ^{60}Co shape-factor analysis methodology. High SF1 values near 51 ft are caused by the rapid change in ^{60}Co activity in this depth interval. The elevated SF1 values from 75 to 90 ft are not meaningful because of the small value of ^{60}Co peak intensity in this range. For this borehole, ^{60}Co shape factors can be reliably interpreted only when the ^{60}Co peak intensity exceeds about 2 c/s.

Figure 14 presents a cross plot of SF2 and SF1 values. One set of points is for the interval from 52 ft, just above the ^{60}Co anomaly, to 56 ft, the lowest depth at which ^{154}Eu contamination is present. The other sets of points are for depths below 59 ft. For the 60 to 70 ft interval, most points cluster near the simulated trend line, between the simulated value for uniformly distributed ^{60}Co and the point for a remote ring source at a radial depth of 30 cm. Other simulated points illustrate ^{60}Co contamination local to the borehole-casing region to show that none of the measured points correspond to ^{60}Co contamination local to the borehole. Points for the 52 to 56 ft interval cluster slightly to the right of the points for the 60 to 70 ft interval, at a higher value of SF1, because of the ^{154}Eu concentration in that depth range. Points at the greater depths from 70 to 75 ft and 90 to 95 ft correspond to regions of relatively low and constant ^{60}Co count rate of about 2 c/s. The higher values of SF2 for these depths could indicate a small amount of the bremsstrahlung-emitter ^{90}Sr accompanying the ^{60}Co , or it could be a reflection of imperfect background compensation to the continuum energy windows used in computing SF2.

Shape factor logs for borehole 51–03–11 indicate the ^{60}Co contamination is somewhat remote from the borehole. There is no clear evidence of the bremsstrahlung-producer ^{90}Sr . The shape factor log is reliable only for ^{60}Co peak intensities in excess of about 2 c/s.

2.4.5 Borehole 22–08–12

^{60}Co contamination was detected at rather low activities in borehole 22–08–12. Figure 15 presents the shape factor logs for this borehole. From 45 to 57 ft and from 69 to 79 ft, the ^{60}Co

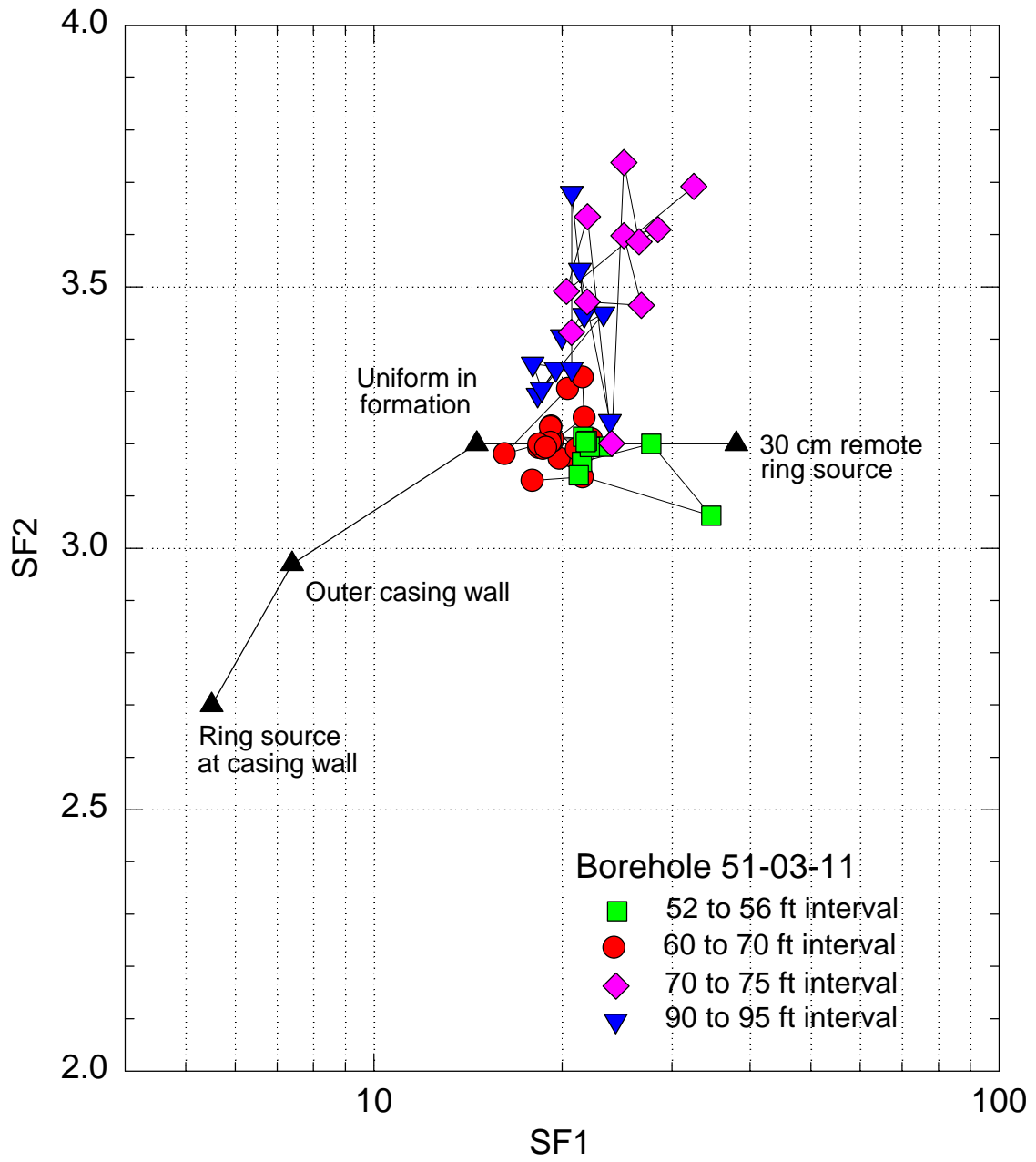


Figure 14. ⁶⁰Co Shape Factor Cross Plot for Borehole 51-03-11

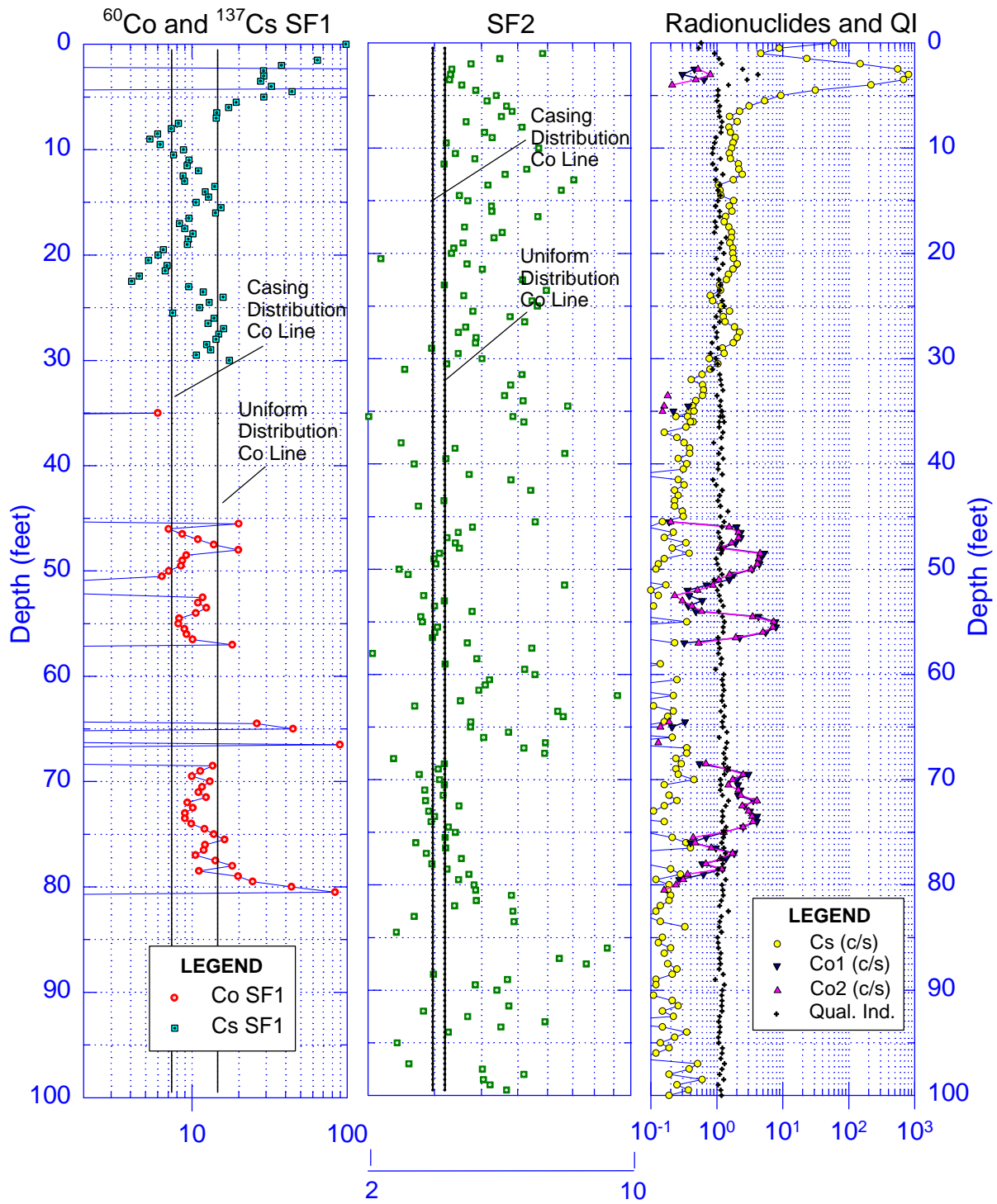


Figure 15. ^{60}Co Shape Factor Logs for Borehole 22-08-12

peak count varies between about 0.5 and 7 c/s. In these zones, ^{137}Cs contamination is detected at low intensity. The ^{60}Co intensities show considerable variation with depth for these intervals. SF1 values are plotted only when the ^{60}Co peak rate exceeds 0.2 c/s. There is a pronounced negative correlation between SF1 and the peak count rates. However, there are regions of stability for SF1 that seem to occur where the ^{60}Co peak count rates are at their greatest. For these intervals, SF1 is between about 8 and 12, indicating the ^{60}Co distribution is intermediate between casing localized and uniform in the formation. As observed in shape factor logs for other boreholes, the shape factor logs for borehole 22-08-12 seem to be reliable only when the ^{60}Co peak count exceeds about 2 c/s. Because the interval from the surface to about 30 ft has a measurable amount of ^{137}Cs contamination, an SF1 value for ^{137}Cs is presented for this interval. SF1 values for the strong ^{137}Cs anomaly at 3 ft may not be considered valid because of the presence of ^{60}Co and elevated values for the quality indicator, QI. Below 3 ft the values of SF1 vary between 6 and 13, indicating the ^{137}Cs is variably distributed between the casing and formation.

2.5 SGLS Tool Depth Response to Thin Zones of Contamination

The negative correlations observed in shape factor logs for depths where the contaminant activity is changing rapidly with depth indicate a need to simulate the variation of shape factor and contaminant log count rates as the tool moves above and below a thin zone of contamination. The availability of thin-zone response profiles would assist in the effort to understand the causes of the negative correlations and to interpret shape factor logs.

Efforts are under way to model the SGLS tool response to a vertically thin contaminant layer. Such models require the use of both Monte Carlo simulations with MCNP and analytical computations that incorporate numerical integration techniques. MCNP is used to simulate spectra for vertical depths within 12 in. or so of the contaminant layer and for the scattered continuum portion of spectra at greater depths. For these greater depths, MCNP cannot simulate the response to the uncollided source gammas because of the severe attenuation they suffer with increasing depth from the source layer. The uncollided flux is computed analytically with a numerical integration package available in Mathematica, which is available from Wolfram Research, Inc. The dependence of this flux on depth from the contaminant layer location is then normalized to the MCNP peak response simulated for depths of 12 in. and less. Early results of this modeling indicate that peak count rates fall rapidly with increasing distance from the thin layer and are negligible for distances greater than about 1.5 ft. SF1 values rise with increasing distance from the thin zone. This behavior would continue indefinitely, in the absence of any activity other than the thin zone, until there was no observable signal. However, in practice, SF1 values reach a maximum away from the high activity zone as the lower activity for zones adjacent to the detector begin to dominate the shape factor calculation. SF2 values show a modest rise with increasing distance from the thin zone. Details of these thin-zone profile simulations will be presented in another report.

Work conducted by Randall (1996) has verified, at least qualitatively, the predicted increase in value of SF1 as the logging tool moves above or below the location of a depth-localized

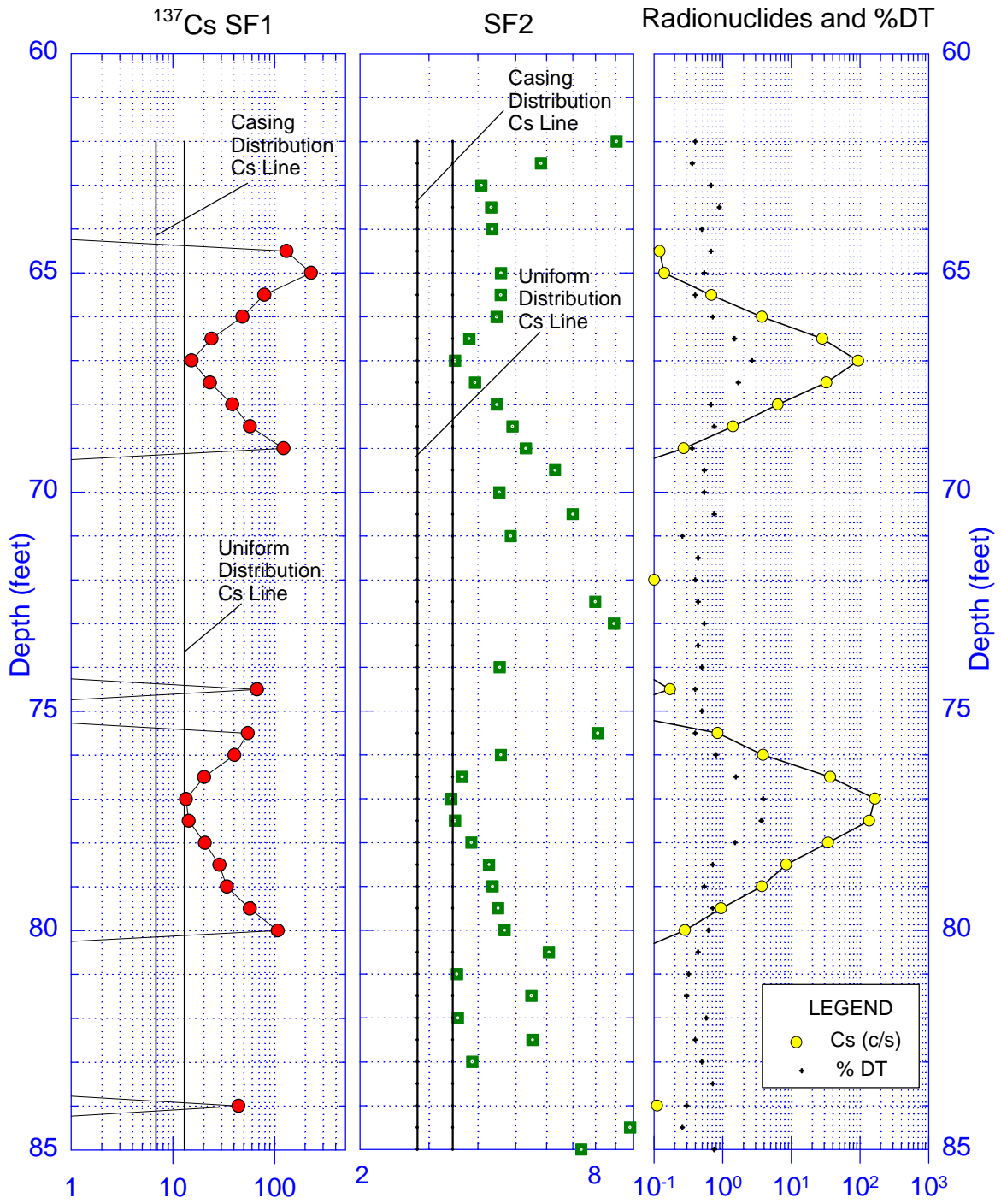


Figure 16. ¹³⁷Cs Shape Factor Logs for Thin Zones in Borehole 41-00-08

contaminant zone. Randall's work also verifies the sharp decrease in contaminant peak count rate for these same logging conditions. These data were taken for an ideal sharp interface between two zones whose activity differed by more than a factor of 100.

Data in some borehole logs indicate the presence of thin zones of contamination. An example is the log for borehole 41-00-08 in a zone from 60 to 90 ft. Figure 16 presents the shape factor log for this section of the borehole and shows the predicted behavior for shape factors SF1 and SF2 as the tool logs through a pair of thin zones at 67 and 77 ft. The minima in SF1 and SF2 at the thin zone depths suggest that the ^{137}Cs is distributed uniformly in the radial direction.

2.6 Summary

^{60}Co shape factor logs were prepared for several boreholes, including a few that are not presented in this report. In general, the method seems to work satisfactorily when ^{60}Co count rates in either peak exceed about 2 c/s and when other contaminants, such as ^{137}Cs or ^{154}Eu , do not contribute interfering count rates. Count rates of 2 c/s correspond to a ^{60}Co activity of about 1.2 pCi/g.

For ^{60}Co count rates less than 2 c/s, the analysis is susceptible to errors in the background correction and to the influence of small concentrations of other contaminants. Shape factor analysis could be extended to lower ^{60}Co count rates (in the absence of other contaminants) if the SGLS count times for each interval were longer. This would improve the ability to perform the background KUT correction to the continuum energy window by improving the statistical precision of the three signature gamma peaks.

A negative correlation observed between SF1 values and ^{60}Co activity is not completely understood. When care is taken in performing the background correction and when there are no apparent interferences from other contaminants, a pronounced negative correlation often remains. The negative correlation can be understood at depths where activity is changing rapidly as being due to the thin-zone response effect, but the change must be greater than about an order of magnitude over an interval of 1 ft or less. Correlations observed elsewhere are not explained by this effect. The negative correlation has been observed for both high and low ^{60}Co activities; dead times are always sufficiently small that pulse pileup is negligible and could not be a contributor to this correlation between spectrum shape and count rate. Efforts are continuing to better understand the negative correlation effect.

Almost all the borehole logs processed for ^{60}Co shape factor logs indicate that the ^{60}Co contamination is uniformly distributed or somewhat localized to the borehole region. An indication of a radially remote source is apparent only for borehole 51-03-11. No indications of bremsstrahlung from the contaminant ^{90}Sr were observed in any of the logs because SF2 always had values in the range expected for the contaminants ^{60}Co and ^{137}Cs .

The continuum window for ^{137}Cs of 60 to 650 keV has also given the best shape factor logs for ^{60}Co . A wider window from 60 to 1100 keV was tried for ^{60}Co but it was not as stable under various logging

conditions, and simulations indicate the sensitivity to contaminant spatial distribution is reduced for the wider continuum window. The initial implementation of ^{60}Co shape factor software will use the 60- to 650-keV continuum window.

Shape factor SF2 is computed from the same continuum windows for both ^{137}Cs and ^{60}Co concentrations and needs to be computed only once for a given borehole, even when both contaminants are present. However, its value for distributed sources of each contaminant are slightly different. Simulations predict the SF2 value is 3.45 for uniformly distributed ^{137}Cs (Wilson 1997) and 3.20 for ^{60}Co . Although the SF1 value is computed from different peaks for each contaminant, they use the same continuum window and, therefore, the values are similar. As simulated by MCNP, the SF1 value for ^{137}Cs is 13 (Wilson 1997) and the SF1 value for ^{60}Co is 14.6.

2.7 Recommendations

Measurements need to be conducted for a point source of ^{60}Co in the sand tank described in Section 3.2 to determine if the true coincidence component of the spectrum is affecting the shape factor calculations. If not, then the simulated values for the shape factors can be used with validity in the interpretation of the SGLS logs at the Hanford Tank Farms.

The software for shape factor log analysis of SGLS data should include the capability to compute ^{60}Co shape factors. Techniques need to be included to switch between ^{137}Cs and ^{60}Co concentrations as the primary shape factor analysis target with user options to correct data when a mixture of the two contaminants occurs, based on assumed shape factors for one of the contaminants.

Error analysis needs to be added to the shape factor methodology for both ^{137}Cs and ^{60}Co . The interpretation of shape factor logs will be improved with such an error analysis and can become the basis for switches that will suppress certain portions of the logs when errors are excessive.

More testing of the ^{60}Co shape factor analysis is required before it can be applied and interpreted with confidence. It may be desirable to relog boreholes of special concern with a collimating arrangement on the tool to minimize the negative correlation between the shape factors and the contaminant count rate.

When ^{137}Cs interferes with the standard ^{60}Co shape factor analysis, it may be better to use a third shape factor SF3, defined as the ratio of counts in a narrow high-energy continuum window to the counts in the two peaks. This factor is not affected by the ^{137}Cs spectral components. A study should be conducted with data where ^{60}Co contamination is detected in the presence of a strong ^{137}Cs signal to determine if SF3 is superior to SF1 in such cases.

3.0 Benchmark Experiments for Validation of Simulated Spectral Shape Factors

Monte Carlo computer models were developed to simulate spectra measured at the Hanford Tank Farms with the SGLS. These simulations are being used to develop spectral shape-analysis techniques to help log analysts determine the radial distribution of gamma-emitting contaminants. The accuracy of these computer models must be validated before the data they produce are used in the log analysis software.

To validate the computer simulations, several experiments were completed with monoenergetic gamma sources. All measurements were performed with a logging tool nearly identical to those in use by the SGLS. These tools contain a large-volume high purity germanium (HPGe) detector (about 35-percent efficient relative to a 3-in.-diameter, 3-in.-long sodium iodide detector at the 662-keV energy of the ^{137}Cs gamma ray) and produce spectra with high-energy resolution.

The comparisons of measured-to-simulated gamma spectra for these various cases substantiated the conclusion that the simulated spectral shapes are quite accurate for most source geometries and energies. These simulations underestimate the flux below about 150 keV for certain source geometries by about 15 percent. The peak count rates, in an absolute sense, are accurate to better than 16 percent.

Some of these experiments prompted the discovery that a physics-based decision made during development of the simulation models to exclude the production of bremsstrahlung from the Monte Carlo tracking of gamma rays, though valid for the lower energy ^{137}Cs gammas, resulted in a significant error at the higher energy of the ^{40}K gamma. The physics of the model was subsequently changed to include bremsstrahlung production, at some cost in processor time. Other refinements made to the materials and the geometry of the simulation model improve the overall agreement with the experiments. Consequently, improved simulations are expected in the future, especially for ^{60}Co shape factors, where the source gamma energies are higher than those for ^{137}Cs . These model improvements have a smaller effect on ^{137}Cs shape factors.

3.1 Potassium Sleeve Experiment

An experiment with a potassium sleeve and an SGLS tool was completed in fall 1996 by James Meisner, formerly of the Westinghouse Hanford Company (WHC) geophysics group, and now with Waste Management Federal Services. A 5-in.-diameter plastic sleeve containing a thin annulus of potassium carbonate was positioned at the midplane of the 8-in.-diameter cased borehole of one of the moisture calibration models at the DOE facility in Pasco, Washington (Engelman et al. 1995). The SGLS tool was then positioned within the sleeve, and gamma spectra were recorded with the instrument in several positions. This arrangement was designed to be an analog of the situation where ^{137}Cs is localized to the inside surface of a cased borehole that is surrounded by sediment. The gamma

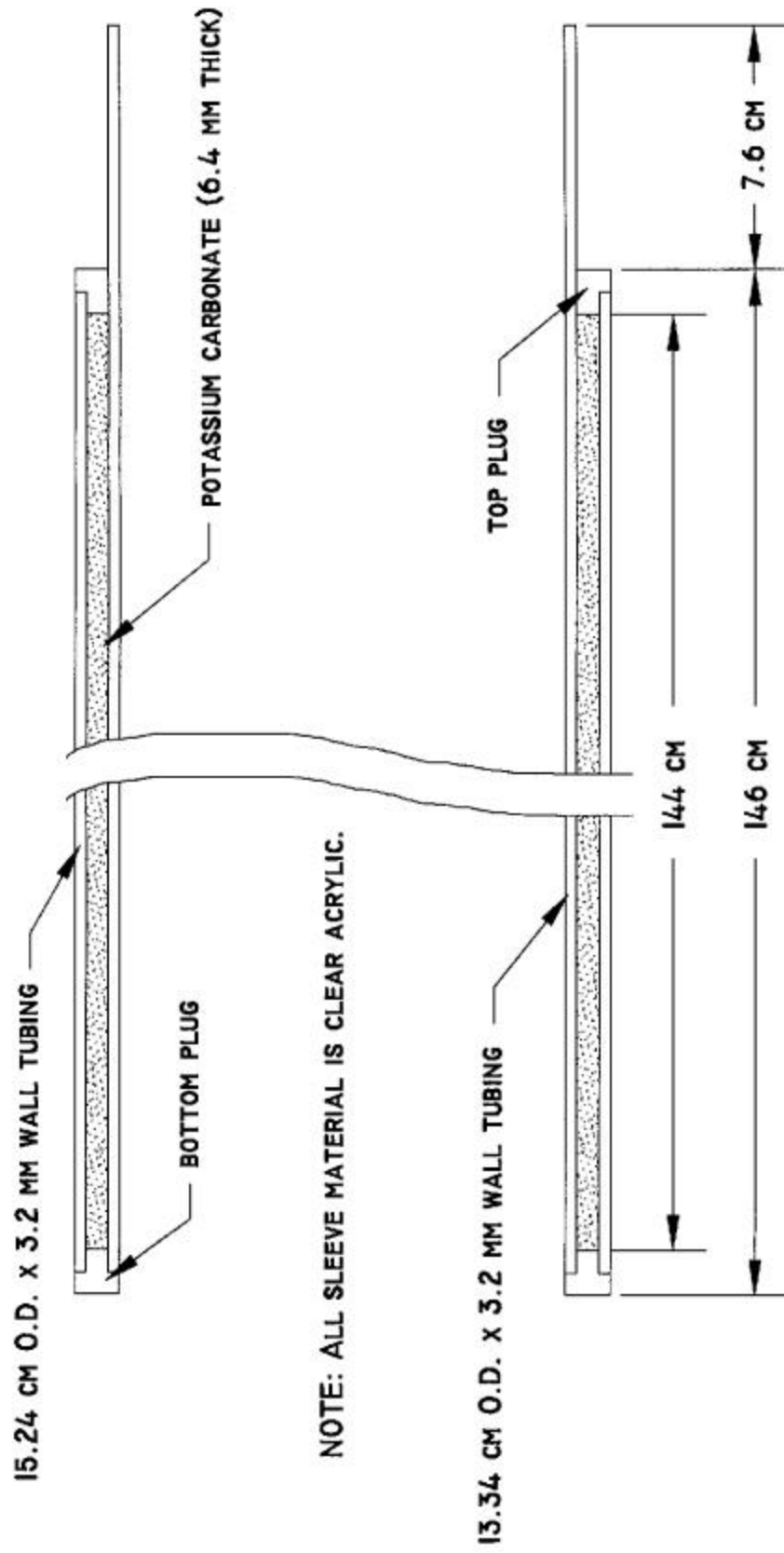


Figure 17. Potassium Sleeve

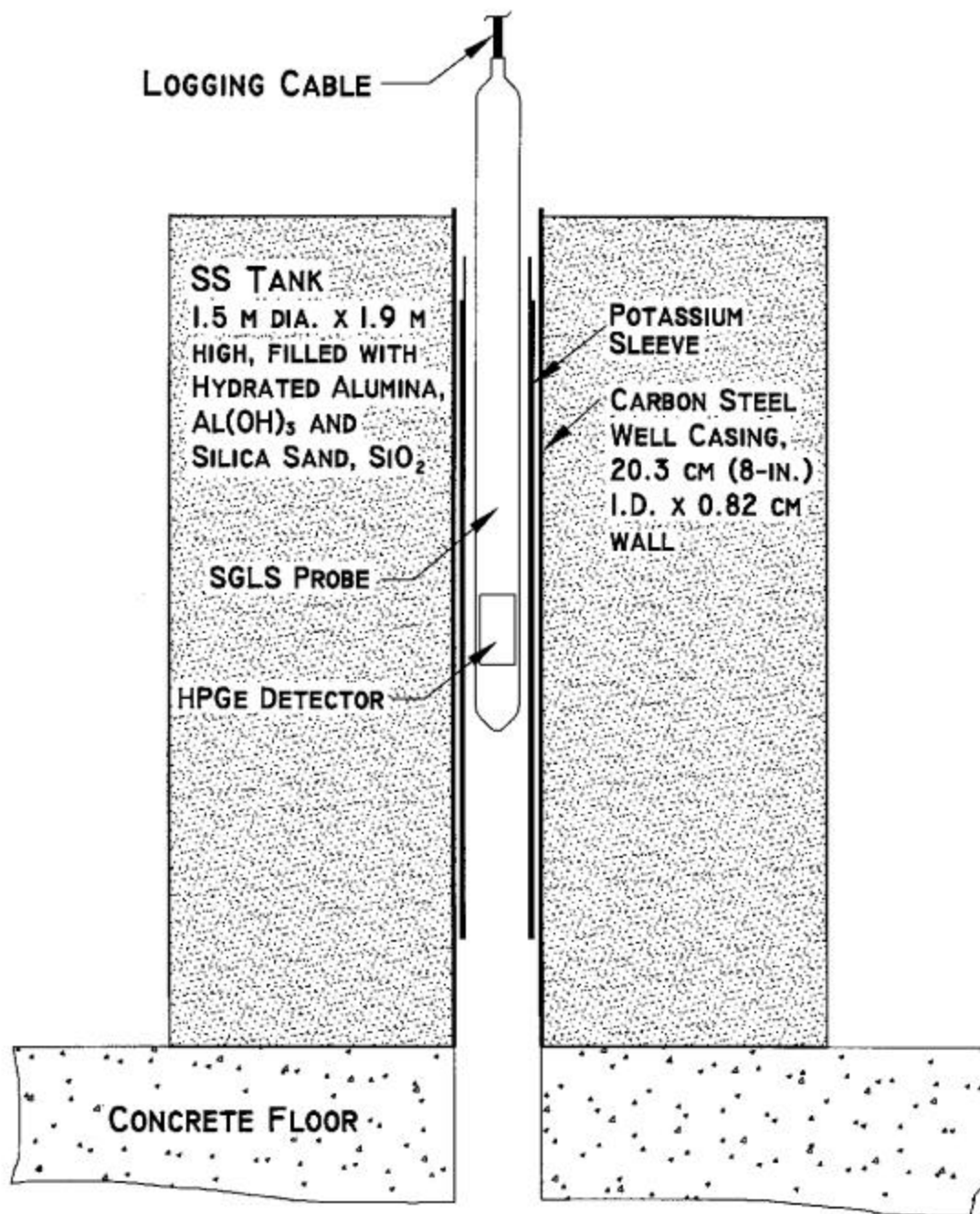


Figure 18. Arrangement for Potassium Sleeve Experiment

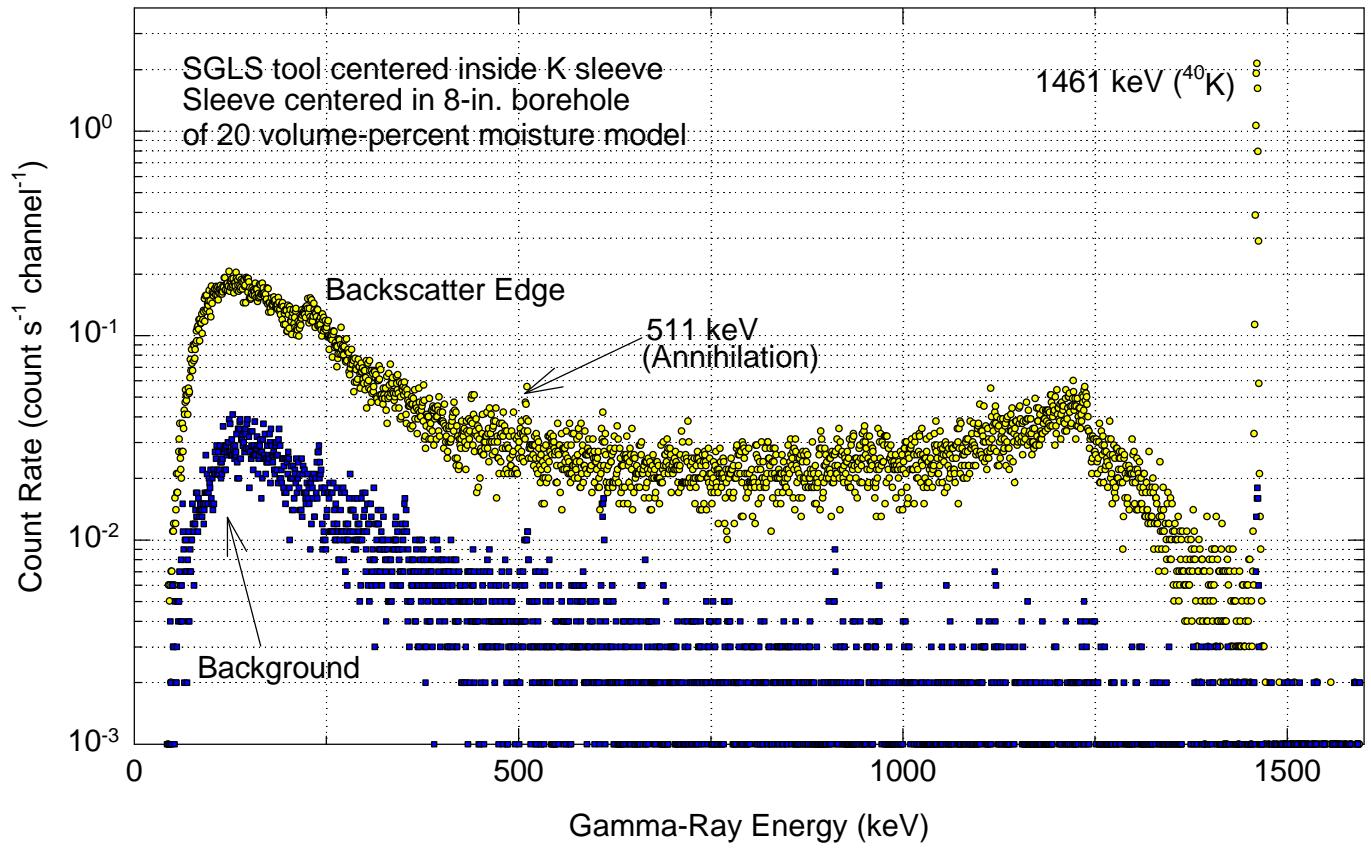


Figure 19. SGLS Spectra Measured Within Potassium Sleeve in Moisture Model

energy from ^{40}K in the potassium carbonate is monoenergetic, as with ^{137}Cs , but has a higher value of 1461 keV. The potassium sleeve was constructed for another project (Wilson 1994) and was well characterized in terms of its materials, dimensions, and source geometry and activity. Figure 17 presents a schematic of the potassium sleeve; Figure 18 shows the logging arrangement with the sleeve centered in the 8-in.-diameter borehole of the moisture model. Figure 19 presents one of the spectra measured with the SGLS tool centered at the midplane of the sleeve.

The 20-volume-percent equivalent moisture model used for the measurements provides significant shielding against the background gammas and a scattering material similar to actual formation sediments encountered in the field. A separate background measurement made with the sleeve removed is shown on Figure 19. This is not exactly the correct geometry for the background measurement because the effect of the sleeve on the background is absent, but the background is relatively small compared to the ^{40}K signal and believed to be an adequate measure of the background contribution to the sleeve spectra. Spectra were also collected with the tool ecentered inside the sleeve and with the tool in several positions above and below the sleeve midplane. Counts were summed in various energy windows and were divided by the measurement live time to give count rates. Before the comparison to simulated count rates, data were corrected for the background contribution. The net count in the 1461-keV photopeak was determined by the peak search option of the Aptec PCMCA/WIN spectrum analysis software, which is available from Aptec Engineering Ltd.

Table 2 presents the count rates for the tool at the sleeve midplane, both centered and ecentered, and with the sleeve removed. The count rates above and below the midplane of the sleeve are within 1 percent of the midplane results, indicating that the sleeve is of sufficient length to represent a potassium source of infinite axial extent. A comparison of count rates for the centralized and ecentered tool positions shows that ecentered count rates are about 2 percent greater, except for the lowest energy window from 60 to 350 keV, where count rates are nearly the same. The effect of tool position would be larger if the difference between sleeve and tool diameters was greater (Wilson and Conaway 1993).

Table 2. Potassium Sleeve Spectral Window Count Rates for the SGLS Tool

| Tool Position | Counts per Second | | | | |
|-----------------------------|-------------------|----------------|-----------------|------------------|-----------------|
| | 60 to 350 keV | 350 to 650 keV | 650 to 1225 keV | 1225 to 1340 keV | 1461-keV Peak |
| Centralized at Midplane | 46.91 | 13.19 | 21.53 | 4.09 (±1%) | 8.43 (±1%) |
| Ecentered at Midplane | 46.88 | 13.4 | 22.11 | 4.13 | 8.64 |
| Background (sleeve removed) | 7.366 (±1%) | 1.836 (±2%) | 1.245 (±3%) | 0.139 (±8%) | 0.035 (±28%) |

For the low-energy window from 60 to 350 keV, the background is 16 percent of the sleeve count rate. For the other windows, the background is a smaller percentage. At the peak energy of

1461 keV, the background is quite small at 0.4 percent. For entries without a percentage in parentheses, the count rate is precise to better than 1 percent.

The MCNP Monte Carlo code (Briesmeister 1993) is used to model the response of the SGLS tool to contaminant distributions surrounding the Tanks Farms monitoring wells. The geometry, materials, and source used in the MCNP model were modified to simulate the SGLS response to the potassium sleeve when placed inside the 8-in.-diameter cased borehole of the 20-percent moisture model. Because the detector used for these benchmark experiments is about 23 percent longer than those used for Tank Farms logging, detector dimensions were changed accordingly in the simulation model. The main effect of this longer length is that the detector is more sensitive to gammas than the field tools, but the difference in length did not greatly affect the shape factors. Simulations performed with a new computer platform using a Pentium Pro 200 processor produced results that were much more precise than earlier SGLS simulations on a slower computer. As a consequence of this improved simulation accuracy, the inaccuracy of a physics assumption of earlier models was discovered. That assumption, the neglect of bremsstrahlung production in the Monte Carlo tracking of the gamma rays, introduced an approximate 10-percent error in simulated spectra for the relatively high 1461-keV source gamma energy from ^{40}K . This effect was not observed in earlier tests conducted for the bremsstrahlung effect on ^{40}K spectra for distributed formation sources because of inadequate simulation precision by the slower computer platform. The effect of bremsstrahlung is not expected to be as great for lower energy spectra, such as those from ^{137}Cs sources. All simulations reported in these benchmark comparisons include the effect of bremsstrahlung production.

Table 3 presents the simulated count rates for the centralized SGLS tool at the midplane of the sleeve and the background-corrected measured count rates from Table 1. Figure 20 presents a comparison of the simulated and background-corrected measured spectra. The ^{40}K activity of the potassium sleeve was computed from published nuclear decay and isotope abundance data (Browne and Firestone 1986) and from the measured mass of the potassium carbonate loaded into the sleeve. This activity was multiplied by the simulated count rates, given per unit source strength, to produce the simulated count rates in Table 3. The ratio of simulated-to-measured count rate shows a systematic trend toward increasing values with increasing energy, ranging from 0.87 at the low energy window to 1.16 for the full-energy peak response. Figure 20 illustrates these differences in spectral shape between the simulation and the experiment. The overall agreement is considered to be quite good. The large drop in experimental response below about 60 keV is due to the electronic discriminator setting and does not appear in the simulations.

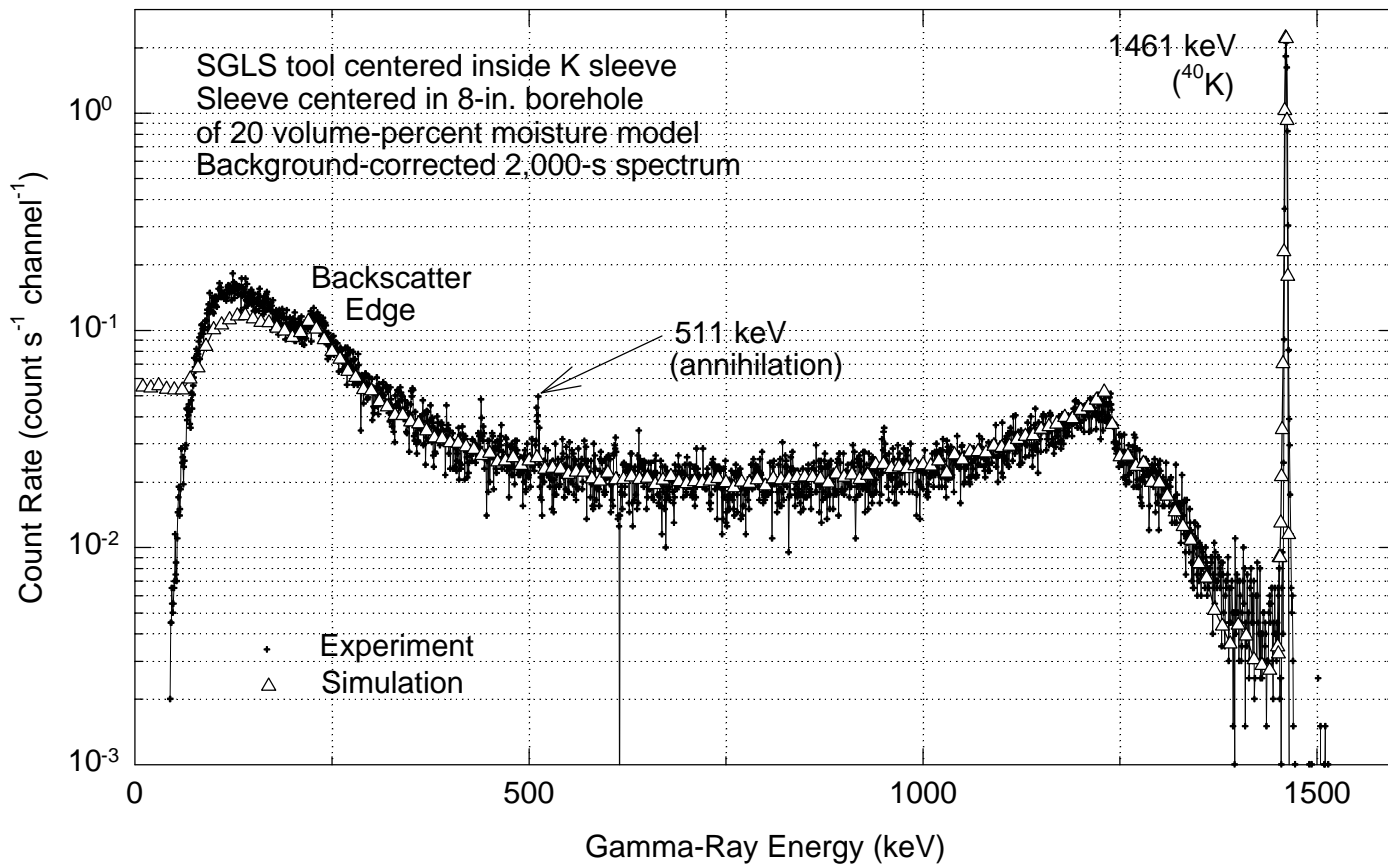


Figure 20. Comparison of Simulated and Measured Potassium Sleeve Spectra

Table 3. Comparison of Simulated and Measured Potassium Sleeve Response

| | Counts per Second | | | | |
|---------------------------------|-------------------|----------------|-----------------|------------------|---------------|
| | 60 to 350 keV | 350 to 650 keV | 650 to 1225 keV | 1225 to 1340 keV | 1461-keV Peak |
| Simulated by MCNP | 34.3 | 11.1 | 20.7 | 4.25 | 9.76 |
| Experiment (net c/s) | 39.54 | 11.35 | 20.29 | 3.95 | 8.40 |
| Ratio (simulated to experiment) | 0.87 | 0.98 | 1.02 | 1.08 | 1.16 |

If shape factors SF1, SF2, and SF3 are defined for the ^{40}K gamma ray in analogy to those introduced in Wilson (1997) for ^{137}Cs , the results are

| | Simulation | Experiment | Ratio (simulation to experiment) |
|--------------------------------------|------------|------------|----------------------------------|
| SF1 (60 to 1340 keV)/1461 keV | 7.18 | 8.94 | 0.80 |
| SF2 (60 to 350 keV)/(350 to 650 keV) | 3.09 | 3.48 | 0.89 |
| SF3 (1225 to 1340 keV)/1461 keV | 0.43 | 0.47 | 0.91 |

These shape factors are similar to those defined for ^{137}Cs but with the continuum energy extended to just below the source energy of 1461 keV. In this comparison, the simulation model underestimates SF1 by 20 percent and SF2 by 11 percent. The simulated high-energy shape factor SF3 is also low by about 9 percent. Part of the problem with these SF1 and SF2 values seems to be the count rate in the lowest energy window. Because this window extends to a low energy of 60 keV (see Figure 20), the imperfect modeling of materials near the detector could be responsible for the disagreement. Another possible explanation is a flaw in the way the code models the low-energy portion of pulse height spectra for gamma detectors. The 16-percent overestimate in the 1461-keV peak count rate by the simulation model is not understood.

This potassium sleeve benchmark comparison represents a test of our ability to simulate thin annular sources on the inside of the borehole casing. An error of a few percent is possible in the source normalization process, based on the quantity of potassium carbonate in the sleeve. Therefore, the differences in absolute count rates of this magnitude probably do not indicate a shortcoming in the simulation model. However, the disagreement in spectral shape is a model deficiency for this particular source geometry. For this experiment, the conclusion is that simulated shape factors for annular gamma sources inside the borehole casing will be too small by about 20 percent. The only documented occurrences of contaminant inside the borehole are at the bottom of the well. However, no attempt is made to interpret spectral shapes at the bottom of the borehole because of the nonstandard source and casing geometry. As benchmark comparisons in Section 3.2 will show, there appears to be a similar but lesser model deficiency for the more consequential case of contaminant on the outer surface of the casing.

The simulation model contains many simplifications to the actual logging tool. Although the tool can, in principle, be modeled in great detail, this modeling can be a time-consuming process in practice. For this reason, and because certain design features are not well-specified by existing drawings or by the manufacturer, simplifications were made. Many calculations were done to determine the sensitivity of the measurements of interest to variations in certain simplified design features. This sensitivity study suggests that the simplifications in the simulation model have not contributed significantly to the observed differences with experimental data. The design parameter that has the greatest effect on tool response is the size of the HPGe detector. Changes in detector length, for instance, have the effect of changing count rates nearly uniformly for all energies without changing the spectral shape. Therefore, if the detector length used in the simulations is incorrect, then the simulated count rates would change but spectral shape factors would remain about the same, though this conclusion is somewhat dependent on the angular distribution of the incident gamma rays.

3.2 ¹³⁷Cs Point Source in Sand Experiment

Experiments to investigate spectral shapes for point sources in a sand medium were conducted in summer 1996 by a consultant to the former WHC geophysics group. Some guidance was provided by the author of this report in planning these measurements. The experiments are described in an informal report (Randall 1996). Additional measurements were performed in late 1996 by Mr. Meisner of Waste Management Federal Services, under my direction, and in early 1997 by Mr. Meisner and Dr. David Stromswold of Pacific Northwest National Laboratory. These measurements have proved useful in the effort to verify the SGLS tool simulation models and have added to the understanding of the SGLS tool response to gamma rays.

A barrel 4.5 ft in diameter and 3.5 ft high was filled with ordinary masonry sand. The measured bulk density of the moist sand was 1.74 grams per cubic centimeter (g/cm^3) and the water content was 5 volume-percent. The composition of the sand is unknown, but the simulations assume pure silica. A 6.62-in. outside diameter, 0.28-in.-thick steel casing passes through the center of the sand barrel and several polyvinylchloride (PVC) tubes are imbedded in the sand in a spiral array, parallel to the casing and at varying radial distances from the casing. The HPGe detector of an SGLS sonde was centered in the casing and spectra were measured for point sources located in each of the PVC tubes. These spectra were compared to simulations performed for each measurement geometry.

Figure 21 presents a schematic of the sand tank showing the casing and measurement tubes. The simulation model included the spiral array of PVC tubes but assumed the walls of the tubes and the source holder were of such low mass that they could be omitted. Therefore, the tubes were modeled as axial voids of 1.5-in. diameter at radial distances of 0, 1, 2, 3, 4, 5, 7, 12 and 17 in. from the wall of the casing. The tubes were located at the azimuthal positions shown on Figure 21. All dimensions are from drawings provided by WHC. The source was modeled as a point isotropic ¹³⁷Cs source at the center of each tube in the detector's midplane. The sand was presumed dry with a bulk density of 1.7 g/cm^3 (the moisture and density measurements were not available until after the simulations were completed).

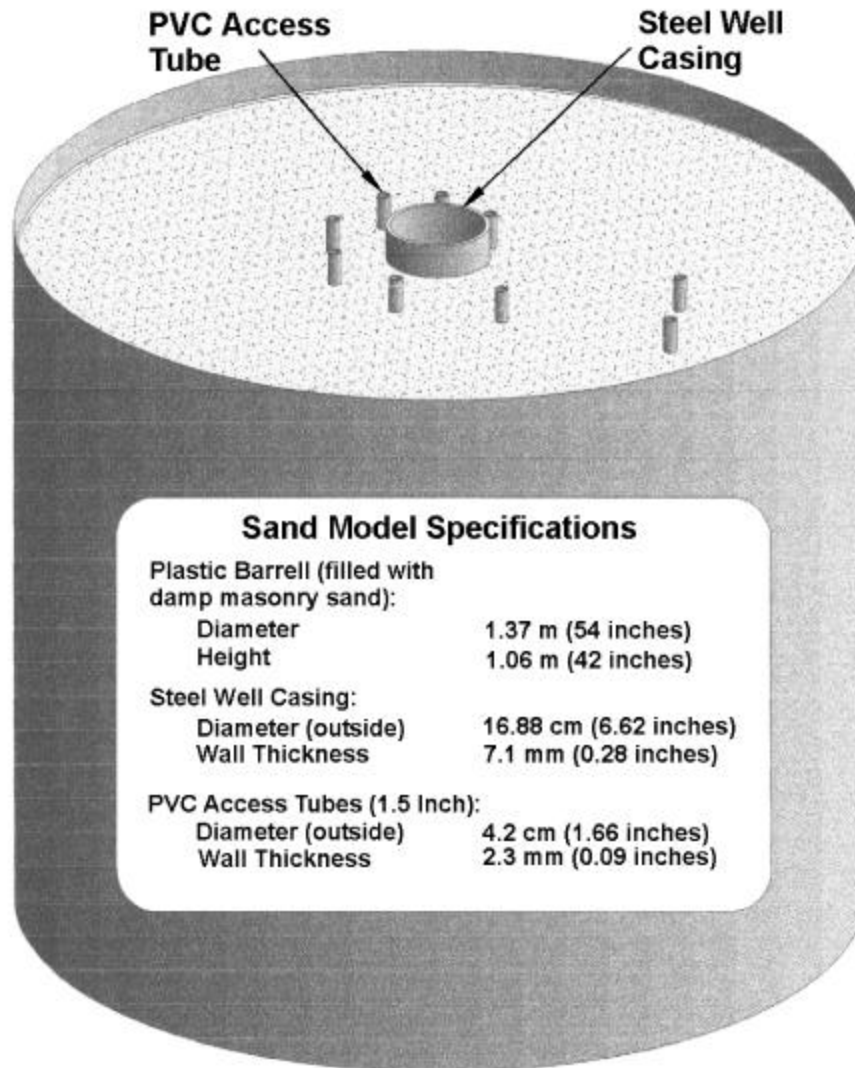


Figure 21. Sand Tank For Point-Source Spectrum Measurements

The small density and moisture differences between the physical and simulation models are not believed to be significant. Count rates measured by Randall (1996) were summed in the several energy windows used for the ¹³⁷Cs shape factor calculations and are tabulated in Table 4 for the several radial source locations and for the background.

Table 4. SGLS Tool Response to Point Sources of ¹³⁷Cs in a Sand Matrix, 4.6-F Ci Source Strength (Randall data of September 1996)

| Radial Source Position (in.) | Counts per Second | | | |
|------------------------------|-------------------|----------------|----------------|---------|
| | 60 to 350 keV | 350 to 650 keV | 610 to 655 keV | 662 keV |
| 0 | 2514 | 971.5 | 62.5 | 549.2 |
| 1 | 1905 | 701.4 | 46.9 | 333.7 |
| 2 | 1237 | 417.5 | 29.5 | 161.4 |
| 3 | 793.8 | 248.9 | 18.4 | 79.09 |
| 4 | 536.3 | 157.8 | 10.5 | 39.28 |
| 5 | 386 | 108.5 | 8.53 | 22.02 |
| 7 | 240.1 | 64.28 | 5.13 | 7.77 |
| 12 (4.3 mCi) ^a | 14305 | 3876 | 249 | 373.9 |
| 17 (4.3 mCi) | 2820 | 637.4 | 41.8 | 47.7 |
| Background | 99.02 | 26.25 | 2.49 | — |

^amCi = millicuries.

The data are corrected for dead time. Because the count rates are sufficiently low, there are no spectral distortions from pulse pileup, except possibly for data taken in the tube in the 12-in. radial source position with a 4.3-mCi source where dead time was 27 percent. Table 5 presents processed data from Table 4 that includes computed shape factors; the shape factors are defined in Wilson (1997). Data at the 12- and 17-in.-radius positions are for a 4.3-mCi source strength. Later experiments conducted by Mr. Meisner verified data acquired by Mr. Randall and, using a third source with a strength of 10.3 microcuries (μCi), provided overlap between the Randall data taken with the weak 4.6-μCi source from 0 to 7 in. and the strong 4.3-mCi source at 12 in. and 17 in. The overlap data are presented in Table 6. Data at 12- and 17-in.-radius positions were normalized to the data at closer positions to give an equivalent 4.6-μCi data set for the full range of positions from 0 to 17 in. Table 7 presents these normalized data results.

Table 5. Processed ¹³⁷Cs Point Source in Sand Measurements, 4.6-F Ci Source Strength (Randall data of September 1996)

| Radial Source Position (in.) | Net Counts per Second | | | 662-keV Peak (c/s) | SF1 Value | SF2 Value | SF3 Value |
|------------------------------|-----------------------|----------------|----------------|--------------------|-----------|-----------|-----------|
| | 60 to 350 keV | 350 to 650 keV | 610 to 655 keV | | | | |
| 0 | 2,415 | 945.3 | 60.0 | 549 | 6.12 | 2.55 | 0.109 |
| 1 | 1,806 | 675.2 | 44.4 | 334 | 7.43 | 2.67 | 0.131 |
| 2 | 1,138 | 391.3 | 27.0 | 161 | 9.47 | 2.91 | 0.168 |
| 3 | 694.8 | 222.6 | 15.9 | 79.1 | 11.6 | 3.12 | 0.201 |
| 4 | 437.3 | 131.6 | 8.0 | 39.3 | 14.5 | 3.32 | 0.204 |
| 5 | 287.0 | 82.25 | 6.04 | 22.0 | 16.8 | 3.49 | 0.274 |
| 7 | 141.1 | 38.03 | 2.64 | 7.77 | 24.1 | 3.74 | 0.340 |
| 12 ^a | 14,206 | 3,850 | 246 | 374 | 48.3 | 3.67 | 0.668 |
| 17 ^a | 2,721 | 611.1 | 39.3 | 47.7 | 69.8 | 4.45 | 0.824 |

^aData for a 4.3-mCi source strength.

Table 6. ¹³⁷Cs Point Source in Sand Measurements Taken by Mr. Meisner With a 10.3-F Ci Source To Provide Overlap of Randall Data

| Radial Source Position (in.) | Net Counts per Second | | | | SF1 | SF2 | SF3 |
|------------------------------|-----------------------|----------------|----------------|---------|------|------|------|
| | 60 to 350 keV | 350 to 650 keV | 610 to 655 keV | 662 keV | | | |
| 7 | 388.8 | 104.2 | 5.28 | 20.4 | 24.2 | 3.73 | 0.26 |
| 12 | 69.2 | 16.6 | 0.57 | 2.14 | 40.1 | 4.17 | 0.27 |

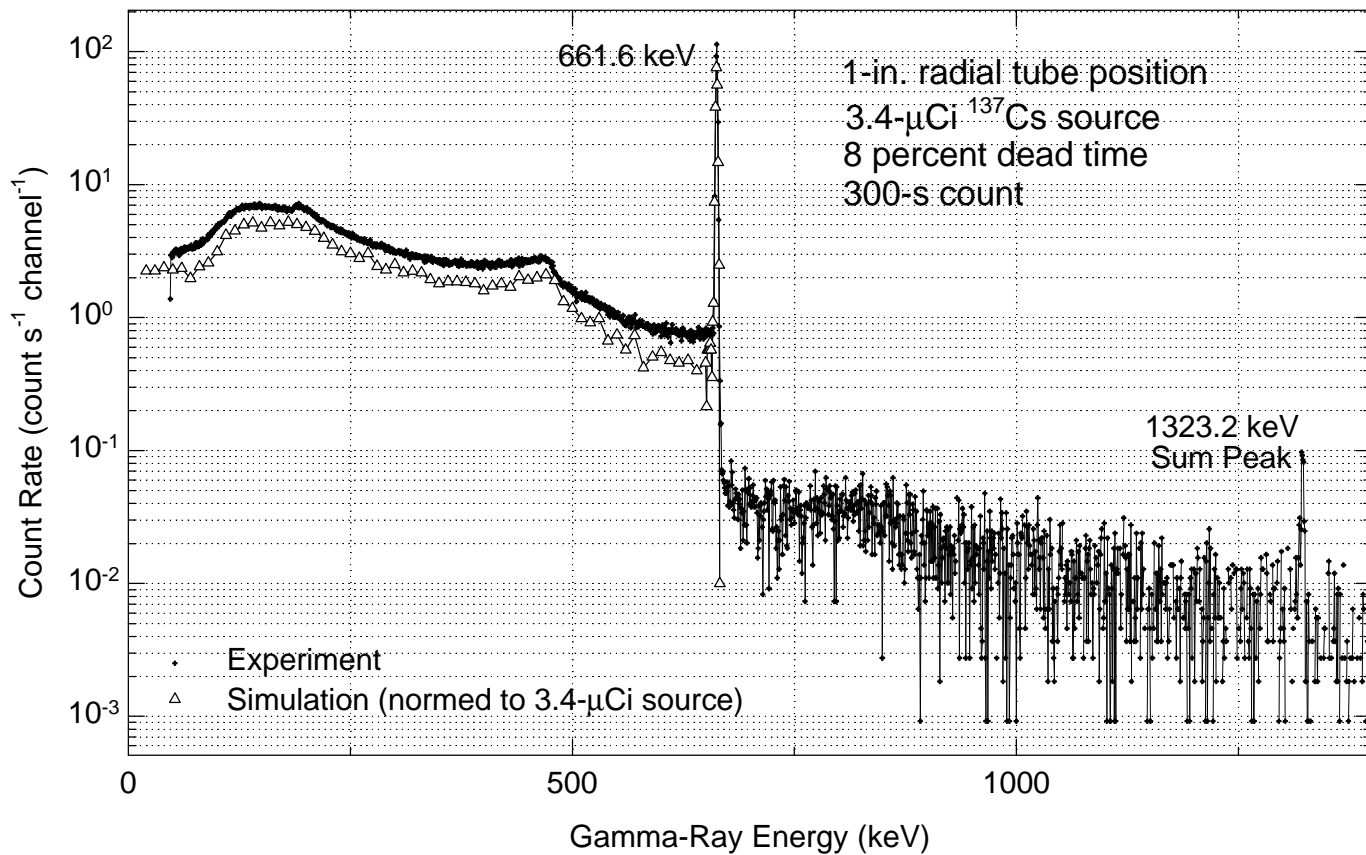


Figure 22. Measured and Simulated Spectra for 1-in. Tube Position

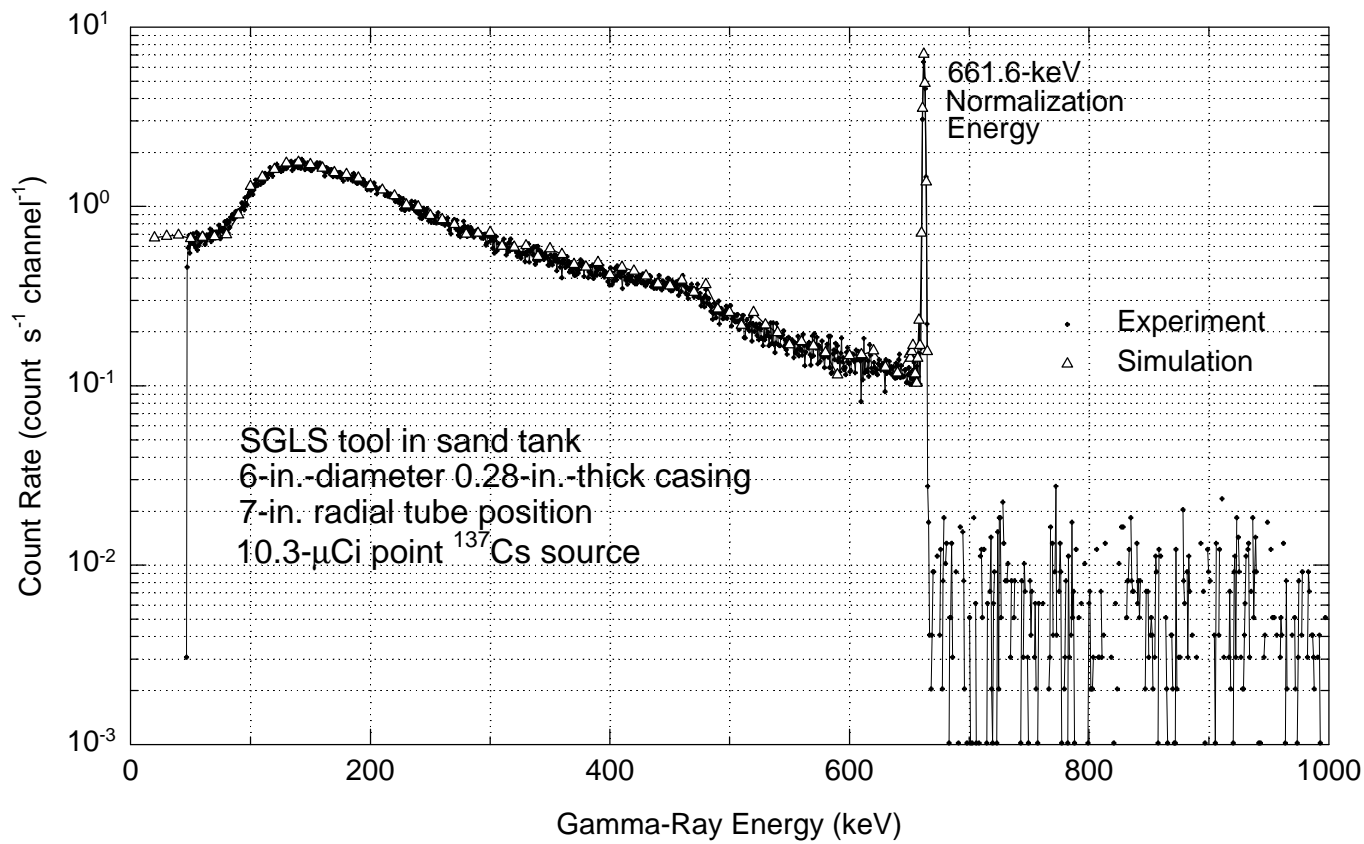


Figure 23. Measured and Simulated Spectra for 7-in. Tube Position

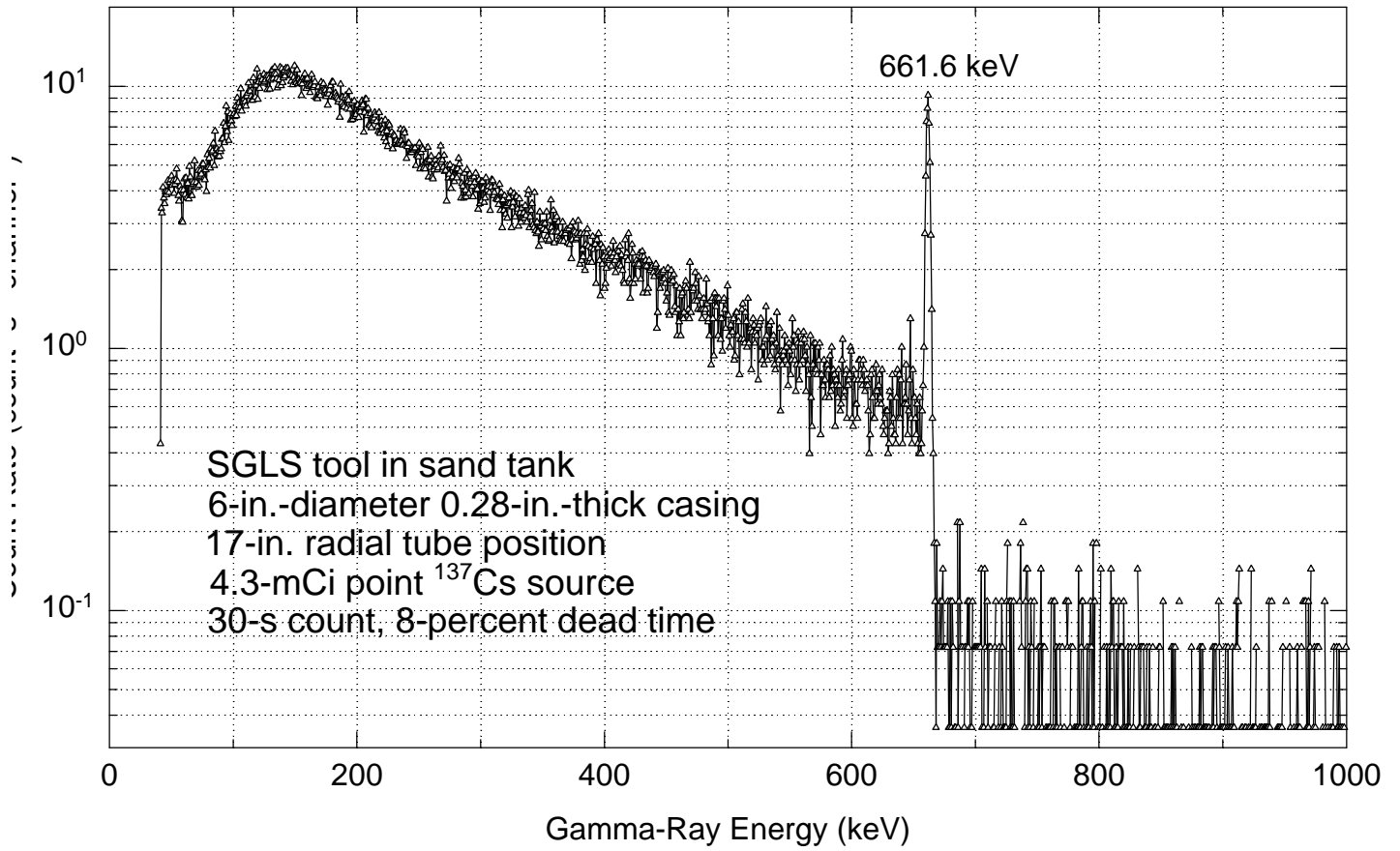


Figure 24. Measured Spectrum for Point Source in 17-in. Tube Position

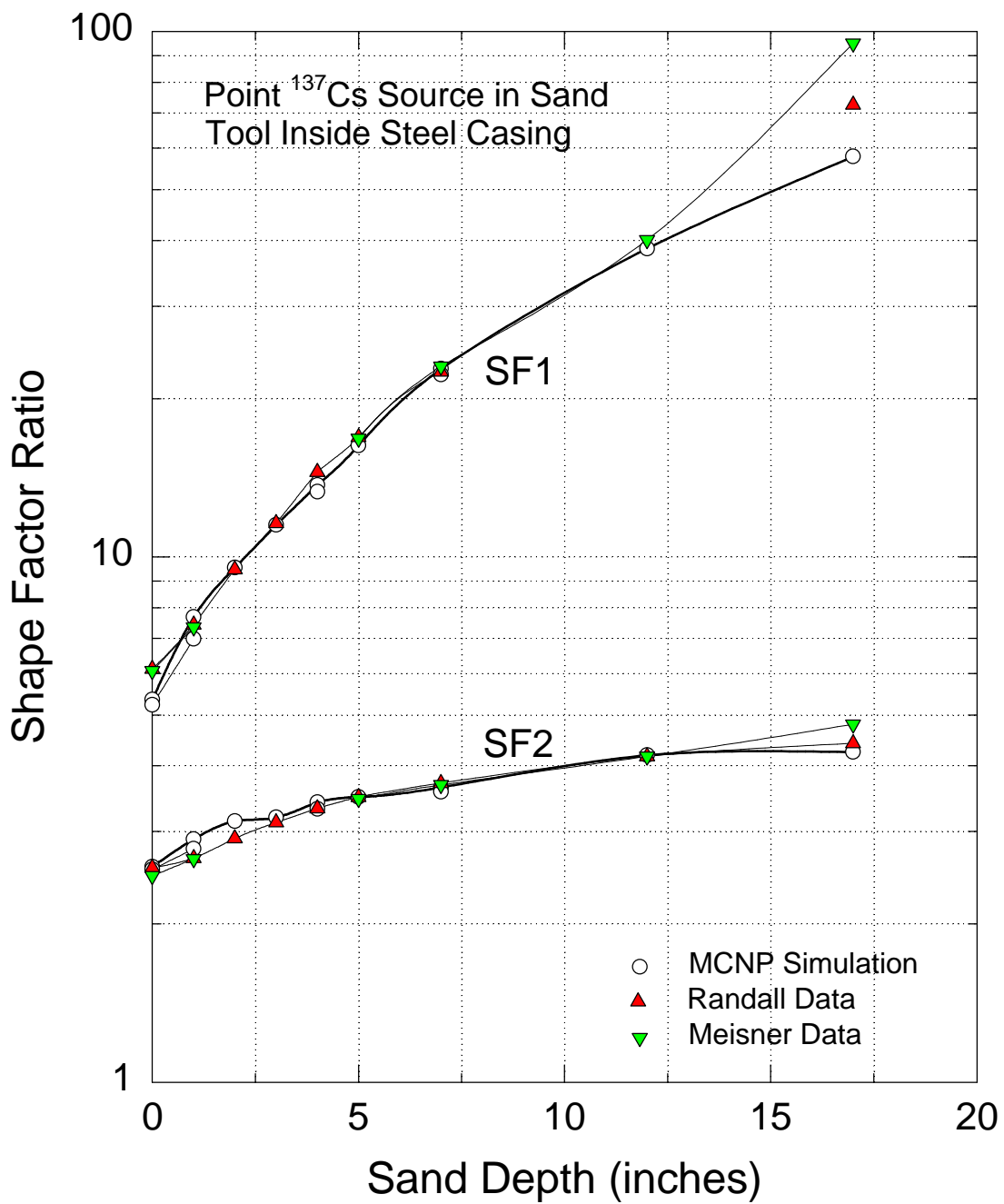


Figure 25. Measured and Simulated SF1 and SF2 Dependence on Radial Source Position

Table 7. Complete Set of ¹³⁷Cs Point Source Data Normalized to 4.6-F Ci Source

| Radial Source Position (in.) | Net Counts per Second | | | 662 keV Peak (c/s) | SF1 | SF2 | SF3 |
|------------------------------|-----------------------|-------------------|-------------------|--------------------|-------------------|-------------------|-------------------|
| | 60 to 350 keV | 350 to 650 keV | 610 to 655 keV | | | | |
| 0 | 2,415 | 945.3 | 60.0 | 549 | 6.12 | 2.55 | 0.109 |
| 1 | 1,806 | 675.2 | 44.4 | 334 | 7.43 | 2.67 | 0.131 |
| 2 | 1,138 | 391.3 | 27.0 | 161 | 9.47 | 2.91 | 0.168 |
| 3 | 694.8 | 222.6 | 15.9 | 79.1 | 11.6 | 3.12 | 0.201 |
| 4 | 437.3 | 131.6 | 8.0 | 39.3 | 14.5 | 3.32 | 0.204 |
| 5 | 287.0 | 82.25 | 6.04 | 22.0 | 16.8 | 3.49 | 0.274 |
| 7 | 141.1 | 38.03 | 2.64 | 7.77 | 24.1 | 3.74 | 0.340 |
| 12 | 26.4 ^a | 6.32 ^a | 0.22 ^a | 0.815 ^a | 40.1 ^a | 4.17 ^a | 0.27 ^a |
| | 30.96 ^b | 8.39 ^b | 0.54 ^b | 0.815 ^b | 48.3 ^b | 3.67 ^b | 0.67 ^b |
| 17 | 5.93 | 1.33 | 0.086 | 0.104 | 69.8 | 4.45 | 0.824 |

^aData acquired with 10.3-F Ci source.

^bData acquired with 4.3-mCi source.

Table 7 presents two sets of shape factor results at the 12-in. position. The first set was taken with the 10.3- μ Ci source and suffers from relatively poor counting statistics. The second set is for the 4.3-mCi source where the dead time was 27 percent. The value of SF3 from the second set is the better result, while the values of SF1 and SF2 from the first set are better because there are adequate counts and no possibility of dead-time distortion.

As with the potassium experiment, a special MCNP simulation model was created for comparison with the sand tank data. Figures 22 and 23 present examples of simulated spectra and comparisons with measured spectra. These spectra correspond to the 1-in. and 7-in. radial thicknesses of sand between the source and the detectors. Because the simulated spectrum for the 1-in. tube position is normalized to the source strength, the comparison is absolute. The simulated spectrum for the 7-in. tube position is normalized to the measured data at the 662-keV peak channel; therefore, the comparison is relative. The simulated spectral shapes are in excellent agreement with experiment data for these source positions. The simulated spectrum at the 1-in. tube position on Figure 22 is lower in magnitude than the experiment spectrum, indicating the source strength is probably inaccurate.

Figure 24 presents the measured spectrum for the 17-in. thickness of sand. The simulations for this position had poor statistical precision and are not shown. Figure 25 shows a plot that compares measured and simulated shape factors SF1 and SF2 as a function of source depth in the sand. The agreement is excellent except at the 17-in. position and at the closest position, against the casing wall. (Note: The simulations were mistakenly done for a detector that is 23 percent shorter than the one used

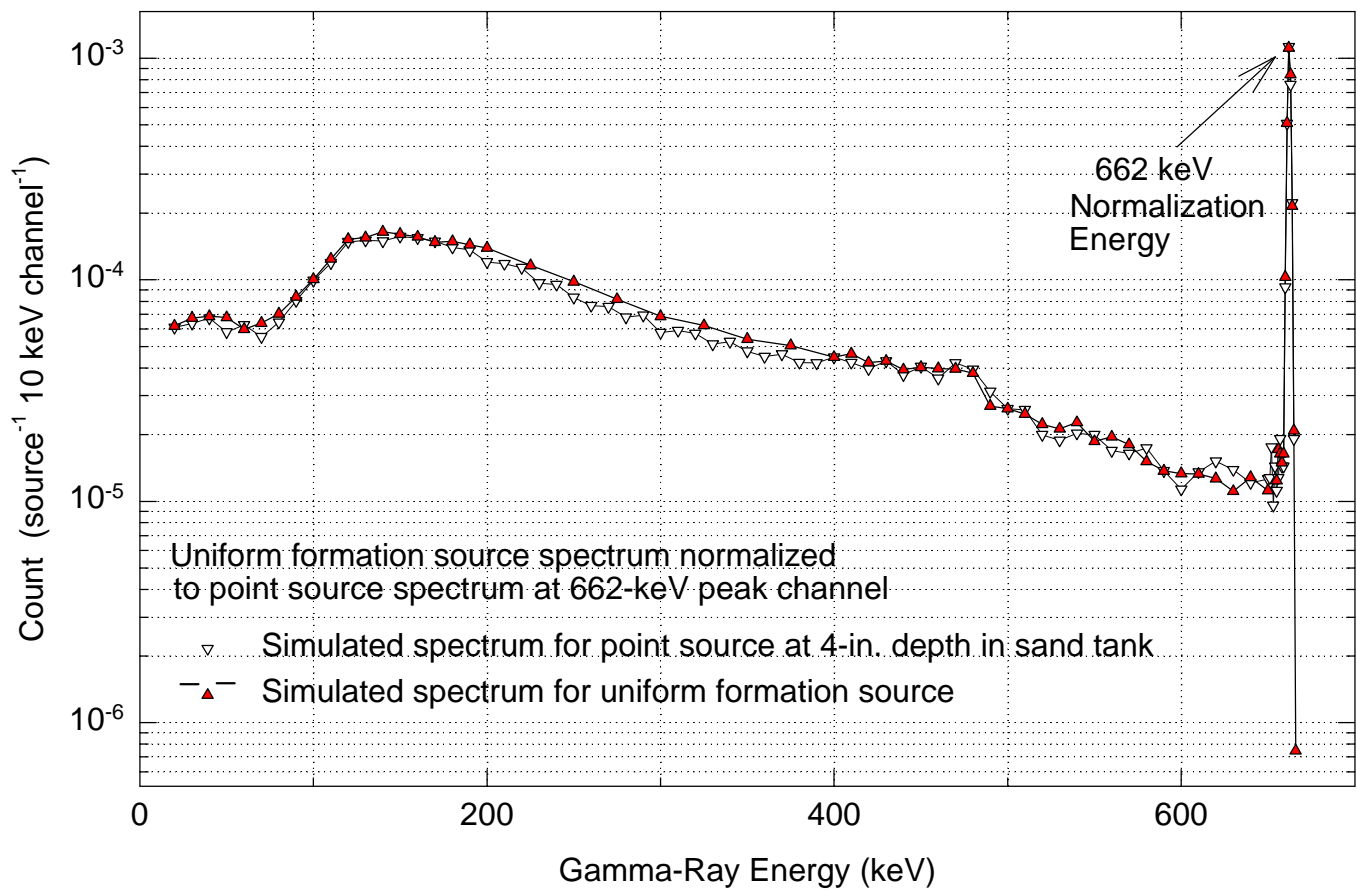


Figure 26. Simulated Spectra at 4-in. Tube Position and for Uniformly Distributed ¹³⁷Cs Contamination

in the sand tank measurements. Certain of the simulations were repeated with the correct length and little effect was observed on the shape factors.) Table 8 presents numerical results for the measured and simulated shape factors.

Table 8. Comparison of Simulated and Measured Shape Factors for a ¹³⁷Cs Point Source at Various Radial Positions in a Sand Matrix With Cased Borehole ^a

| Radial Source Position (in.) | SF1 (60 to 650/662) | | | SF2 (60 to 350/350 to 650) | | | SF3 (610 to 655/662) | | |
|------------------------------|----------------------|-------|-------|-----------------------------|-------|-------|----------------------|-------|-------|
| | Sim. | Expt. | Ratio | Sim. | Expt. | Ratio | Sim. | Expt. | Ratio |
| 0 | 5.48 | 6.12 | 0.89 | 2.59 | 2.55 | 1.02 | 0.077 | 0.109 | 0.71 |
| 1 | 7.32 | 7.43 | 0.98 | 2.81 | 2.67 | 1.05 | 0.103 | 0.133 | 0.78 |
| 2 | 9.54 | 9.47 | 1.01 | 3.14 | 2.91 | 1.08 | 0.145 | 0.168 | 0.86 |
| 3 | 11.5 | 11.6 | 0.99 | 3.19 | 3.12 | 1.02 | 0.19 | 0.201 | 0.94 |
| 4 | 13.7 | 14.5 | 0.945 | 3.41 | 3.32 | 1.03 | 0.223 | 0.204 | 1.09 |
| 5 | 16.3 | 16.8 | 0.97 | 3.49 | 3.49 | 1.00 | 0.261 | 0.274 | 0.95 |
| 7 | 22.8 | 23.0 | 0.99 | 3.64 | 3.71 | 0.98 | 0.352 | 0.340 | 1.03 |
| 7L | 22.8 | 24.1 | 0.95 | 3.64 | 3.74 | 0.97 | 0.352 | 0.365 | 0.96 |
| 12L | 38.6 | 40.1 | 0.96 | 4.19 | 4.17 | 1.00 | 0.585 | 0.27 | 2.17 |
| 12RR | 38.6 | 48.6 | 0.79 | 4.19 | 3.69 | 1.14 | 0.585 | 0.666 | 0.88 |
| 17RR | 57.8 | 69.8 | 0.80 | 4.25 | 4.45 | 0.96 | 0.83 | 0.824 | 0.95 |

^a "L" designates 10.3-FCi source; "RR" designates 4.3-mCi source; remainder of the results are for the 4.6-FCi source.

The comparison shows certain trends in the ratio of simulation-to-experiment with increasing radial position of the source in the sand medium. When the source is against the casing, the simulated SF1 is less than the measured value, the difference being -11 percent. This difference is consistent with a similar difference reported for the potassium sleeve experiment where the source was local to the borehole region. For the non-zero radial positions, simulated SF1 values are in good agreement with the experiment, except for the 17-in. radius where both experiment and simulation suffer from large statistical uncertainties.

Figure 26 presents a comparison of a simulated spectrum for a radial depth of 4 in. to the spectrum simulated for uniformly distributed ¹³⁷Cs contamination. The spectral shapes are similar, as are the computed shape factors. This result shows that for this particular sand medium, and for a ¹³⁷Cs gamma source, a point source placed at the 4-in. depth produces a spectral shape about the same as for a uniformly distributed source. This correspondence could prove useful in later experiments to determine, for example, the effect of dead time on uniformly distributed ¹³⁷Cs spectra. Point sources with varying activity could be placed at the 4-in. position and the spectrum shape could be measured as a function of dead time.

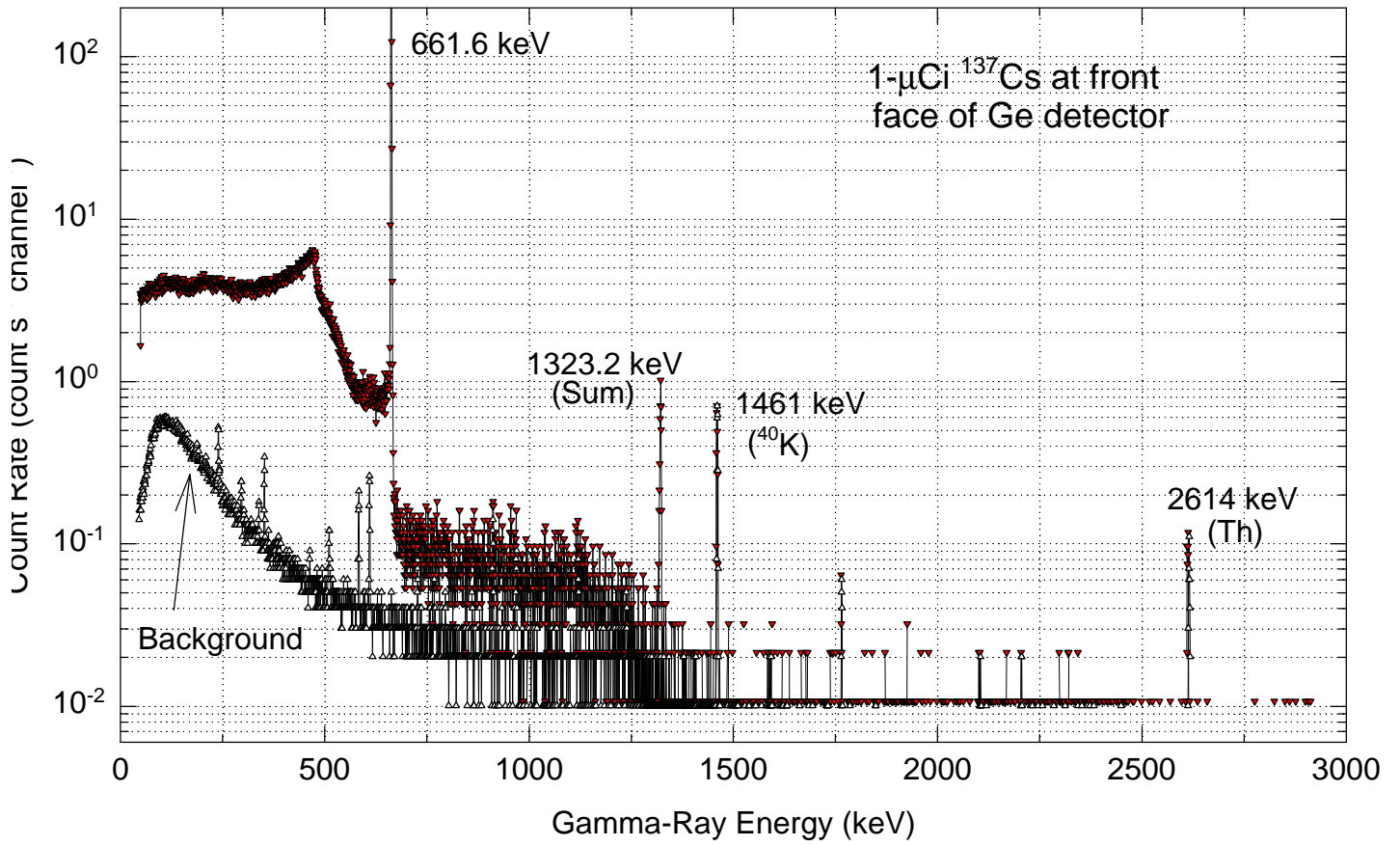


Figure 27. Measured Spectrum for ^{137}Cs Source at Front Face of Detector

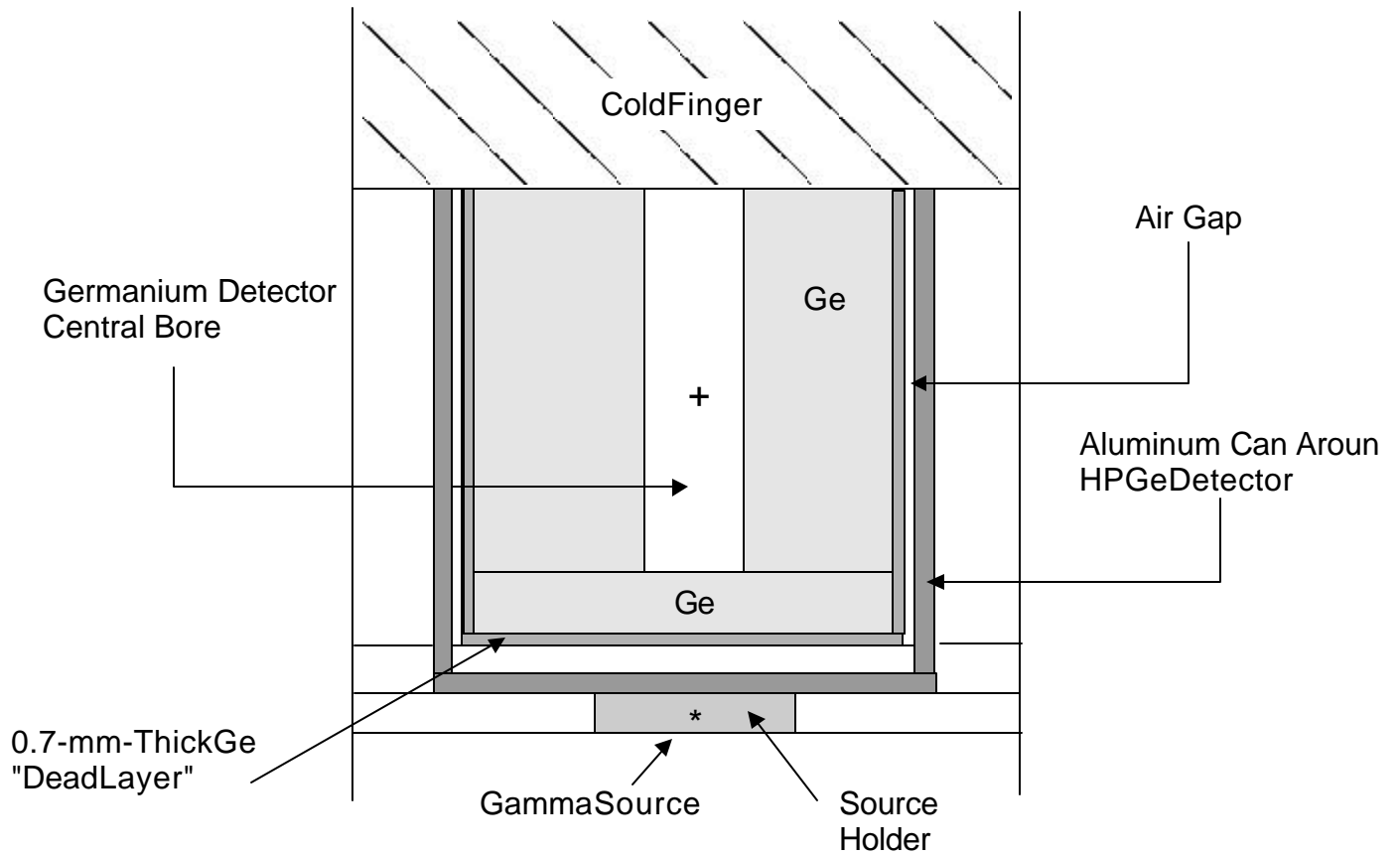
3.3 ¹³⁷Cs Point Source Experiments With Scattering Materials Removed

The SGLS tool housing was removed and the detector assembly was suspended in air to obtain spectra that do not contain scattered gammas from materials external to the detector. This arrangement is a more direct test of the validity of the MCNP code in simulating the germanium detector response to incident gamma rays. A point source of ¹³⁷Cs gammas was placed at various positions from the detector, both along its axis and along a radius in the midplane of the detector. Figure 27 shows the spectrum measured with the 1-μCi source against the front face of an aluminum can surrounding the detector and the measured background spectrum. A similar shape and counting rate were obtained with the source at the detector midplane against the curved surface of the can. This result shows that the detector responds in about the same way for gammas incident from below and from the side of the detector. The background correction is significant only at low energies. Spectra were also measured for distances of 2, 4, and 8 in. from the detector in each direction to determine the effect of increasing the monodirectional character of the gamma flux. For all these distances, the spectral shapes were nearly the same as when the source was against the detector can, indicating little directionality effect. Table 9 presents the count rates in the energy regions used in ¹³⁷Cs shape factor analysis.

Table 9. Measured Count Rates for a ¹³⁷Cs Point Source at Several Axial and Midplane Positions Relative to Detector With Housing Removed and Tool Suspended in Air

| Source Position (in.) | Counts per Second | | |
|-----------------------|-------------------|----------------|------------|
| | 60 to 350 keV | 350 to 650 keV | 662 keV |
| Axial, $z = 0$ | 1,580 | 1,227 | 1,079 |
| Axial, $z = 4$ | 210.2, 207.5 | 99.4, 97.3 | 67.7, 66.0 |
| Midplane, $r = 0$ | 1,508 | 1,178 | 1,049 |
| Midplane, $r = 2$ | 433.5 | 281.0 | 236.4 |
| Midplane, $r = 4$ | 246.8 | 124.6 | 91.3 |
| Background | 127.6 | 25.5 | — |

Table 10 presents shape factors computed from these data, along with shape factors simulated for the $z = 0$ axial source position. To properly simulate these measurements, the MCNP model of the detector and nearby materials had to be modified to more accurately represent the geometry. In particular, air gaps between the germanium detector and the aluminum can were added because they were omitted in the model used for borehole simulations. Also, the center bore inside the germanium was corrected to terminate at the proper distance of about 0.5 in. from the front face of the crystal. The original simulation model had the bore passing completely through the crystal for simplicity. Another addition to the model was the dead layer at the front surface of the detector.



| Materials | Density (g/cm ³) | Composition |
|--------------|------------------------------|------------------|
| SourceHolder | 1.20 | Lucite (H, C, O) |
| AluminumCan | 2.70 | Aluminum |
| HPGe | 5.32 | Germanium |
| ColdFinger | 3.00 | Copper + Iron |

Regions Without Shading or Hatching Are Voids

Figure 28. MCNP Simulation Geometry for Source at Front Face of Detector

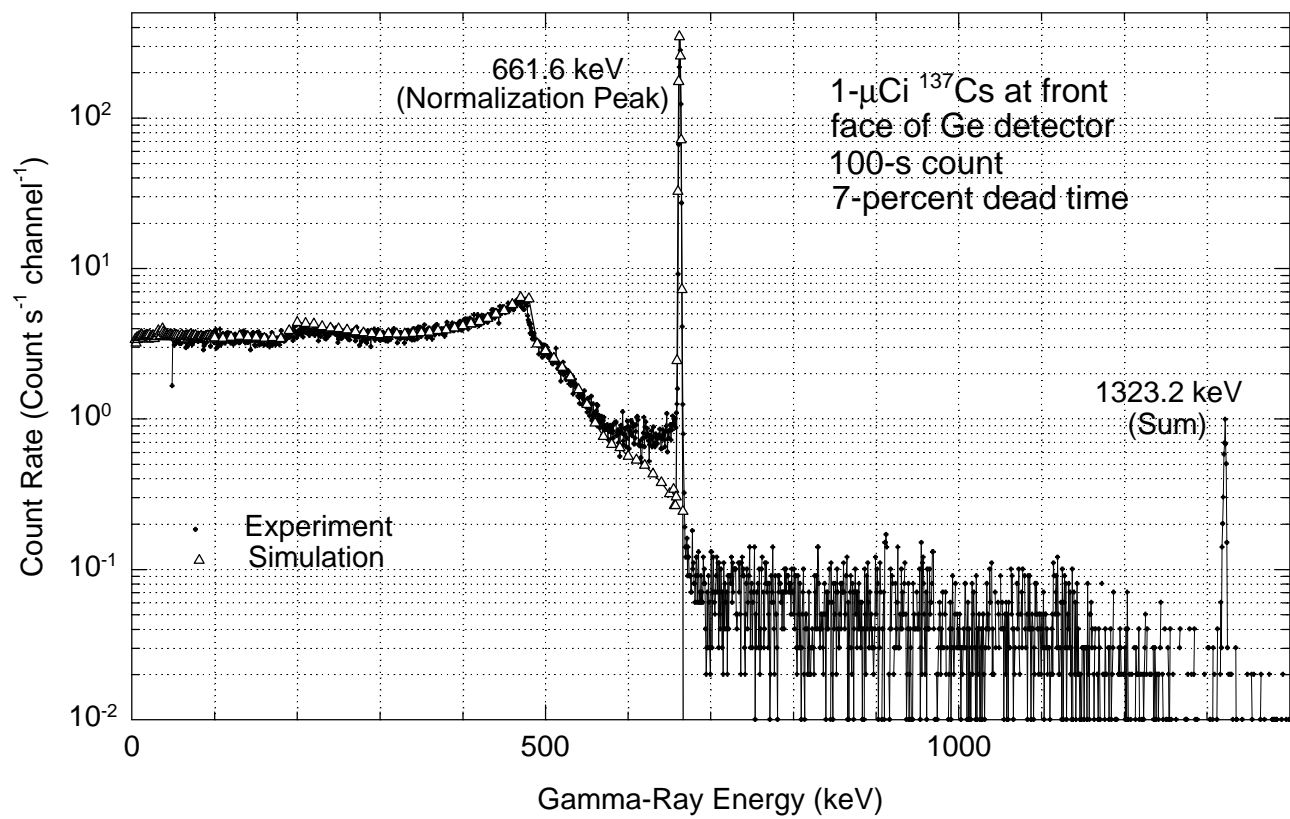


Figure 29. Comparison of Simulated and Measured Spectra for ^{137}Cs Source at Front Face of Detector

Table 10. Comparison of Simulated and Measured Shape Factors for a ^{137}Cs Point Source at Various Radial and Axial Positions From Detector With Tool in Air and Housing Removed

| R or Z (in.) | SF1 (60 to 650/662) | | | SF2 (60 to 350/350 to 650) | | |
|-----------------|----------------------|-------|-------|-----------------------------|-------|-------|
| | Sim. | Expt. | Ratio | Sim. | Expt. | Ratio |
| $r = 0$ | — | 2.41 | — | — | 1.20 | — |
| $r = 2$ | — | 2.37 | — | — | 1.20 | — |
| $r = 4$ | — | 2.39 | — | — | 1.20 | — |
| $z = 0$ | 2.16 | 2.46 | 0.88 | 1.28 | 1.21 | 1.06 |
| $z = 4$ | — | 2.31 | — | — | 1.18 | — |

This dead layer was needed to model the response properly to low energies where the x rays from $^{137\text{m}}\text{Ba}$, the decay product of ^{137}Cs , would otherwise be detected. The plastic holder for the source was added to the model and all housing, borehole, and formation materials were deleted from the model. Figure 28 presents a side view of the refined SGLS detector model.

Although these changes improved the agreement between simulation and experiment values, the simulations tended to underestimate the measured shape factor SF1 for this point-source measurement arrangement with the tool housing removed. This disagreement is apparent from the SF1 ratio (simulated to measured) of 0.88 in Table 10. The only way this discrepancy could be removed was to make an arbitrary reduction in the mass density of the germanium from its theoretical value of 5.32 g/cm^3 to about 5.0 g/cm^3 . This reduction in mass density has an effect similar to a reduction in the diameter of the germanium crystal. Because it is not possible to measure the detector diameter or mass density, the ORTEC data sheet was used for the diameter, which appears to be a nominal value and not one that was actually measured for the detector used in this study. Simulations were conducted only for the source against the front face of the detector. The nominal detector dimensions and the theoretical mass density of 5.32 g/cm^3 were used in the simulation. The SF2 values are in good agreement, with a simulated-to-measured ratio of 1.06. This ratio value indicates that the discrepancy for shape factor SF1 is traceable to a simulated peak intensity that is too high in relation to the scattered continuum.

Figure 29 shows plots of the simulated and measured spectra for this source geometry. The continuum spectral shapes agree well from the lowest measured energy of about 40 to 600 keV. The simulation underestimates the counts from 600 keV to the peak energy of 662 keV. Although not apparent on Figure 29, the simulated peak area is somewhat overestimated, relative to the continuum, and is reflected as a simulated SF1 value that is too small by about 12 percent (see Table 10).

3.4 ^{60}Co Point Source Experiments With Scattering Materials Removed

Spectra were also measured for a ^{60}Co source against the front face of the detector can with the tool housing removed. Figure 6 (presented in Section 2.2), compares the measured and simulated spectra

for this geometry. The simulated and measured shape of the continuum part of the spectrum below the 1173-keV energy of the lower peak agree quite well, although the simulated continuum count rates are lower in relation to the peak intensities. The simulated continuum between the photopeaks is underestimated. The sum spectrum with a peak at 2505 keV and associated continuum are due to the true coincidence effect (Knoll 1987) and not because of the pileup effect that is observed for high count rates from ^{137}Cs (see Figure 29). The true coincidence effect is caused by the random detection of both gammas emitted by a single decay, is dependent on the solid angle between detector and source location, and, therefore, is greatest for the source close to the detector. This effect cannot be simulated by MCNP. The discrepancy between simulation and experiment for the continuum between the photopeaks is likely due to the true coincidence continuum that extends to the smallest energies. Section 2.2, "Comparison of Simulated and Measured Point-Source ^{60}Co Spectra," presents a discussion of the potential effect of the true coincidence effect on shape factor analysis. Additional ^{60}Co measurements are planned in the sand tank using the procedures described for ^{137}Cs .

3.5 Distributed Potassium Source Benchmark Comparisons

Early in the study of spectral shape effects from variations in the gamma source distribution, simulations were conducted of the spectra measured by the SGLS tool in one of the concrete borehole calibration models at the DOE Grand Junction Office facility. These spectra were taken in the uncased borehole of the potassium-enriched model. Spectra were simulated using a MCNP model that includes the published geometry, materials, and bulk densities for this physical model (Leino et al. 1994). Absolute simulated count rates were determined by using the published dry-bulk mass potassium concentrations for the model (Leino et al. 1994) and by computing a normalization factor that multiplies the simulated responses, which are given as counts per gamma ray emitted by the source. The measured potassium spectrum was corrected for uranium and thorium contributions for the several energy windows of interest by using additional measured calibration data (Koizumi 1996). The benchmarking process for the uniform-distribution potassium spectrum is still in progress.

3.6 Summary and Recommendations

The comparison of simulated and measured spectra for the various experiments indicates that the simulated shape factors are quite accurate except for sources located close to the detector and when there is a minimum of scattering material between source and detector. In this situation, simulated values of SF1 tend to be too small. It is estimated from these comparisons that for contaminant on the outer wall of the steel casing, the simulated values of SF1 will be too small by from 10 to 15 percent, while the simulated SF2 values will be accurate for all source conditions. These estimated inaccuracies in the simulations should be kept in mind by analysts as they use simulated trend lines to interpret shape factors from spectra measured by the SGLS in the Tank Farms.

Additional experiments should be performed with the point-source sand model to determine the thin zone response of the SGLS tool to both ^{137}Cs and ^{60}Co concentrations. The true coincidence sum

spectrum from ^{60}Co should be investigated further to determine if it is a significant effect for ^{60}Co shape-factor analysis.

Studies should be conducted to understand the cause of the discrepancy between measured and simulated spectra reported for sources close to the detector and where there is a minimum of scattering material between source and detector.

4.0 Identification of the Bremsstrahlung-Producing Beta-Emitting Contaminant ^{90}Sr

Previous work (Wilson 1997) showed that spectral shape analysis techniques can be used to identify the presence of ^{90}Sr from its bremsstrahlung radiation, even in the presence of gamma-emitting contaminants such as ^{137}Cs . This identification is accomplished with the use of a cross plot of shape factors SF1 and SF2. In Wilson (1997), at least one occurrence of ^{90}Sr in the presence of ^{137}Cs was detected in the processing of logs from the SX Tank Farm. The present study applied the shape factor methods to logging data from a crib in which ^{90}Sr contamination was suspected to exist in the absence of other gamma-emitting contaminants. Measurements were also conducted with a prepared ^{90}Sr source of known activity placed in a sand-filled tank. This study permitted determination of a signature value for SF2 when ^{90}Sr alone is present and verified earlier simulations of the detection limit for ^{90}Sr when logged by the SGLS in steel-cased boreholes.

This study determined that the spectral shape factor SF2 has a value of about 10 when only ^{90}Sr is present. This value is significantly above the values obtained for gamma-emitting contaminants such as ^{137}Cs and ^{60}Co and is the basis for detecting the presence of ^{90}Sr in borehole spectra. The detection limit for ^{90}Sr is about 2,000 pCi/g in the presence of typical gamma background levels. When gamma-emitting contaminants are also present, the detection limit will be higher and will depend on the intensity of the additional contaminants. ^{90}Sr concentrations can be approximately quantified from the background-corrected low-energy count rate using a simulated sensitivity factor, but only if other gamma-emitting contaminants are absent or their presence has been properly compensated. There are likely many other occurrences of ^{90}Sr contamination at the Hanford Site that are suitable for this spectral gamma log analysis method and for which the location and approximate concentration values would be of use.

the much smaller bremsstrahlung signal in this depth range (Figure 32). The SF2 values above 10 ft also suffer from the same statistical problem.

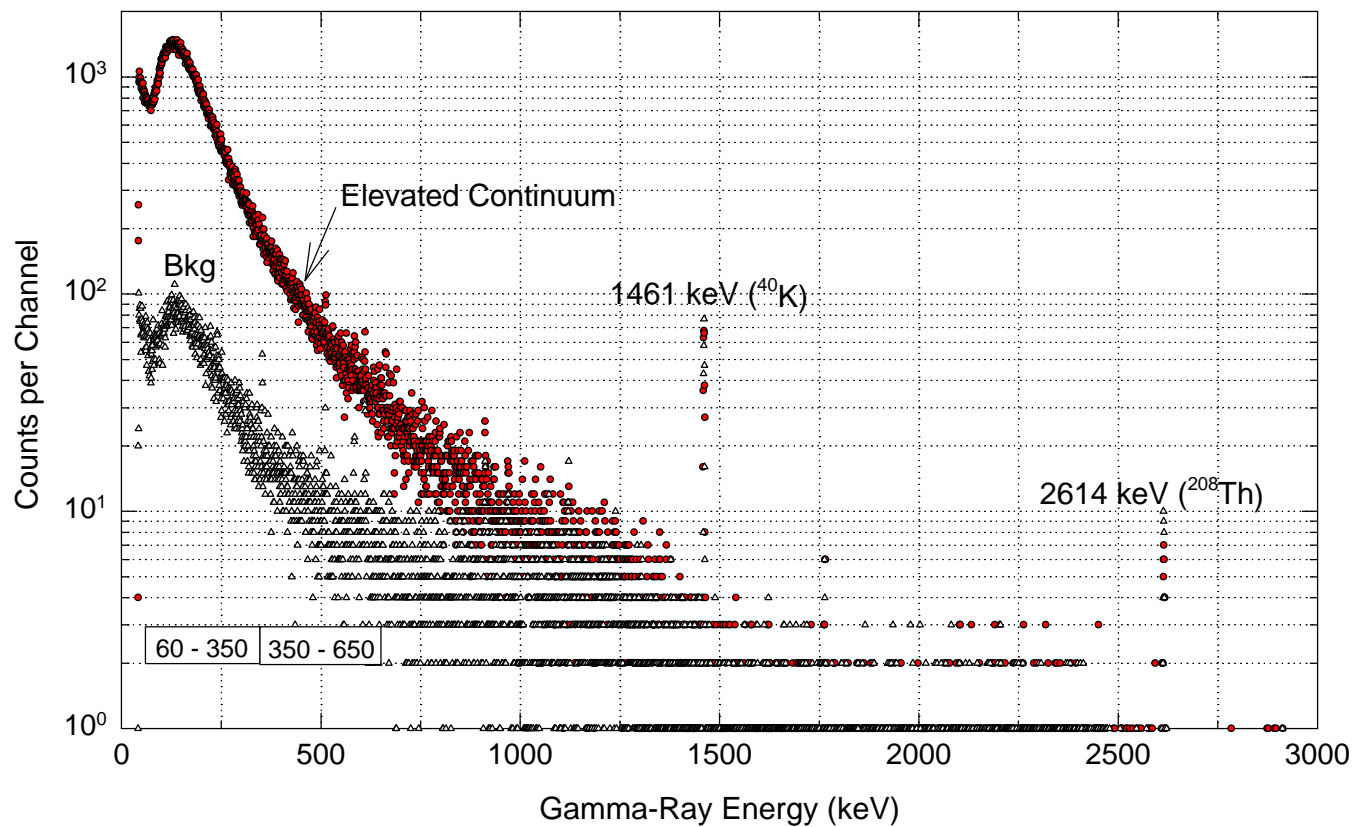


Figure 30. RLS Spectra at the 14.5-ft Depth in Crib Borehole 299-E25-191

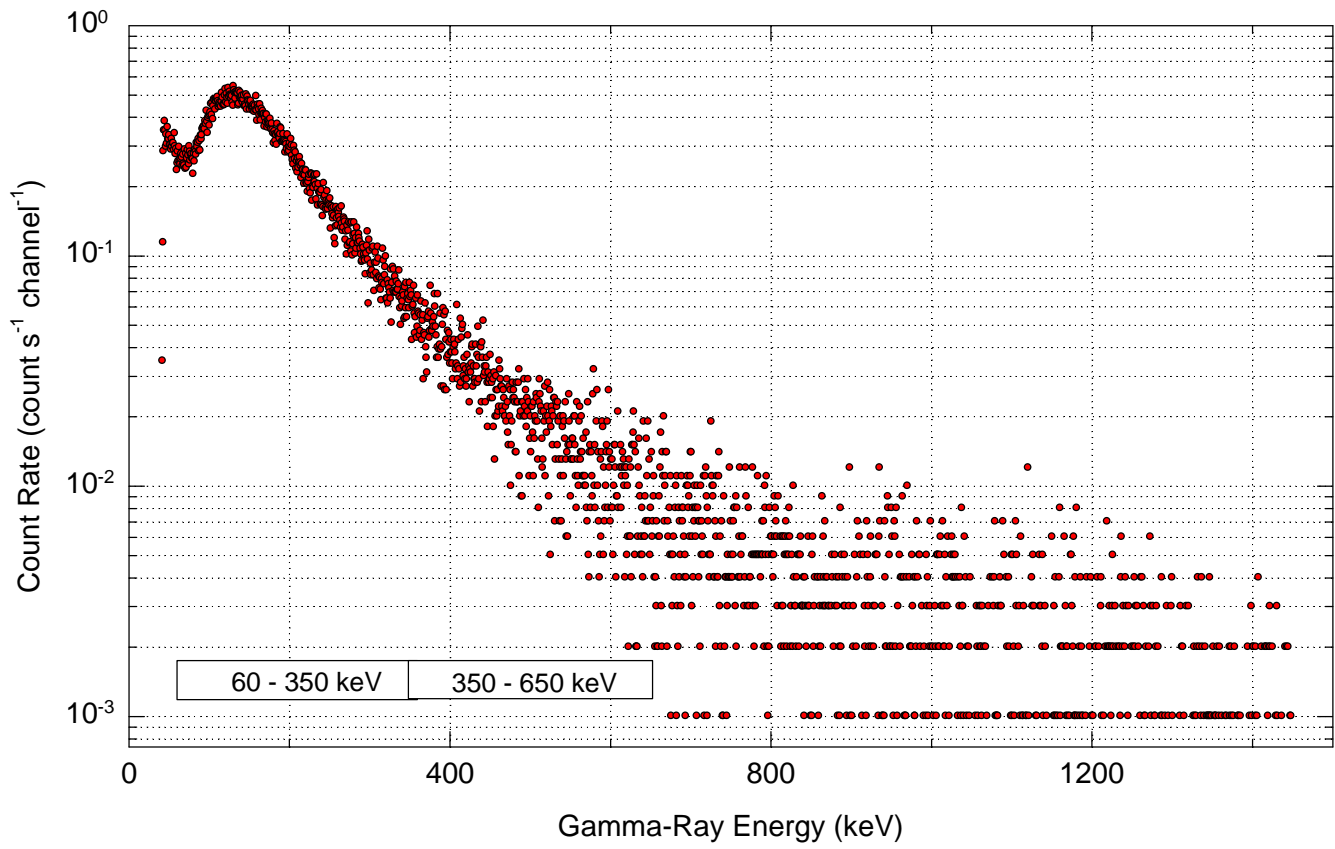


Figure 31. Background-Corrected Spectrum at 14.5 ft in Borehole 299-E25-191

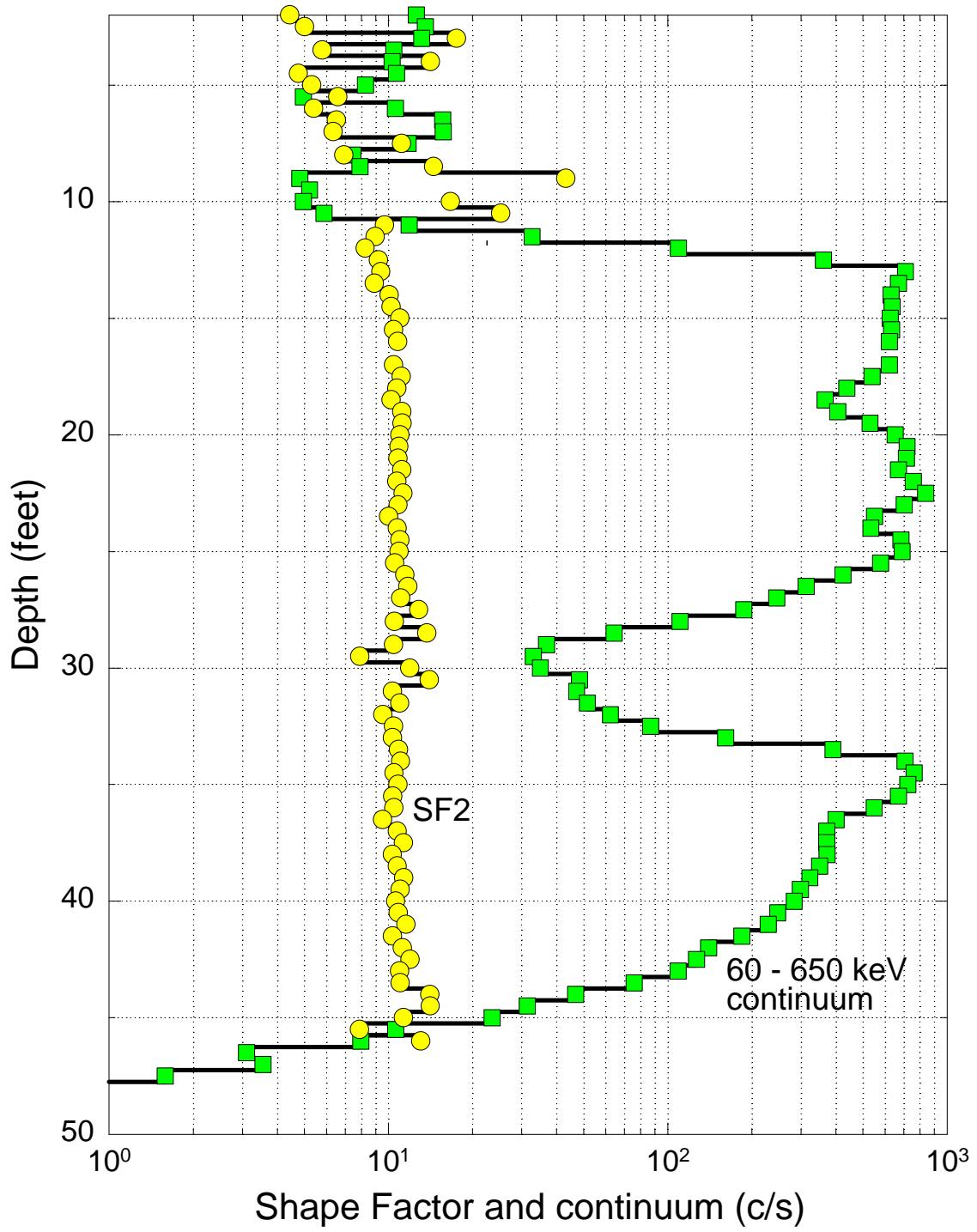


Figure 32. Shape Factor SF2 and Continuum Logs for Borehole 299-E25-191

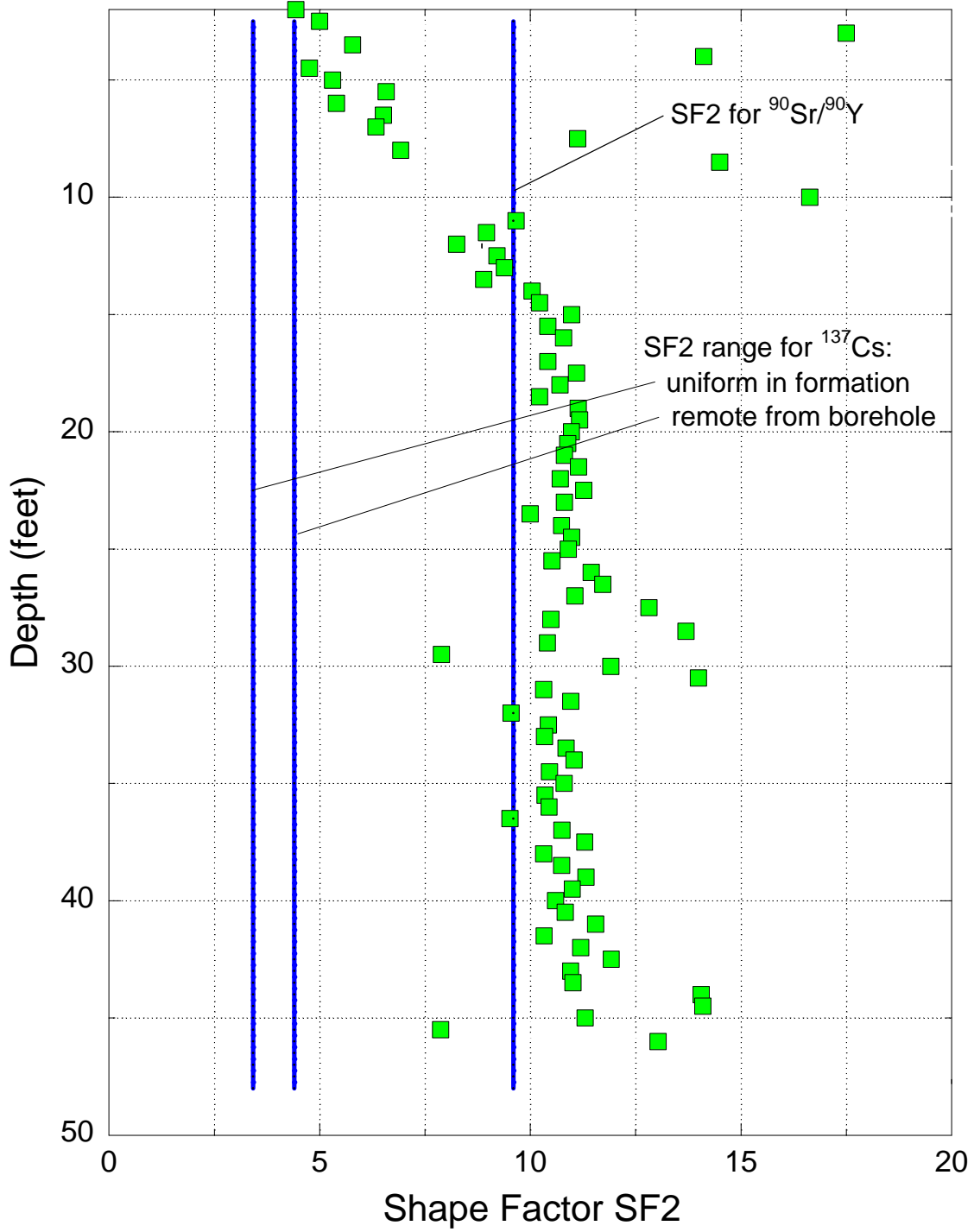


Figure 33. Linear Shape Factor Log SF2 for Borehole 299-E25-191

4.1 Shape Factor Analysis of Spectral Logs From Crib Borehole 299-E25-191

The WHC Radiological Logging System (RLS) logged borehole 299-E25-191 located near crib 216-A-30 in 1992. Information recorded in a WHC Engineering Data Transmittal report (WHC 1993) states that this crib received 102 Ci of ^{90}Sr , 117 Ci of ^{137}Cs , 751 Ci of ^{239}Pu , and smaller quantities of other contaminants from 1961 through 1989. The RLS logs detected ^{137}Cs contamination from the surface to a depth of 8 ft, but no gamma emitters were detected from 10 ft to total depth of 48 ft. However, a zone of strong continuum counts was observed in the low-energy range at depths below about 13 ft. The spectra files for this log were obtained from R.K. Price, now employed by Waste Management Federal Services at the Hanford Site (Price 1997) and were processed using shape-factor analysis software (DOE 1997b). Unfortunately, there are no drill core samples from this well that could be analyzed to identify and quantify the contaminant concentration whose decay is responsible for the intense continuum counts below about 300 keV.

Because no contaminant gamma peaks were detected for the depths where the continuum counts were observed, it was suspected by WHC analysts that the bremsstrahlung-emitter ^{90}Sr may be present.

Figure 30 shows a spectrum taken for 500 s at a depth where the continuum activity was elevated and a spectrum taken near the bottom of the well that recorded only the potassium, uranium, and thorium background. Figure 31 presents the difference between these two spectra, which is the background-corrected continuum spectrum. Figures 30 and 31 present the two energy regions used to compute shape factor SF2, the ratio of counts from 60 to 350 keV to the counts from 350 to 650 keV. The shape of the difference spectrum resembles earlier simulations of the bremsstrahlung from ^{90}Sr (Wilson 1997). This shape is also close to that reported in a measurement with a prepared ^{90}Sr source.

Figure 32 presents the depth log of SF2 and the net continuum counts for the 60- to 650-keV range for depths below 2 ft. For depths above 8 ft the continuum counts and SF2 are affected by the presence of ^{137}Cs . Below 8 ft, the net continuum counts, if from the bremsstrahlung-emitter ^{90}Sr , indicate the contaminant concentration ranges from approximately 30,000 to 60,000 pCi/g from 13 to 25 ft and from 34 to 35 ft. This estimate is based on a simulated sensitivity for the summed bremsstrahlung counts from ^{90}Sr (Wilson 1997).

Figure 33 shows a linear plot of the SF2 log and trend lines for the values expected for uniformly distributed ^{137}Cs contamination and for ^{137}Cs contamination that is radially remote from the borehole. Also shown is a trend line for ^{90}Sr obtained from measurements with a prepared ^{90}Sr source. Clearly, the elevated SF2 values are consistently in the range from 10 to 12, far above the values expected for any distribution of gamma-emitting contaminant, such as ^{137}Cs , but close to the value of 9.4 obtained with the ^{90}Sr source. Although the expected values of SF2 for ^{137}Cs were simulated for the larger detector of the SGLS, the values for the RLS detector are expected to be nearly the same. The fluctuation in SF2 from 28 to 31 ft is statistical in nature and is due to the much smaller bremsstrahlung signal in this depth range (Figure 32). The SF2 values above 10 ft also suffer from the same statistical problem.

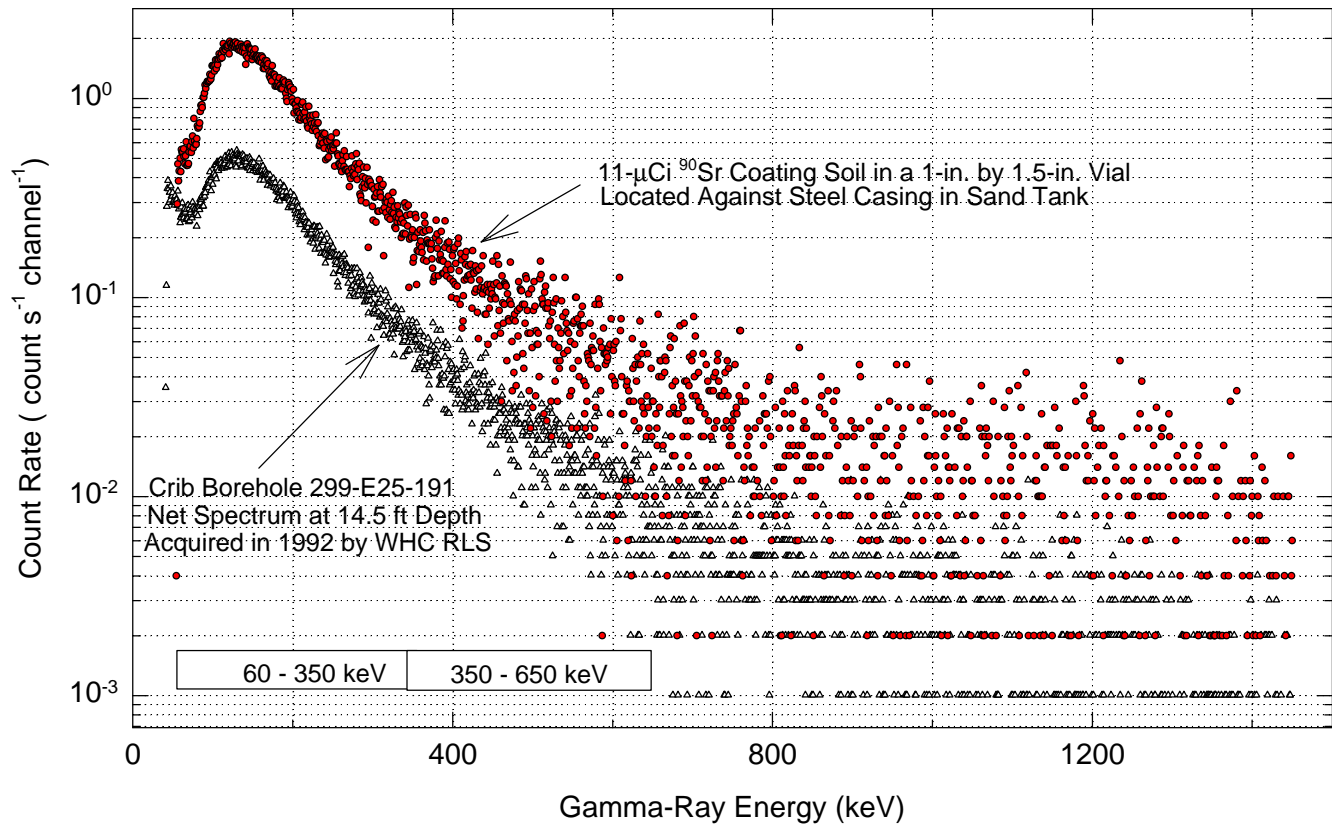


Figure 34. Comparison of Continuum Spectra From Borehole 299-E25-191 and Bremsstrahlung Spectrum From ⁹⁰Sr Source in Sand Tank

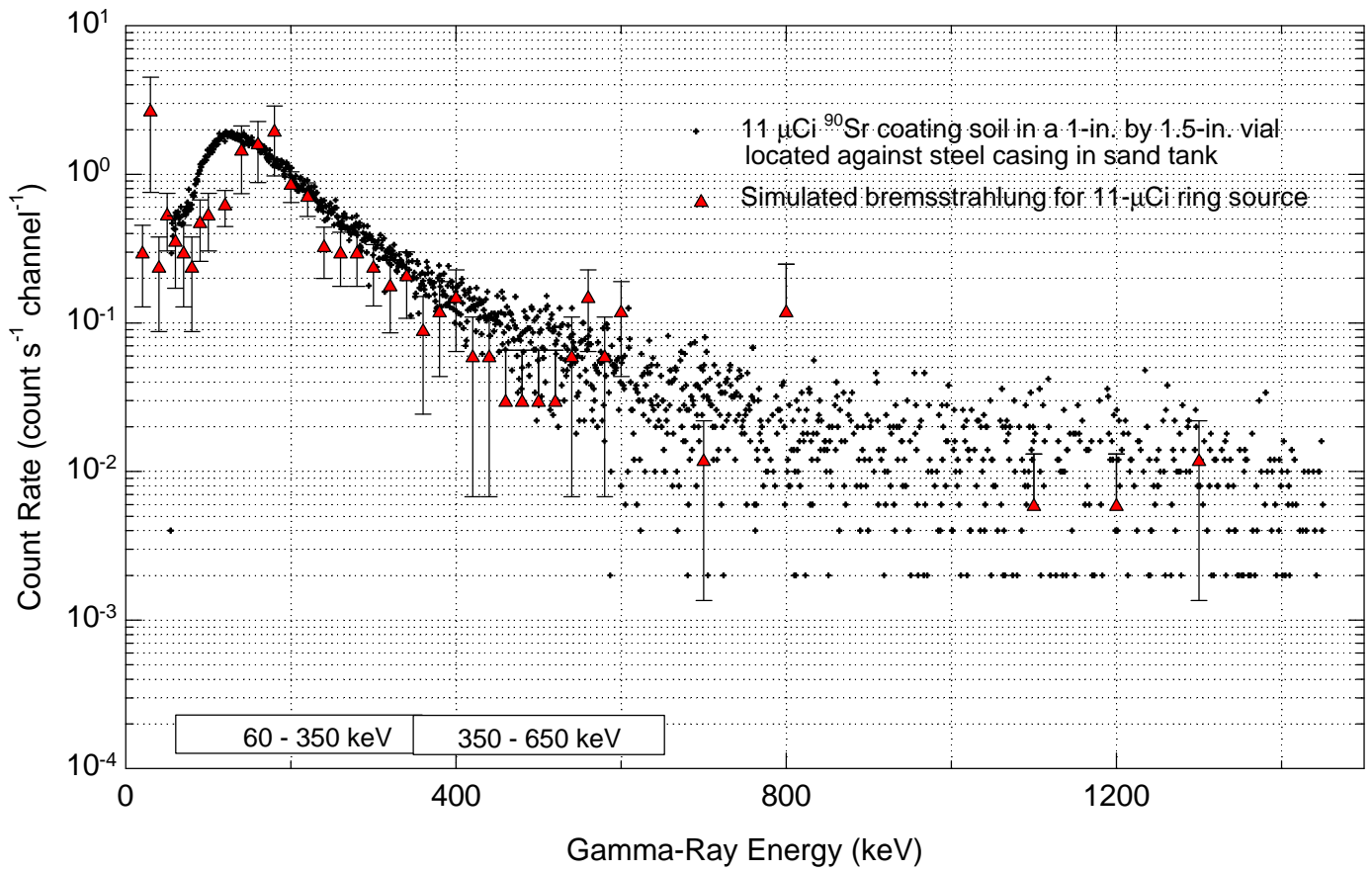


Figure 35. Comparison of Simulated and Measured Bremsstrahlung Spectra From ⁹⁰Sr Source in Sand Tank

The shape-factor log analysis methodology contains tests that suppress the SF1 log when contaminant-peak count rates are below certain values. However, SF2 is not suppressed by these tests. The plot for borehole 299–E25–191, with its strong net continuum signal in the absence of contaminant peaks, is a good example of why SF2 should never be suppressed. In this instance, ^{90}Sr could not be detected without the SF2 log. The analyst, when convinced of the presence of a bremsstrahlung signal from ^{90}Sr (after correction for background and in the absence of other contaminants), should estimate the corresponding ^{90}Sr concentration by applying the approximate sensitivity factor of 28 counts per second per 1,000 picocuries per gram (for the SGLS detector) to the net counts from 60 to 650 keV. The RLS detector volume is about a factor of 2 smaller than the volume of the SGLS detector. Therefore, the sensitivity factor is approximately 14 counts per second per 1,000 picocuries per gram. If this factor is applied to the continuum log value at 15 ft in Figure 32, the approximate (probably within a factor of 2) ^{90}Sr concentration is $(600 \text{ counts per second}) / (14 \text{ counts per second} / 1,000 \text{ pCi/g}) = 43,000 \text{ pCi/g}$. The approximate detection limit for ^{90}Sr under these measurement conditions corresponds to the continuum count rate where SF2 becomes statistically noisy at 30 ft. The activity at this depth is about 2,000 pCi/g.

4.2 Measured Spectra for a Prepared ^{90}Sr Source in a Sand Tank

To provide verification of the bremsstrahlung spectral shape from the beta-emitter ^{90}Sr and to verify predicted sensitivities based on computer simulations, a source with known activity was prepared by Pacific Northwest National Laboratory (Stromswold 1997). The source was placed in a sand model that was used to benchmark computer simulations of SGLS spectra from gamma-emitting contaminants. The sand model contains a 6-in.-diameter steel casing at its center and several PVC access tubes parallel to the borehole with varying radial thicknesses of sand between the casing and the tubes (see Figure 21). The source was prepared by coating soil grains contained in a 1-in.-diameter, 1.5-in.-long vial with 11 FCi of ^{90}Sr . The choice of source strength was guided by the simulated SGLS sensitivity to ^{90}Sr distributed in silica sand around a steel borehole.

Figure 34 presents the background-corrected spectrum measured with the SGLS for the ^{90}Sr source located in an access tube adjacent to the casing. For comparison, Figure 34 also shows the background-corrected spectrum measured in borehole 299–E25–191 at a depth of 14.5 ft. The spectra are similar in shape, but the magnitudes are dissimilar because of activity differences. The difference in spectral shape at low energies (below about 100 keV) may be due to differences in system electronic noise. The computed value of SF2 for the spectrum from the prepared ^{90}Sr source adjacent to the casing in the sand tank is 9.2 and 9.6 for the two measurements that were performed. These values are similar to the values of 10 to 12 obtained from the borehole spectra. Figure 35 shows a comparison of the spectrum measured in the sand tank and a simulation with the Monte Carlo code MCNP for a ring-shaped source adjacent to the borehole casing. The source geometry is not quite the same as that used in the experiment, but the magnitude of the response is similar to the measured count rate when the strength of the prepared source is used to normalize the simulated spectrum. This comparison validates the simulated count-rate response of the SGLS tool to the bremsstrahlung from ^{90}Sr , though the spectral shapes do not agree well at the lower

energies. The peak in simulated response at about 30 keV is not understood, but it lies below the approximate 50-keV threshold of the SGLS counting system and does not contribute to the measured response. The value of SF2 from the simulated spectrum is 7 with an uncertainty of ± 2 , considerably lower than the measured values and lower than simulations reported in Wilson (1997). The differences are not presently understood but all simulated values of SF2 should be used with caution because of the large uncertainties.

4.3 Summary

The shape factor analysis of spectral gamma borehole logs that contain elevated continuum counts in the absence of gamma-emitting contaminants produced SF2 (continuum shape factor) values of about 10 and are consistent with values obtained from experiments in a sand tank with a prepared ^{90}Sr source. These results strongly suggest that ^{90}Sr contamination is distributed in the sediment surrounding the borehole when logging data yield SF2 values of 10. With these conditions, a ^{90}Sr concentration value can be computed on the basis of approximate sensitivity of the SGLS for bremsstrahlung radiation in the energy window from 60 to 650 keV of 28 c/s per 1,000 pCi/g of $^{90}\text{Sr}/^{90}\text{Y}$ as determined from Monte Carlo simulations. The resulting concentration values should be considered to be uncertain by about a factor of 2.

4.4 Recommendations

Experimental data that verify the use of SF2 to identify the presence of ^{90}Sr and the predicted detection limit are quite limited. In addition, the Monte Carlo method is of limited use in simulating borehole bremsstrahlung spectra. Therefore, work was begun to develop alternative computer simulation models based on deterministic computer codes capable of solving the coupled electron-photon transport problem numerically without the large statistical errors inherent in Monte Carlo simulations. Such a code has been installed and tested but it is not yet possible to simulate SGLS spectra because the effect of detector response has not been incorporated in the model.

It is recommended that work to improve computer simulation capabilities for bremsstrahlung spectra from contaminants such as ^{90}Sr be completed. This effort will result in the ability to simulate accurately the detection thresholds for ^{90}Sr for a variety of logging conditions and to determine the contaminant distribution conditions for which the observed SF2 signature value is valid. The experiment with a prepared ^{90}Sr source was limited in scope. Additional measurements need to be made with this source. Because the sand tank, source, and logging tool are already available, the expenditure will be modest and the knowledge base of bremsstrahlung spectra from subsurface contaminants measured in boreholes will be greatly expanded.

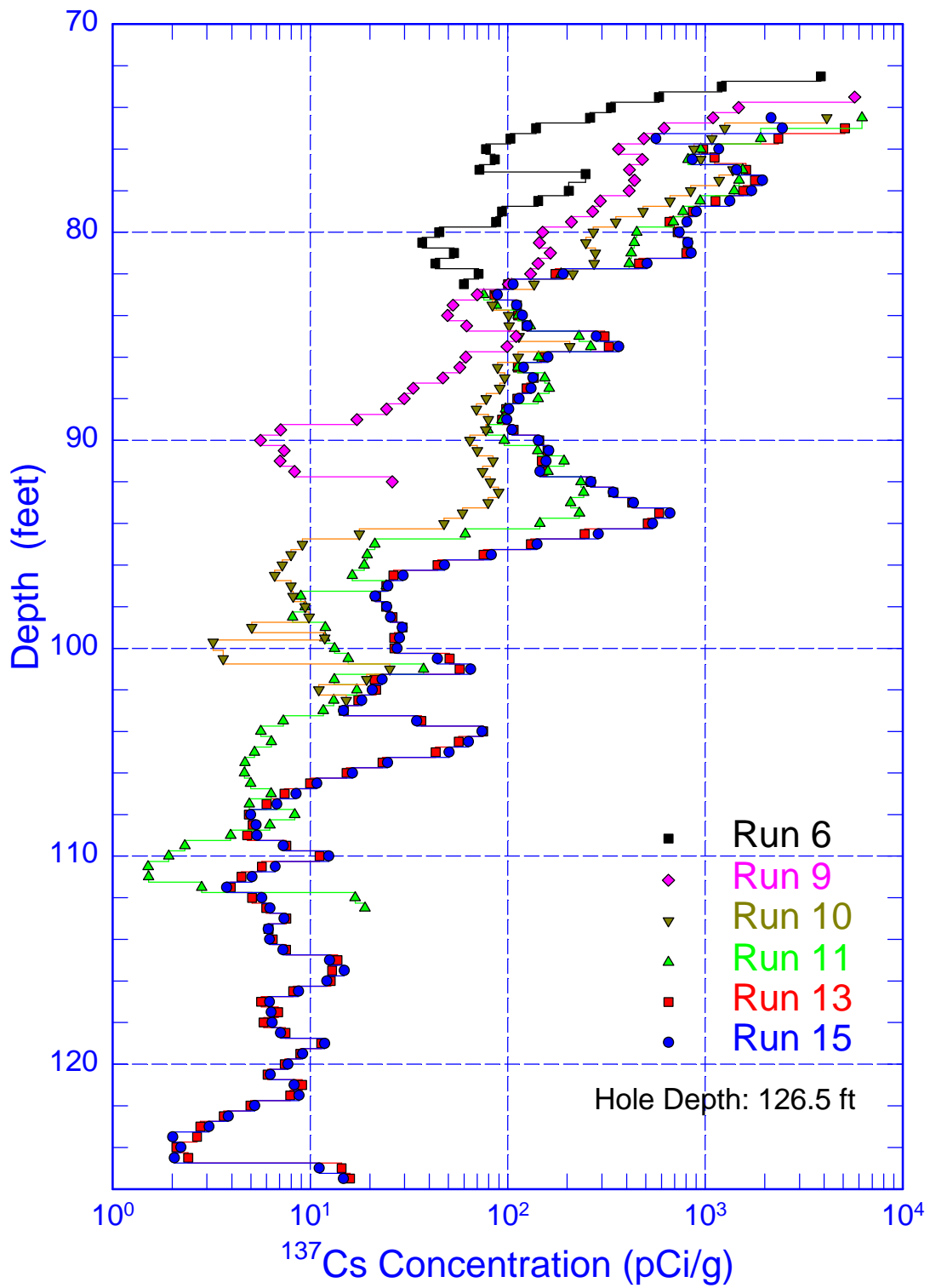


Figure 36. ^{137}Cs Logs for Expert Panel Borehole 41-12-01

5.0 Spectral Shape Factor Analysis for Expert Panel Borehole 41-12-01 Near Tank SX-112

At the request of an Independent Expert Panel established to assess vadose zone contamination, a new borehole (41-12-01) was pushed to a depth of 125 ft near existing borehole 41-12-02 in the vicinity of tank SX-112 (DOE 1997a). The Independent Expert Panel requested that a spectral shape analysis be performed on the data taken by the SGLS during and after the drilling process. Information about the drilling and logging of this borehole is in an informal report by Brodeur (1996). The methodology employed in the shape factor analysis is described in Wilson (1997).

The SGLS logs for this borehole show that contamination was “dragged down” the borehole by the drill casing from the high-contamination zone at about 70 ft. Figure 36 presents a composite of several logs showing this drag-down behavior as the borehole was deepened in 10-ft increments (Brodeur 1996). From the character of these logs, it appears that a fixed ^{137}Cs source is associated with the tip region of the drill pipe, and possibly at other locations on the casing.

Presumably, as the pipe penetrated to greater depths, more and more of this contamination was transferred to the sediment, gradually building up the ^{137}Cs profile observed at the completion of the drilling. Run 15 is a repeat of run 13 and provides a measure of log reproducibility.

Shape-factor analysis verifies the near-casing location of the detected ^{137}Cs contamination. The shape factor logs also suggest that the contamination is not confined to the casing wall but extends somewhat into the formation surrounding the casing. Alternatively, the ^{137}Cs contamination could consist of two components, one at the casing wall and the other present in the formation before the new borehole was drilled.

5.1 Shape Factor Logs

Because the new borehole was completed with 0.5-in.-thick casing with an inside diameter of 7 in., it was necessary to determine new potassium, uranium, and thorium stripping factors to correct the ^{137}Cs shape-factor energy windows for background. New simulations were also conducted with MCNP for this casing size to obtain shape factors for ^{137}Cs contamination uniformly distributed in the formation, at the outer casing wall, and at the inner casing wall. Table 11 presents new shape factors that were used to derive expected ranges for comparison to the actual shape factor logs.

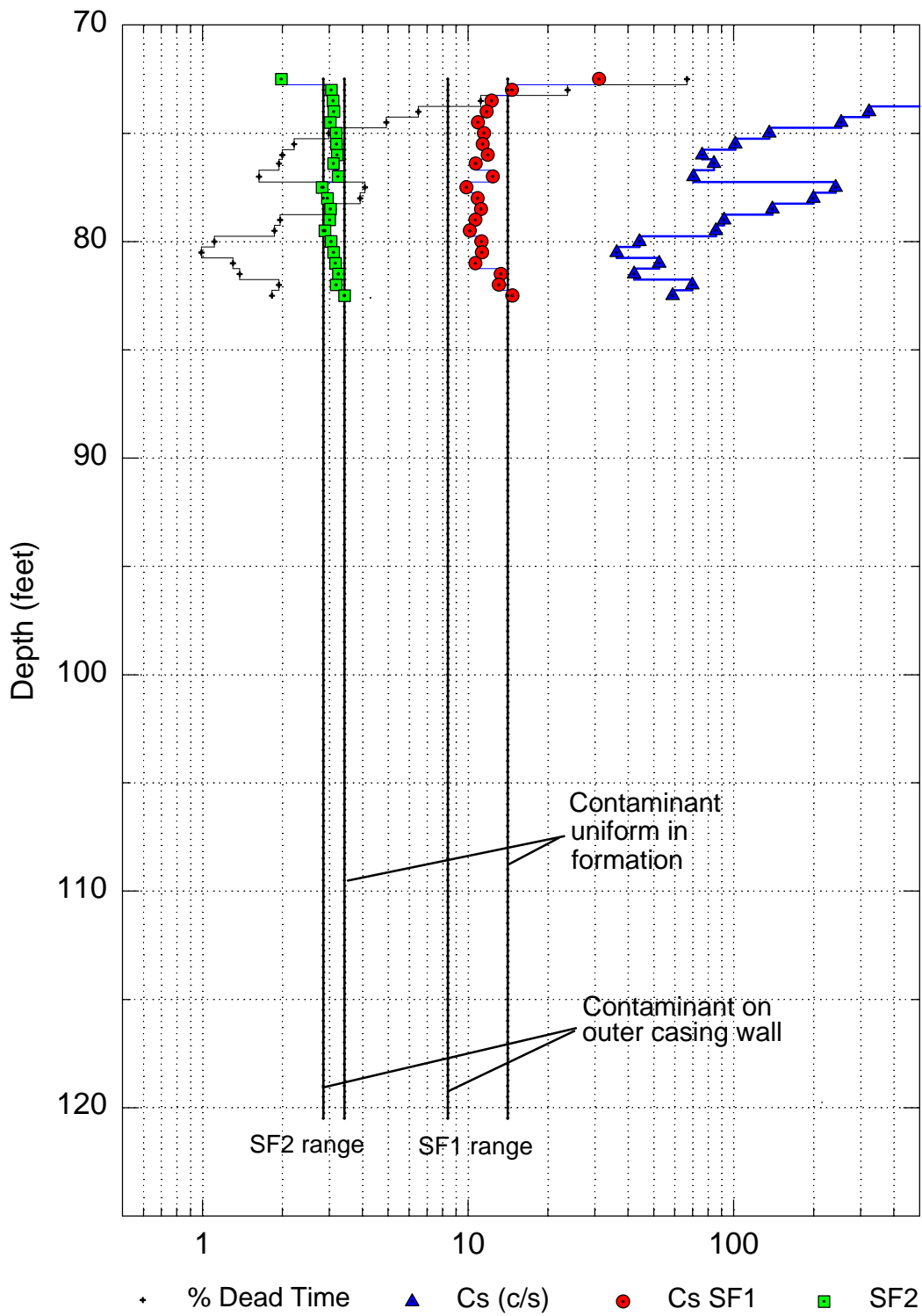


Figure 37. Shape Factor Logs for Run 6, Borehole 41-12-01

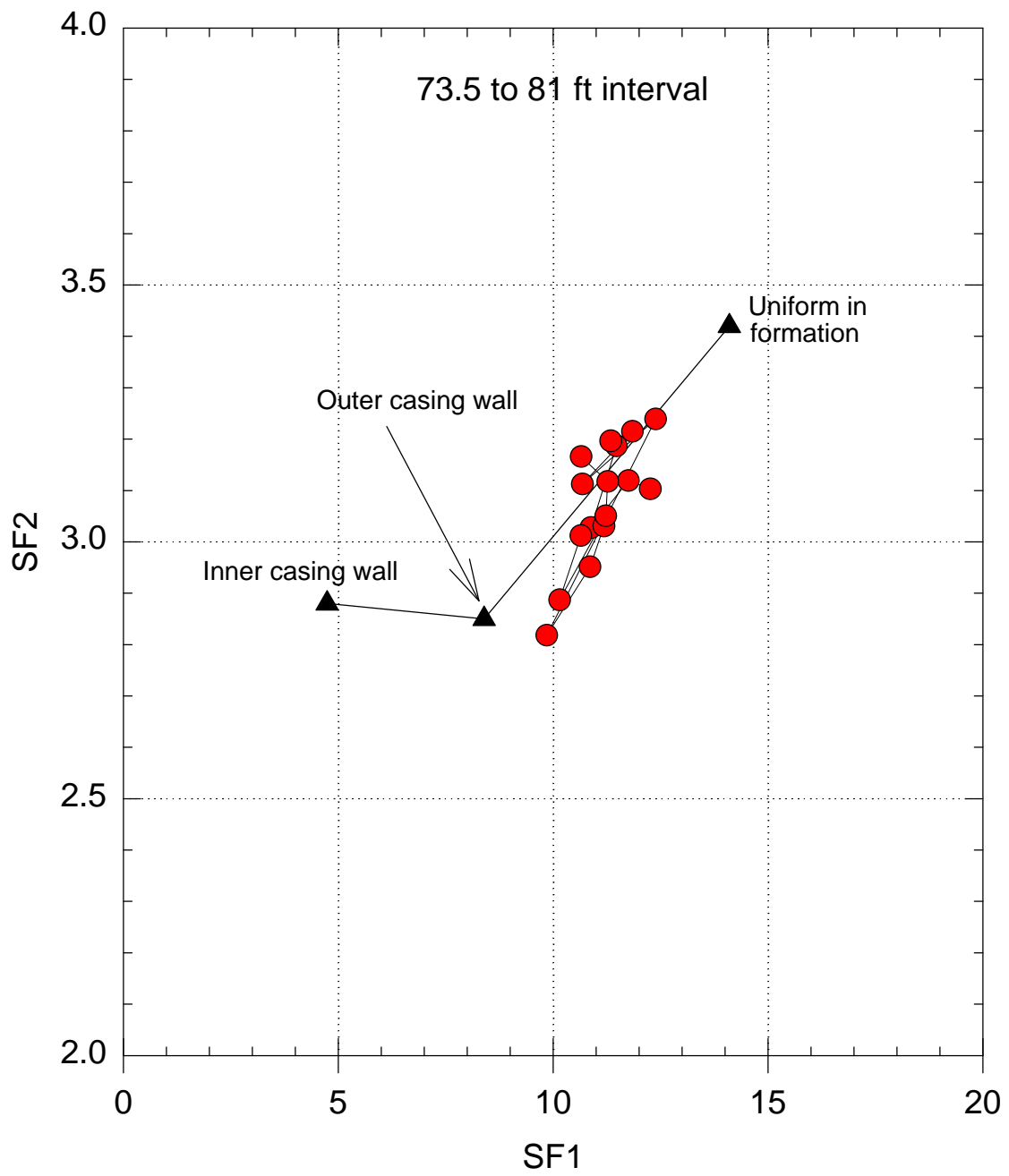


Figure 38. SF1 and SF2 Cross Plot for Run 6, Borehole 41-12-01

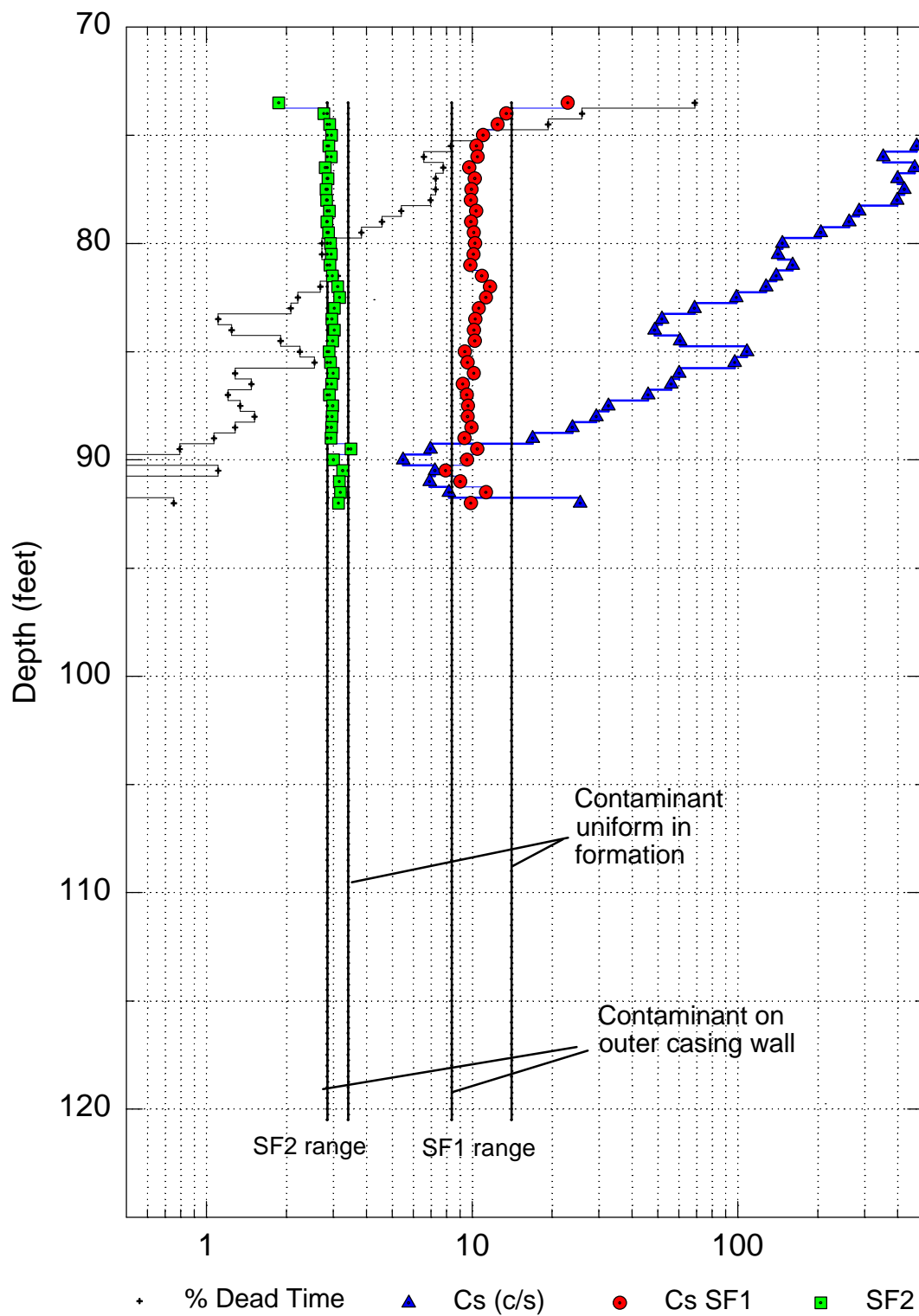


Figure 39. Shape Factor Logs for Run 9, Borehole 41-12-01

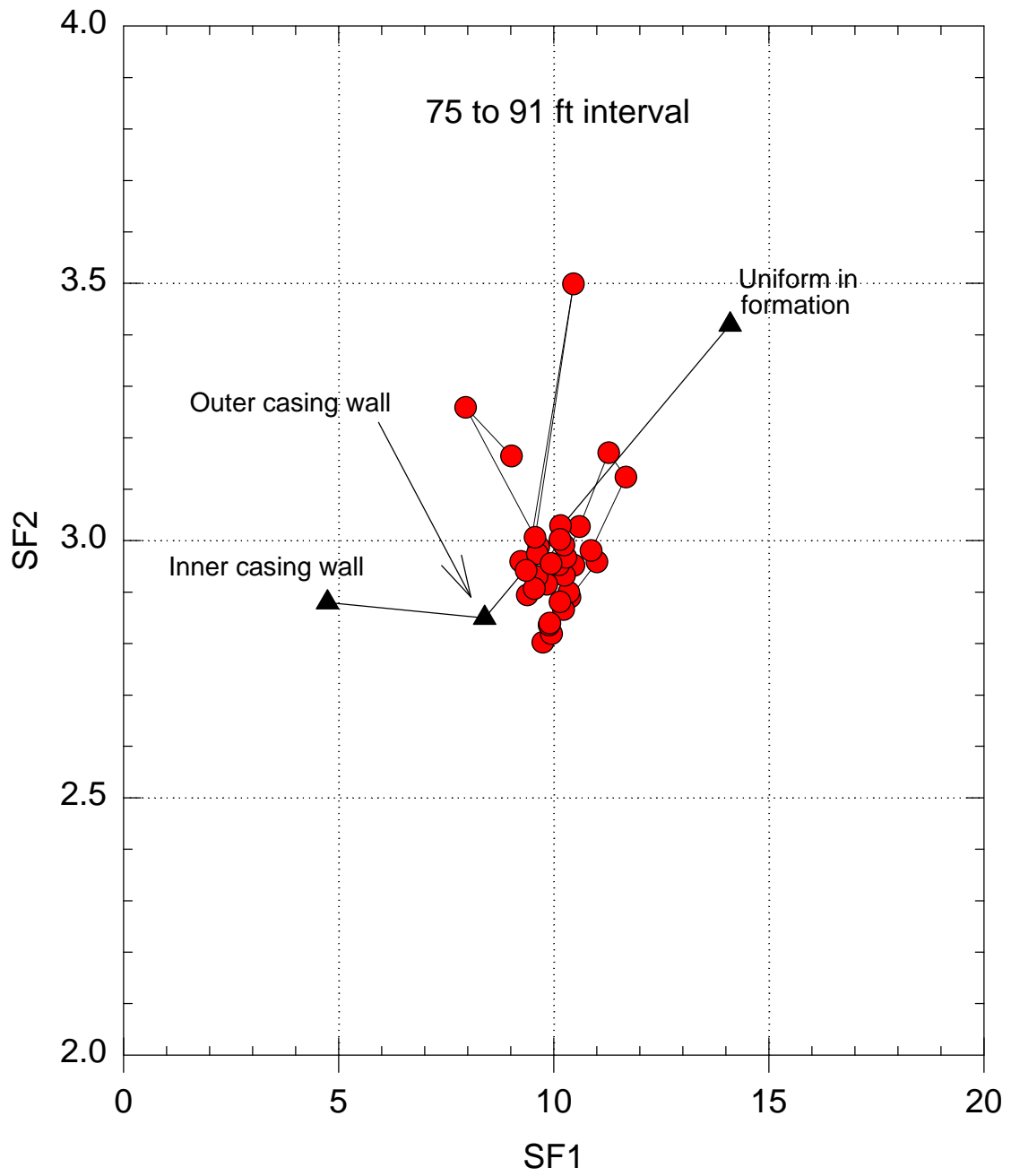


Figure 40. SF1 and SF2 Cross Plot for Run 9, Borehole 41-12-01

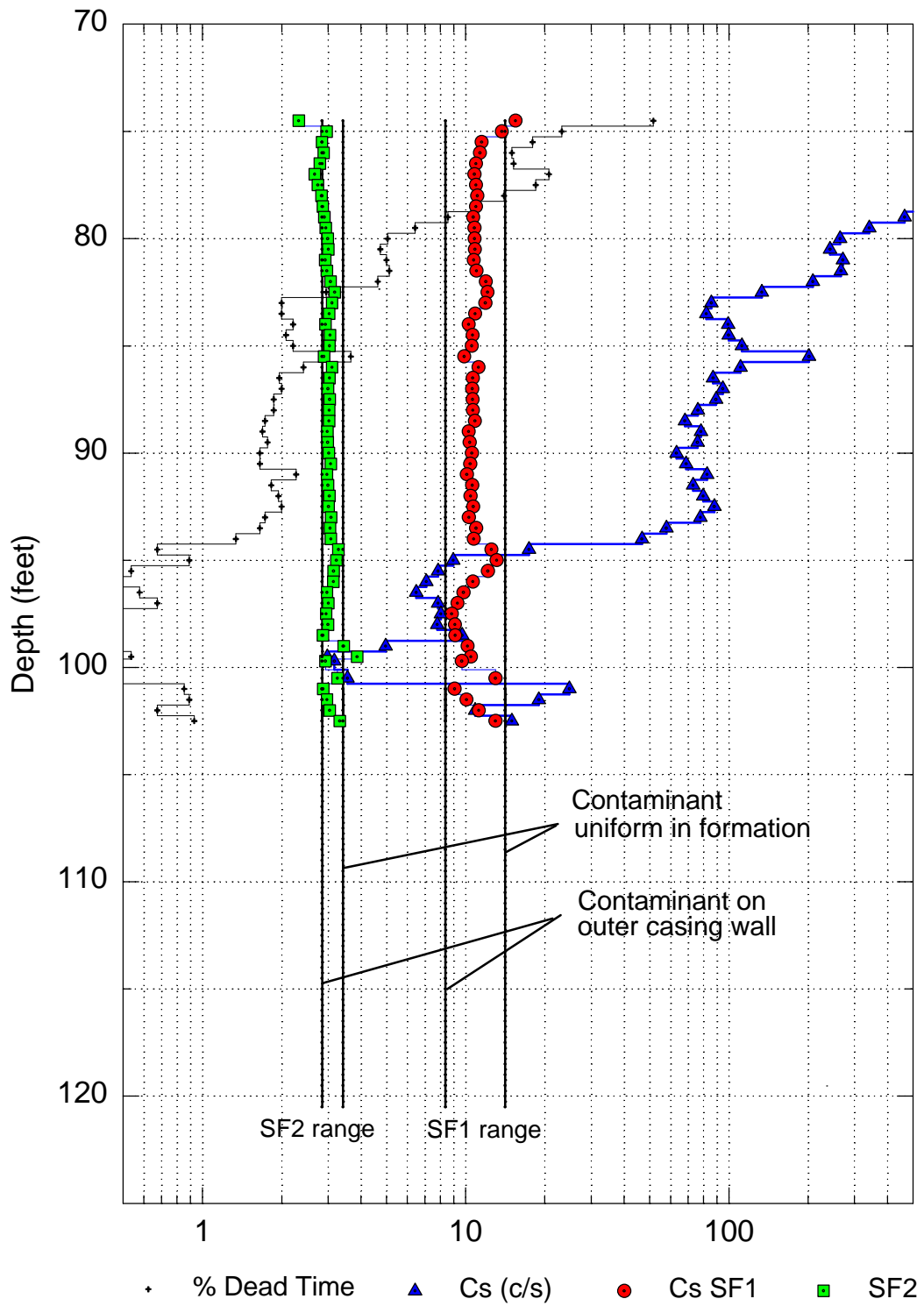


Figure 41. Shape Factor Logs for Run 10, Borehole 41-12-01

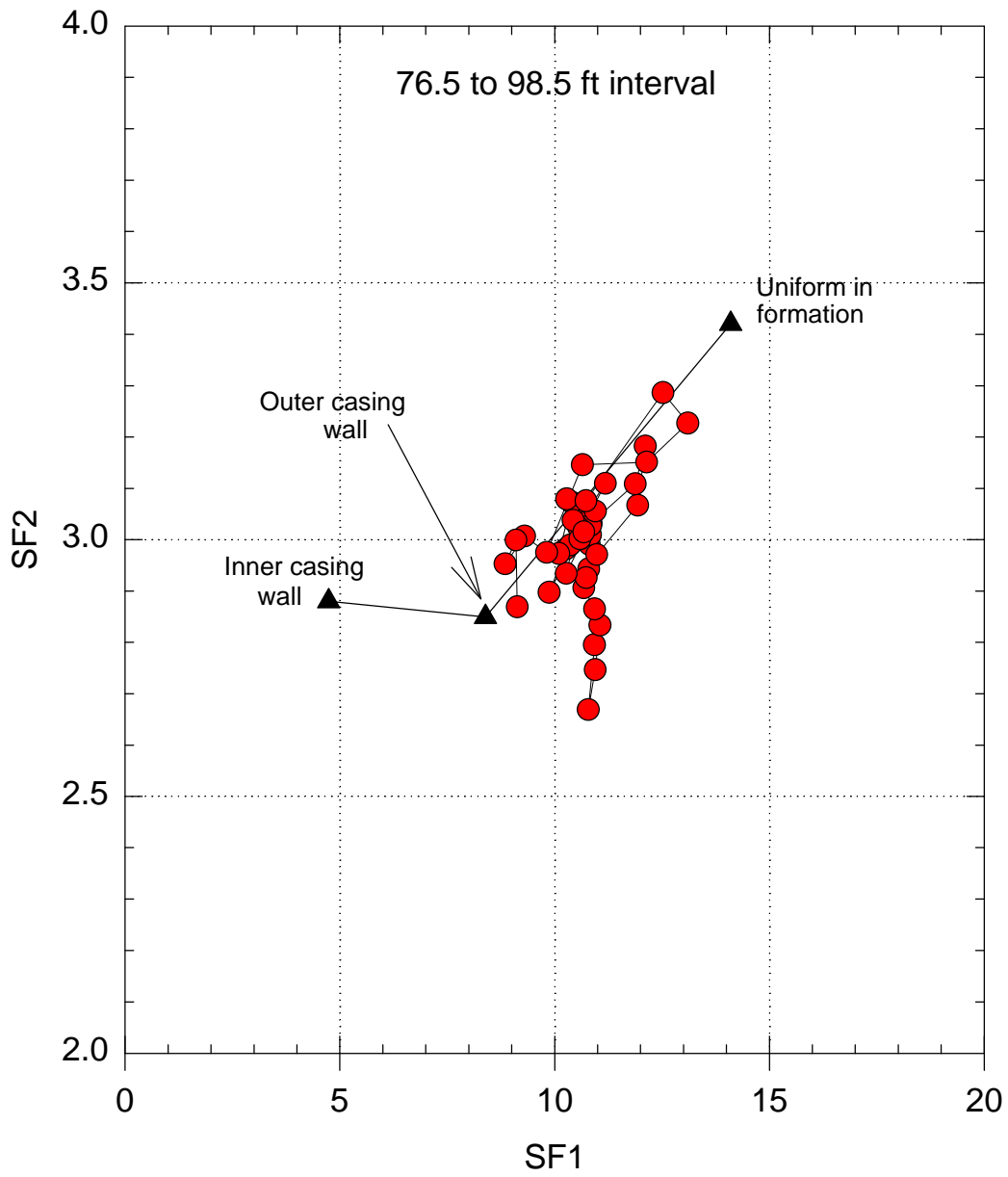


Figure 42. SF1 and SF2 Cross Plot for Run 10, Borehole 41-12-01

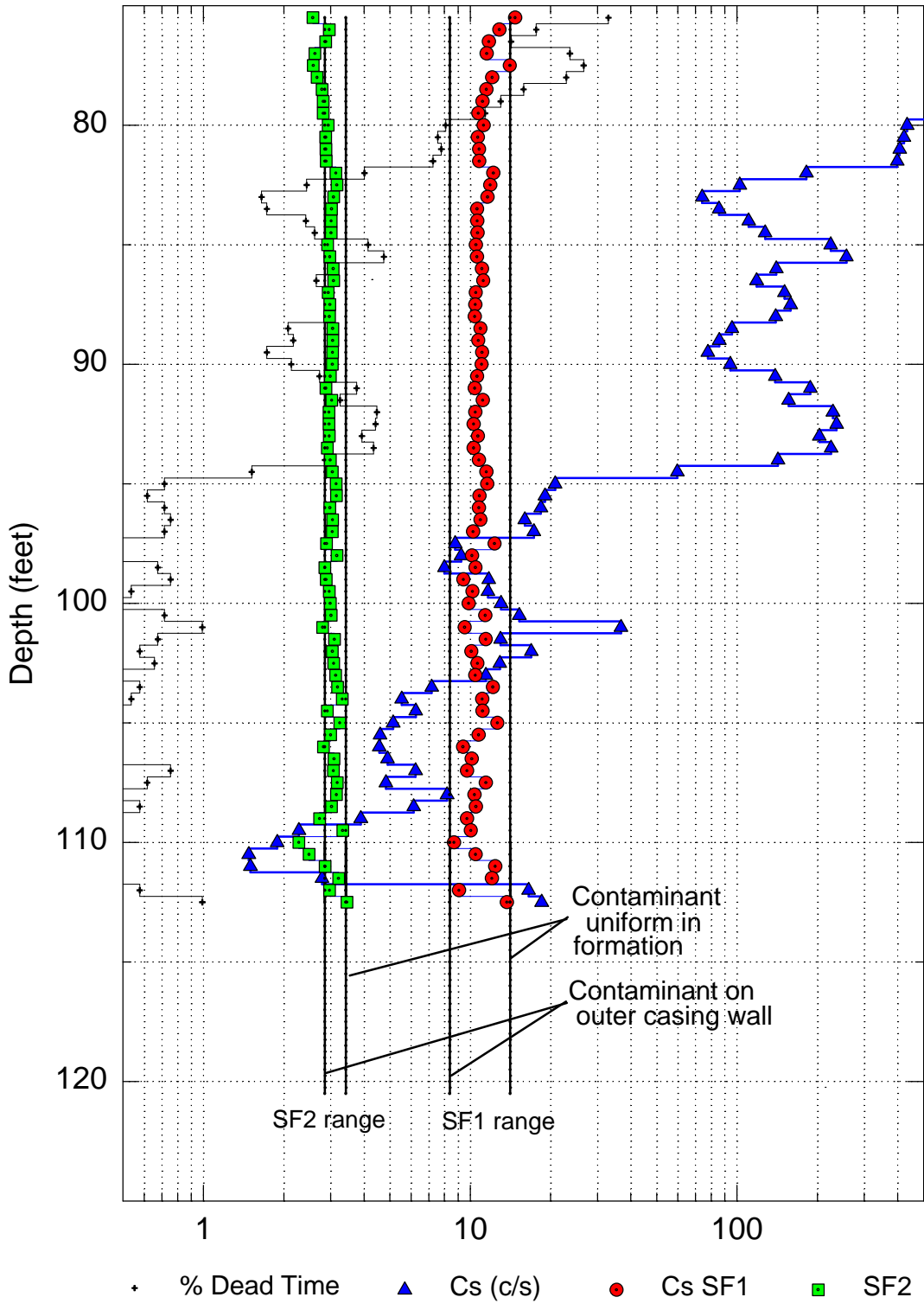


Figure 43. Shape Factor Logs for Run 11, Borehole 41-12-01

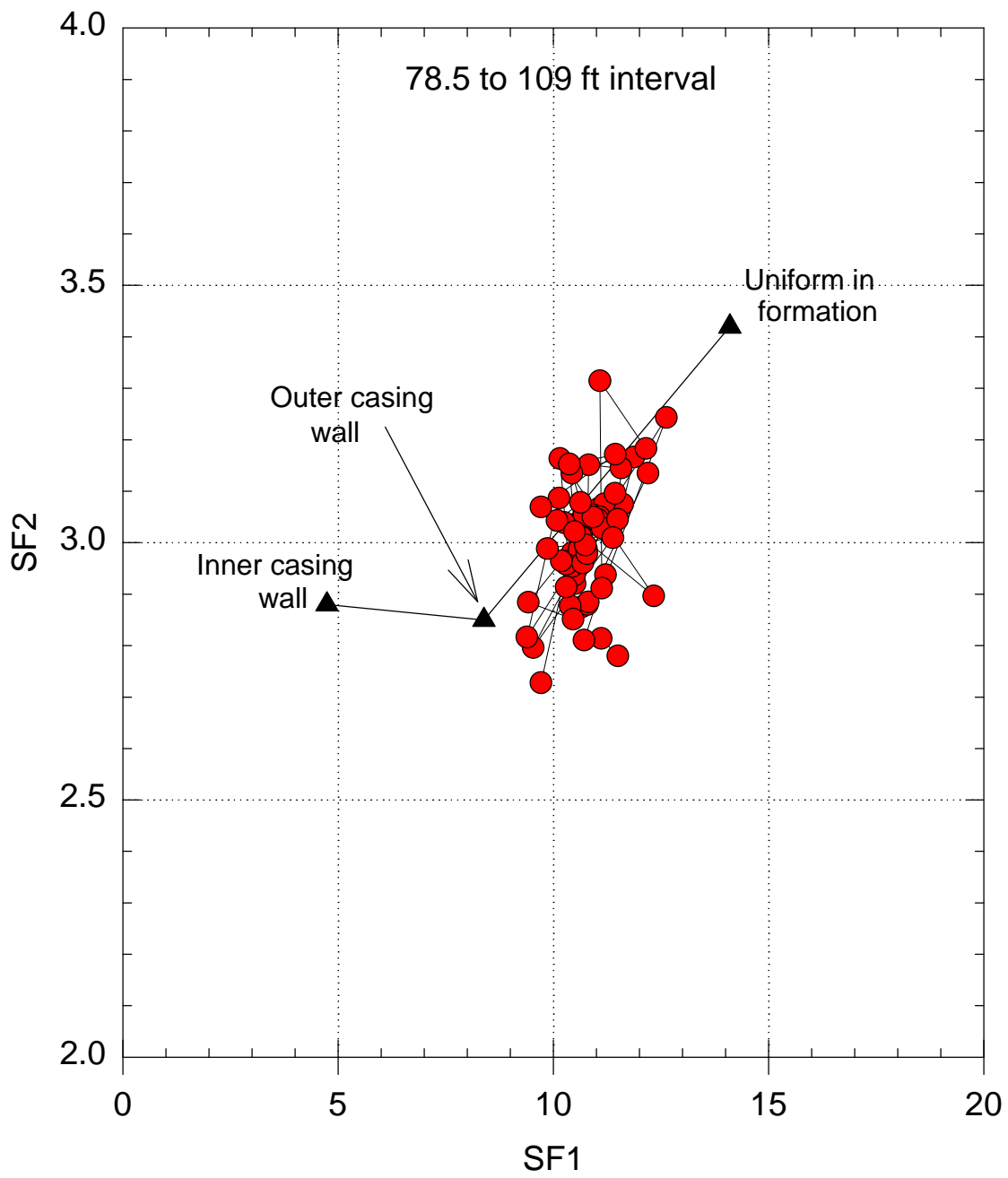


Figure 44. SF1 and SF2 Cross Plot for Run 11, Borehole 41-12-01

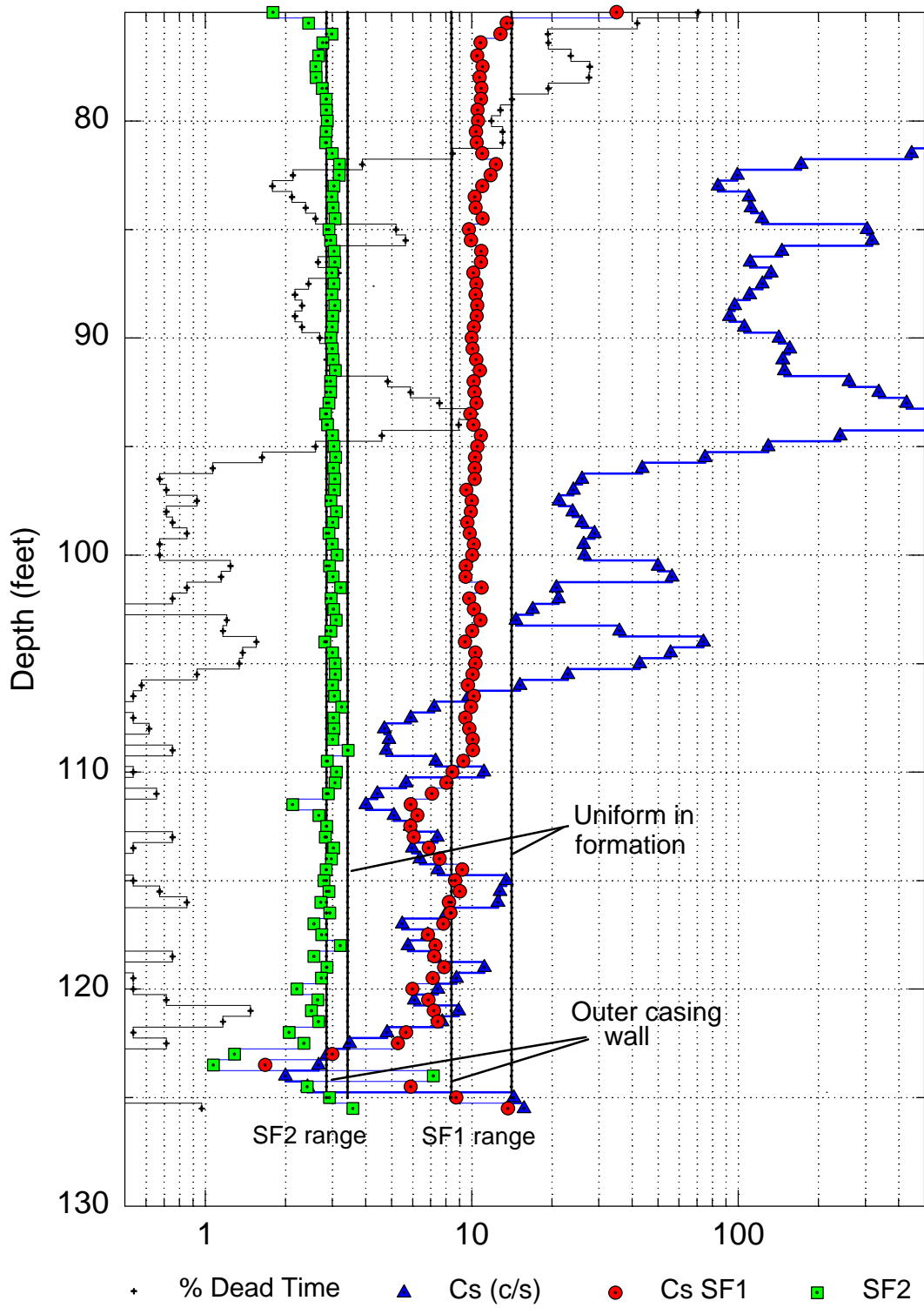


Figure 45. Shape Factor Logs for Run 13, Borehole 41-12-01

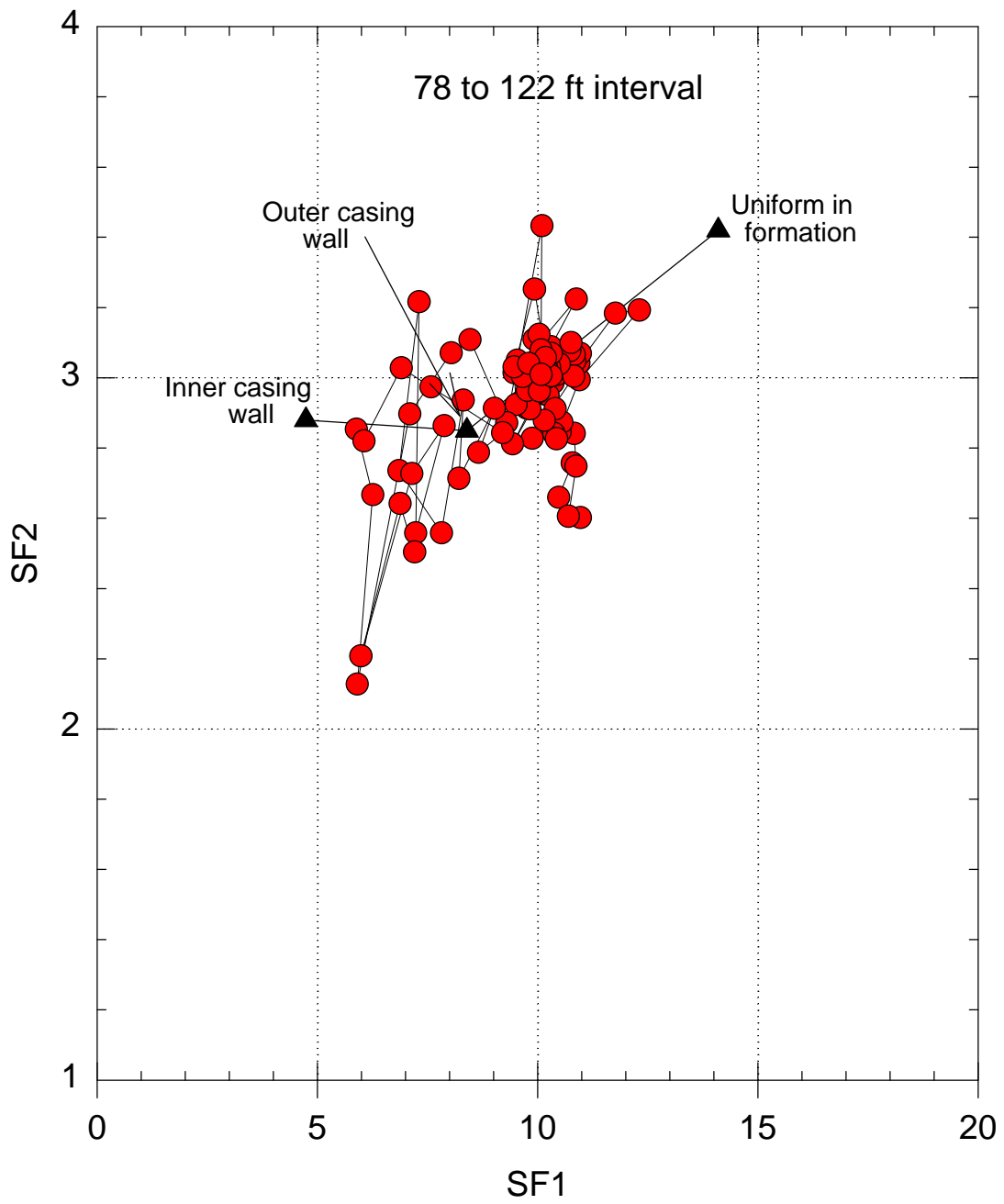


Figure 46. SF1 and SF2 Cross Plot for Run 13, Borehole 41-12-01

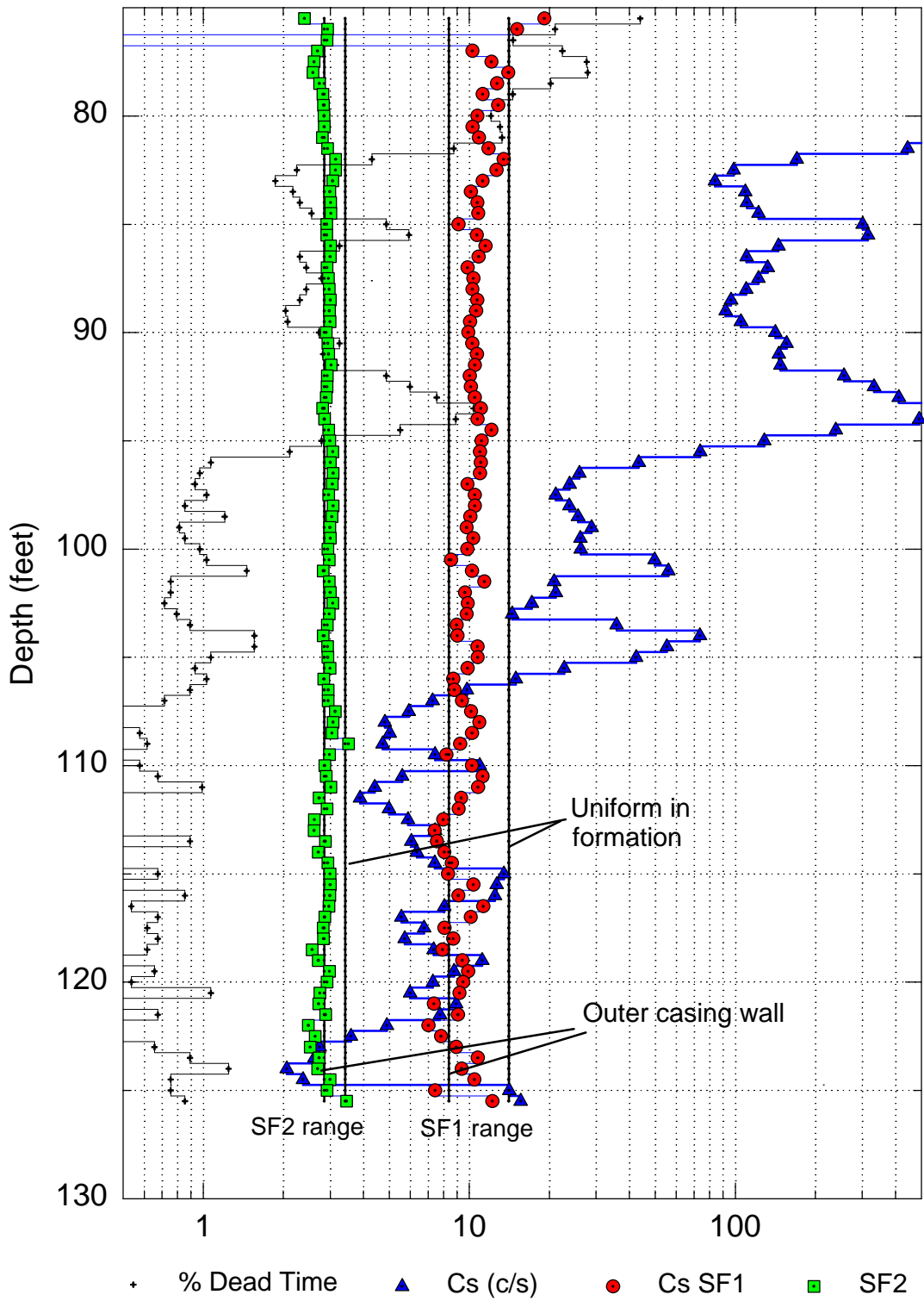


Figure 47. Shape Factor Logs for Run 15, Borehole 41-12-01

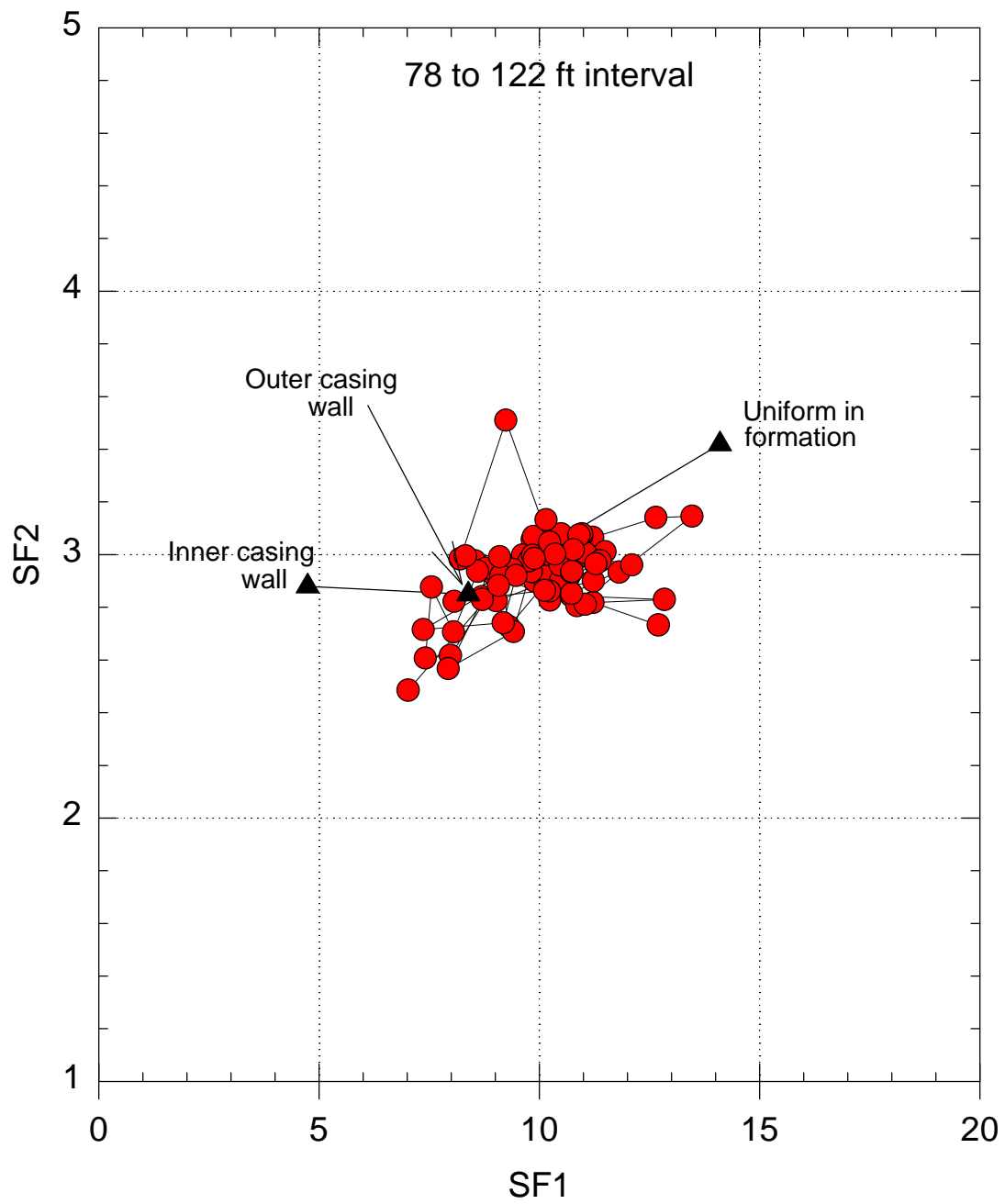


Figure 48. SF1 and SF2 Cross Plot for Run 15, Borehole 41-12-01

Table 11. ¹³⁷Cs Spectral Shape Factors for 0.5-in.-Thick Steel Casing

| ¹³⁷ Cs Source Distribution | SF1 (60 to 650 keV)/662 keV | SF2 (60 to 350 keV)/(350 to 650 keV) | SF3 (610 to 655 keV)/662 keV |
|---------------------------------------|--------------------------------|---|---------------------------------|
| Uniform Formation | 14.1 | 3.42 | 0.23 |
| Outer Casing Wall | 8.39 | 2.85 | 0.122 |
| Inner Casing Wall | 4.74 | 2.88 | 0.037 |

The potassium, uranium, and thorium stripping ratios for the continuum-window background corrections were obtained for the new borehole conditions by processing the ¹³⁷Cs-free zone from about 10 to 45 ft and demanding that the net counts in the two energy ranges of 60 to 350 keV and 350 to 650 keV be zero for the summed results over the entire depth interval. The nominal potassium, uranium, and thorium stripping factors (for 0.313-in.-thick casing) had to be adjusted upward by factors of 1.23 and 1.31 for the two energy ranges of 60 to 350 keV and 350 to 650 keV, respectively, and by a factor of 1.25 for the full continuum energy range from 60 to 650 keV.

Shape factor analysis was done for runs 6, 9, 10, 11, 13, and 15, which are the runs presented in Figure 36. Figures 37 through 48 present the shape factor logs for these runs and the corresponding cross plots of SF2 and SF1 values. The shape factor log plots include solid lines bracketing the expected ranges for SF1 and SF2 from the source on the outer casing wall to a uniform sediment-source distribution. The ranges are 8.4 to 14.1 for SF1 and 2.85 to 3.42 for SF2. The plots also include the ¹³⁷Cs count rate and the percent dead time (DT). The SF3 log is not presented in these plots. The cross plots include a trend line connecting the simulated points for the source on the inner casing wall, on the outer casing wall, and uniform in the sediment.

Figures 37 and 38 show the shape factor results for the first interval drilled through the high-contamination zone to a depth of 82.5 ft. SF1 values shown on Figure 37 fall between the two range lines, indicating the source material is somewhere between the extremes of being on the outer casing wall and uniform in the sediment. There is a gradual decrease in SF1 with depth. At the bottom of the well, shape factor values are affected by the change in geometry for source and casing as the open bottom is approached. Values close to the hot zone above about 73 ft are affected by the rapid change in contaminant concentration with depth and by pulse pileup from excessive dead time. The trend from 73.5 to 81 ft suggests that some of the contamination may be uniformly distributed and present before drilling, while near the bottom of the well more of the contamination is local to the borehole casing region. Figure 38 shows how the SF1 and SF2 values for depths from 73.5 to 81 ft tend to conform to the trend line.

Figures 39 and 40 are shape factor plots for the SGLS data taken after the pipe was pushed another 10 ft in depth to 92.5 ft. The trend toward decreasing SF1 values with increasing depth continues; a comparison of Figures 37 and 39 shows that the SF1 values become smaller for the repeat depth zone from 73.5 to 82.5 ft, indicating a larger fraction of the contaminant is local to the borehole casing. This contaminant distribution is consistent with the hypothesis that each new increment of drilling carries

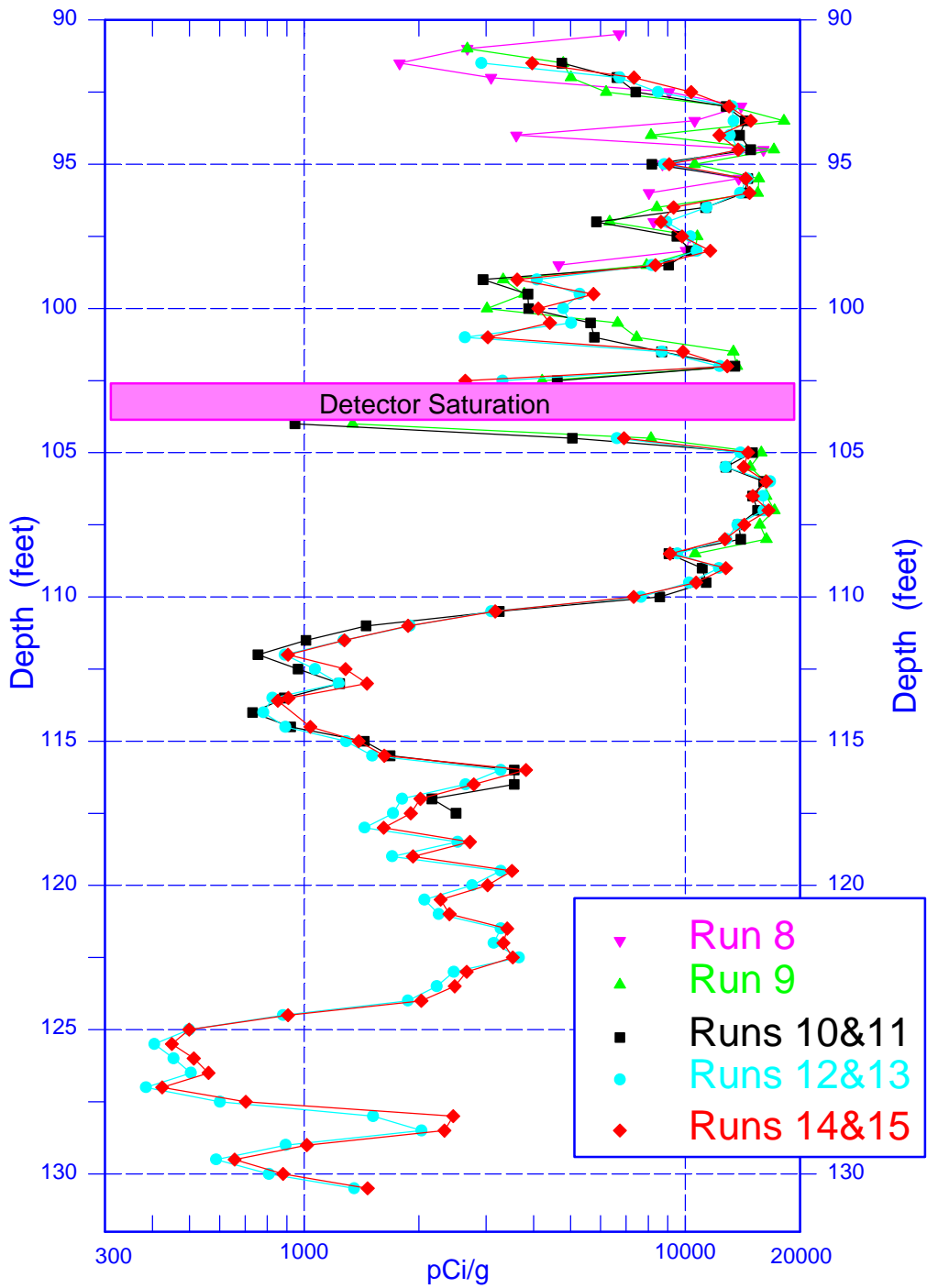


Figure 49. ^{137}Cs Logs for Expert Panel Borehole 41-09-39

more contamination down to a given depth. Again, the rise in casing is strong evidence that there was no drag down of contamination and that the activity was in place before emplacement of the well (Brodeur 1997a).

A ^{137}Cs shape-factor analysis was conducted for the zone from 103 ft to total depth at 130 ft. Although there are uncertainties in the shape factor analysis interpretation process of logs for this borehole, the results of the analysis indicate that the ^{137}Cs contamination detected in this depth range is at least somewhat local to the borehole region. The shape factor SF1 is intermediate between that expected for the casing-localized source and the source uniform in the formation. This result seems to conflict with the observation of no drag down of ^{137}Cs from above.

The SGLS count rates are generally high for the depth zone processed, with dead times ranging from 10 to nearly 100 percent. These data provide valuable information concerning the effect of high dead times on spectral shape and lead to the conclusion that the shape factor analysis can be performed at dead times much higher than previously thought.

6.1 Shape Factor Logs and Analysis

Because the contaminant activity is high for the depths of interest, shape factor processing of the logging data is not affected by small inaccuracies in the KUT background correction. Therefore, the nominal KUT background stripping factors used for logs of the first new borehole (41-12-01) were also used for logs of the second new borehole. ^{137}Cs shape factors simulated earlier for the 0.5-in.-thick steel casing of the first new borehole are also appropriate for the second new borehole. These values are shown on the log plots to define the range of expected values as the source distribution changes from being borehole localized to uniform in the formation. The simulated shape factors are for spectra unaffected by pileup distortion.

Because the shape factor log analysis was performed for two independent log runs with similar results, only one set of shape factor logs will be shown in this report. Figure 50 presents SF1 and SF2 logs, along with vertical lines defining the simulated ranges. The right-most track presents logs of percent dead time, a pulse pileup indicator, and ^{137}Cs count rate. No attempt was made to correct the simulated shape factor ranges for spectral distortion from the high count rates. The detector was saturated and no data were recorded at the 103-ft interval. There is a gap in the data from 108.5 to 110 ft because the two runs for producing these logs (runs 9 and 15) do not include these depths. For depths above 110.5 ft, the dead times are too high to make a meaningful analysis. The computed SF1 values below 110.5 ft are quite stable, a reflection of the excellent counting statistics for these data and the absence of severe count-rate-dependent distortion. The separation of the vertical lines defines the expected range for SF1 (8.4 to 14.1) and SF2 (2.85 to 3.42) in the absence of dead-time distortion. Dead times range from about 7 percent to nearly 100 percent. The pulse pileup indicator is the count rate in an energy window from 1350 to 1450 keV, placed just above the first ^{137}Cs sum peak at twice 662 keV, or 1324 keV. This spectral quality indicator (QI) is a measure of the second-order pileup effect occurring for energies above the first sum peak and is a better gauge of pileup distortion of the

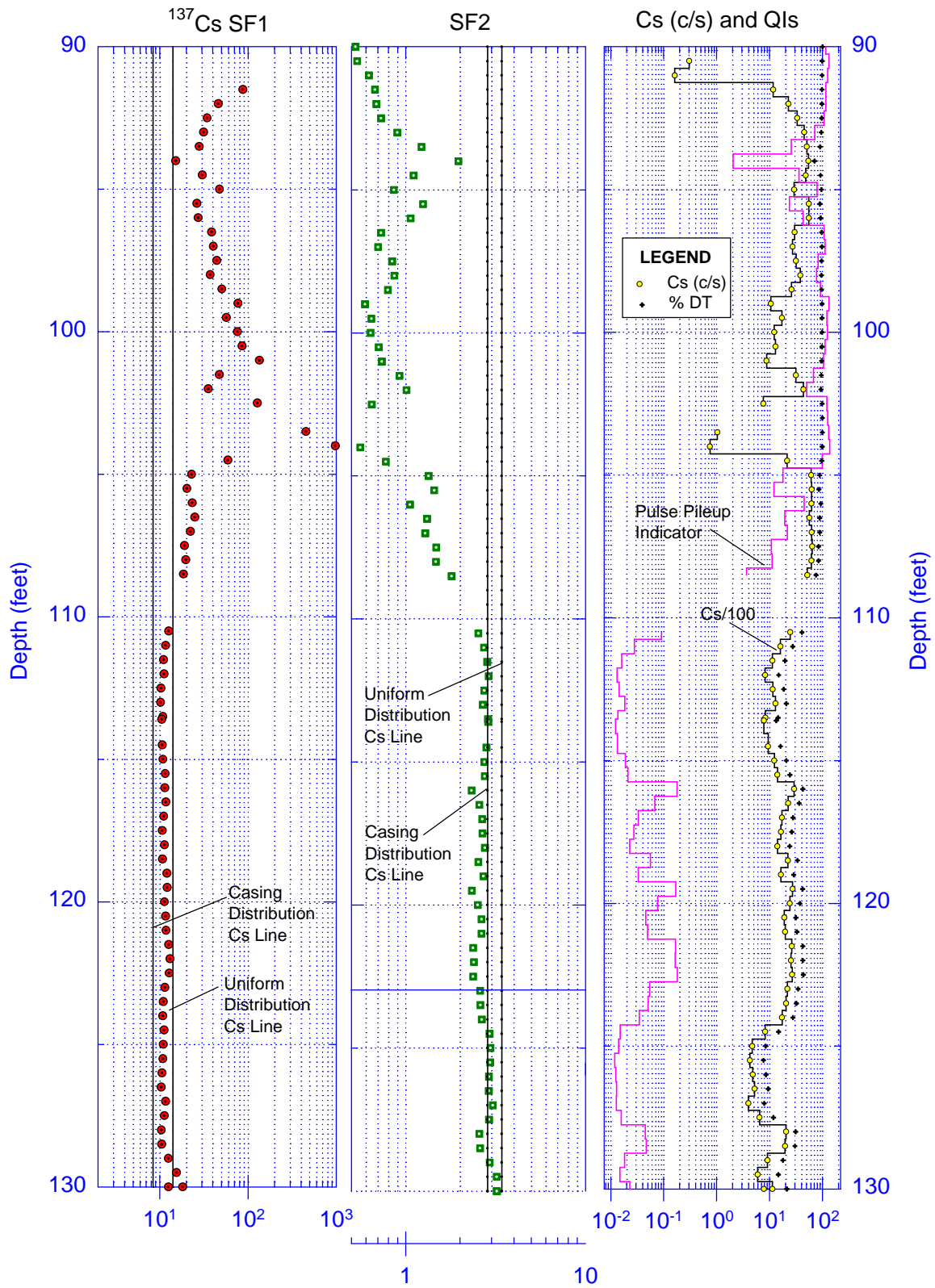


Figure 50. Shape Factor Logs for Runs 9&15, Borehole 41-09-39

shape factors than previous QIs. Note how this indicator falls dramatically for depths below 110 ft, where dead time falls from about 70 percent to values in the 10- to 30-percent range. For the depth range from 111 to 128 ft, where the value of the pile-up indicator is small, shape factor SF1 is not believed to be affected by the mild count-rate distortion that exists in these spectra.

The indication from SF1 is that the ^{137}Cs distribution is intermediate between a casing-localized source and a uniform formation source. SF2, however, is believed to be significantly affected by spectral distortion for the 111 to 128 ft depth interval (evidence for this is presented in Section 6.2, “Dead-Time Effect on Spectral Shape”). This results in SF2 values that tend to be too small, falling somewhat below the vertical line corresponding to ^{137}Cs localized to the outer casing wall.

Recent concerns (Brodeur 1997b) about the effect of compaction during drilling on shape factors have been considered. Simulations show that the compaction effect on a casing-localized source is small, causing SF1 to increase by about 2 percent. On theoretical grounds, compaction is not expected to affect the uniformly distributed ^{137}Cs SF1 value, though this point is still under study. Presently, it is believed that the SF1 results for the 111 to 128 ft depth interval are defensible, in spite of the high count rate and concerns about compaction during drilling.

Figure 51 presents a cross plot of SF1 and SF2 values for this depth range that shows simulated points for the casing-localized and formation-uniform source distributions. The location of all the points somewhat below the trend line is attributed to a slight spectral distortion effect on SF2 (dead times are in the range from 7 to 40 percent for this depth interval). This effect is discussed in Section 6.2, but there is a definite trend for SF2 to decrease with increasing dead time while the effect on SF1 is small for these dead times. Points near the bottom of the borehole were omitted because spectral shape is affected by the nonstandard source geometry.

At this time, there is an unresolved contradiction between results of repeat logging and the shape factor analysis. The results of logging after each push imply the contamination is in the formation, while the shape factor analysis indicates the contamination is distributed more local to the borehole than expected for a uniform distribution.

6.2 Dead-Time Effect on Spectral Shape

Before examining these high dead-time data for new borehole 41-09-39, attempts were under way to determine the effect of high count-rate spectral distortion on shape factors SF1 and SF2 by measurements with point sources in a sand tank. Results from such measurements show that SF1 increases at high dead times, while SF2 decreases. However, the magnitude of the effect as a function of dead time has not been determined from these experiments because of difficulty in obtaining the proper range of source strengths and because of uncertainties concerning source encapsulation effects on spectral shape.

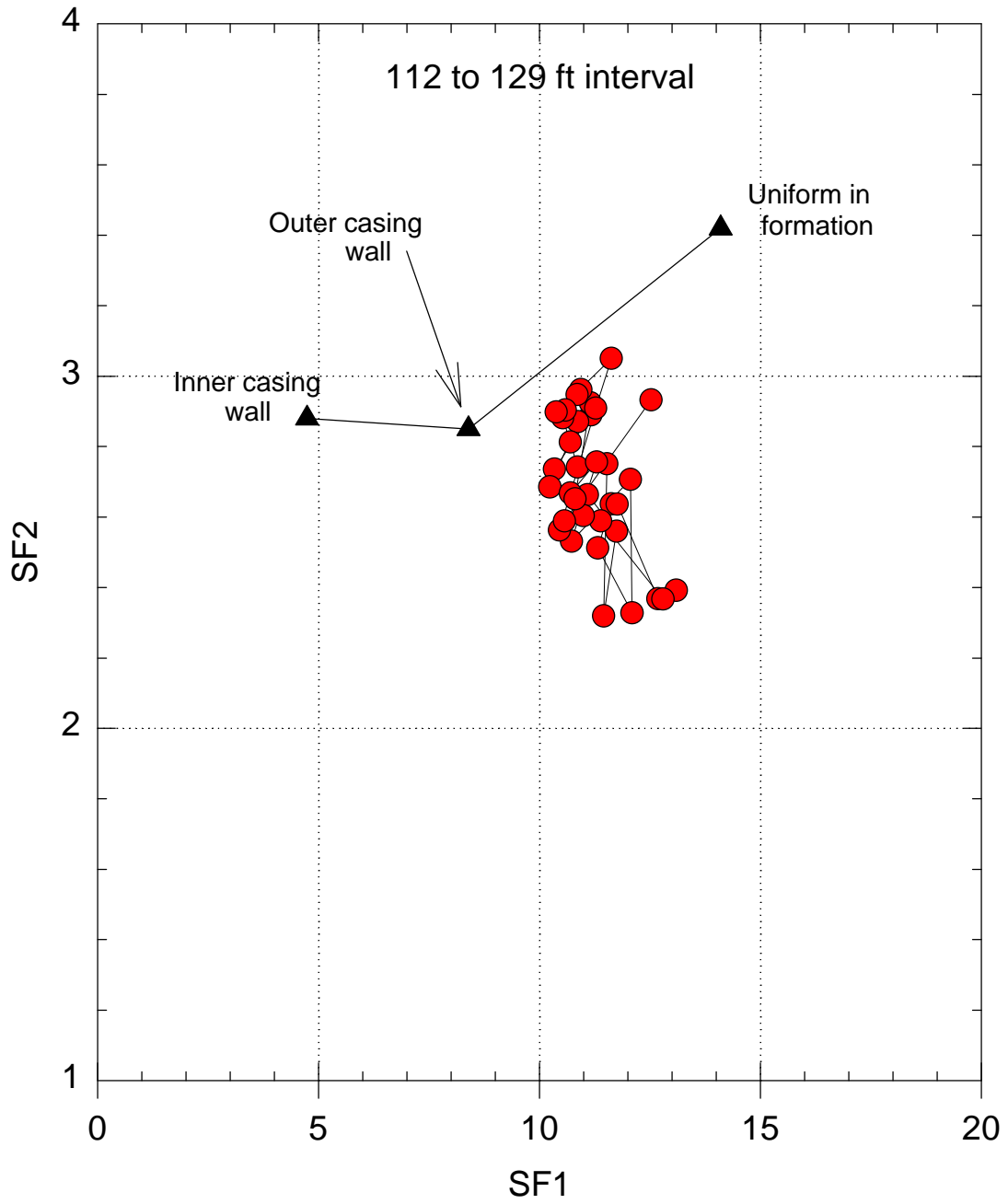


Figure 51. SF1 and SF2 Cross Plot for Depth Interval 112 to 129 ft, Borehole 41-09-39

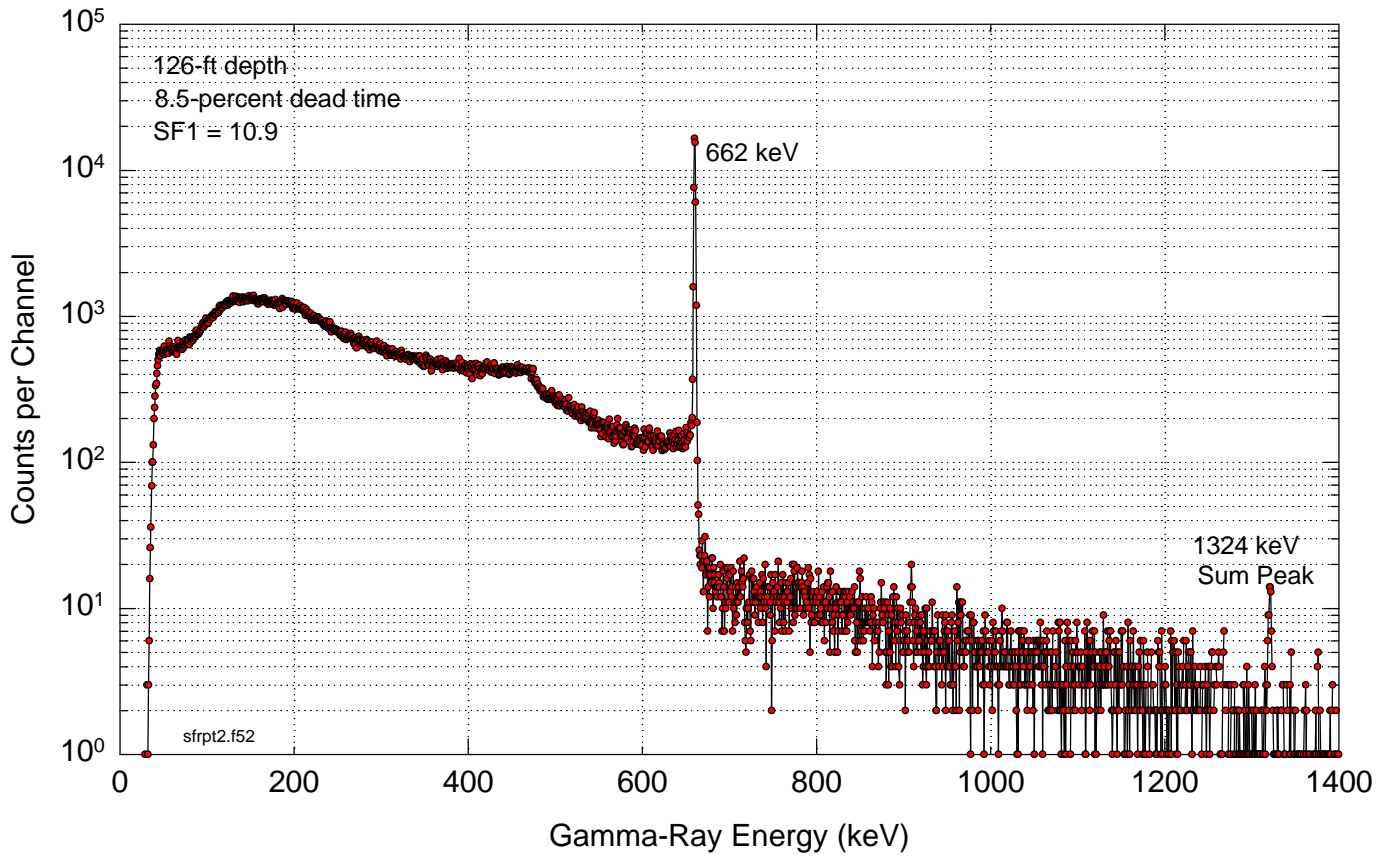


Figure 52. Gamma Spectrum at 126-ft Depth in Borehole 41-09-39

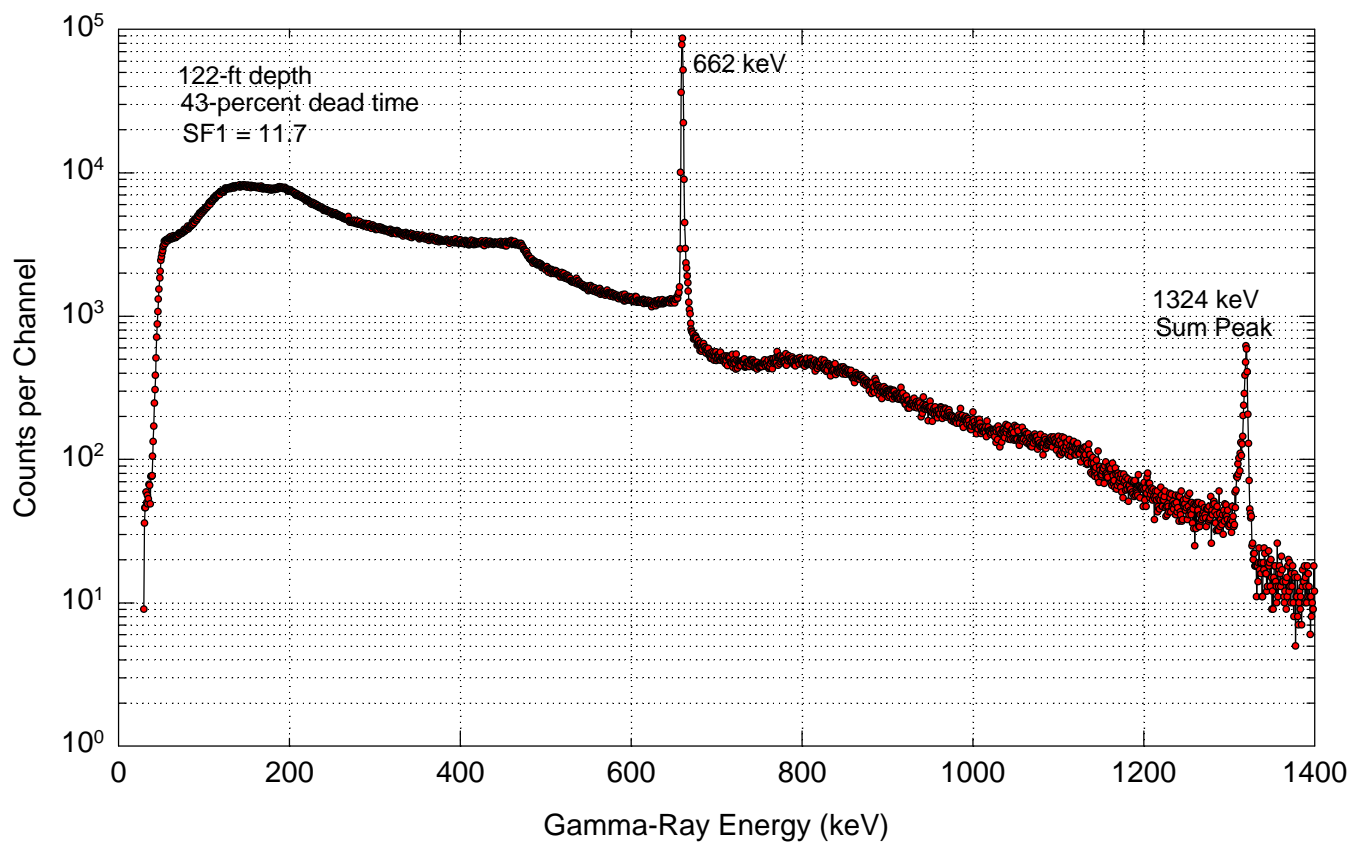


Figure 53. Gamma Spectrum at 122-ft Depth in Borehole 41-09-39

Previously, a rule of thumb for the application of shape factor analysis was that dead time must be less than about 15 percent to ensure there are no shape factor changes because of pulse pileup distortions of the spectra. Because most of the spectra for this second new borehole do have dead times in excess of 15 percent, it was initially believed that the measured shape factors would be greatly affected by pileup distortion and that simulated shape factors would not be useful as an interpretation tool for this borehole. However, the effect of high count rates on spectral shape, especially on the value of SF1, is not as great as feared and the shape factor analysis can be performed on data with dead times as high as 40 percent. This conclusion is based on an examination of how measured shape factors for borehole 41-09-39 depend on dead time.

The examples of spectra from borehole 41-09-39 shown on Figures 52 and 53 correspond to dead times of 8 percent and 43 percent, respectively. Although the effect of pileup is dramatically different for energies above 662 keV, the effect on the primary spectrum shape at lower energies is not as great. It is this primary portion of the spectrum that is processed for shape factor information and, therefore, the pileup distortion does not greatly affect SF1 and SF2 computations for this dead-time range. Note that the effect on SF1 is relatively small, increasing from 10.9 at 8-percent dead time to 11.7 at 43-percent dead time. Of course, it is assumed that the source distribution is the same for the contaminant at 122 ft and at 126 ft, the depths at which these spectra were measured. This may be a good assumption because when all the spectra are examined, a smooth trend is observed for the dependence of shape factor on dead time, regardless of depth in the borehole. This trend is demonstrated on Figure 54, where the dependence of SF1 and SF2 on dead time are plotted for the depth range from 92 to 129 ft with the exclusion of the saturated zone from 102.5 to 104 ft and the 1-ft interval at the bottom of the borehole. The SF1 plot shows little effect from spectral distortion until dead times reach values of about 40 percent. Unfortunately, a gap in dead times between 43 and 70 percent does not permit determination of the trend for this critical range. At 70 percent, SF1 is nearly a factor of 2 greater than at low dead times. SF2 shows a more continuous dependence on dead time, beginning at the lowest dead times of about 10 percent.

It is hoped that curve fits to these data can provide dead-time corrections to SF1 and SF2 values for future use in the log analysis software so that shape-factor analyses can be performed for dead times as high as 70 percent. Experiments should continue in an attempt to measure this dependence on dead time for a range of source distributions. At this point, the dead-time dependence is known only for the source distribution of borehole 41-09-39. Early results of the benchmark experiments have shown that the value of SF1 increases with dead time, while SF2 decreases with increasing dead time. This behavior is in agreement with data shown on Figure 54. For a spectrum shape similar to that for a uniformly distributed ^{137}Cs source, limited data indicate that SF1 increases by about 10 percent as dead time increases from small values to a value of 31 percent. For a spectrum shape similar to that for ^{137}Cs at the casing wall, limited data indicate that SF1 increases more rapidly with increasing dead time than for the uniform-source spectrum. SF1 values for borehole-localized sources could increase by as much as 20 percent as dead times rise to 40 percent.

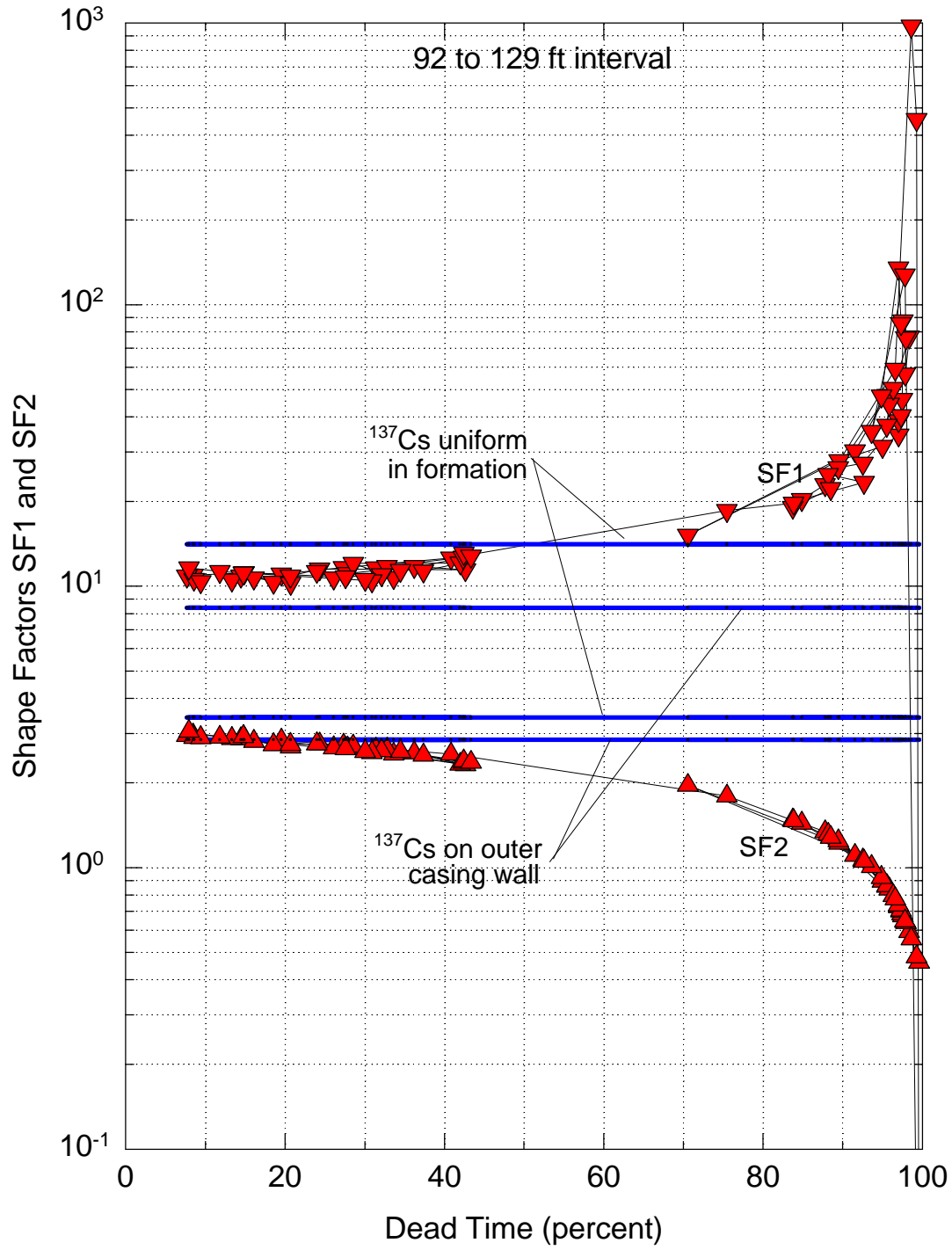


Figure 54. SF1 and SF2 Compared With Dead Time for Borehole 41-09-39

7.0 Summary and Recommendations

The shape factor analysis of gamma-ray spectra collected at the Hanford Tank Farms by the SGLS high-resolution germanium logging systems has been enhanced by the addition of the contaminant ^{60}Co to the methodology previously developed for ^{137}Cs (Wilson 1997) and by the addition of a bremsstrahlung signature value for shape factor SF2 that provides for the identification and quantification of the contaminant ^{90}Sr . The effect of dead time on the measured values of SF1 and SF2 has also been determined and has led to the extension of the useful range of the shape factor analysis method to dead times of about 40 percent. The new boreholes pushed to depths of about 130 ft in the vicinity of borehole 41-12-02 were processed for shape factors to help determine if the high ^{137}Cs activity detected at depth is from the formation or local to the borehole. The shape factor results from one of these new boreholes (41-09-39) indicate that the ^{137}Cs contamination is radially distributed, but with somewhat more contaminant local to the borehole region than expected for a uniform distribution. This result conflicts with the repeat logging results that imply ^{137}Cs contamination was in the formation before placement of the new borehole. This apparent conflict in results needs to be resolved.

Comparison of simulated and measured shape factors for several source distributions indicates that simulated shape factors are quite accurate except for certain borehole localized sources where simulated values of SF1 are too small by about 15 percent. The analyst should be aware of this discrepancy when interpreting shape factor logs.

The shape factor analysis of borehole data can be improved by increasing the SGLS count time at each depth station and by adding a collimator to minimize the detection of gammas from directions not adjacent to the detector position. This procedure lengthens and complicates the logging process but it may be warranted for boreholes and intervals of special concern.

The shape-factor studies activity in the vadose zone characterization project at the Hanford Site should continue in fiscal year 1998. Some of the objectives would include:

- Complete software enhancements to SGLS tool computer modeling capability.
- Evaluate production version of shape-factor analysis software and resolve any difficulties that arise in its routine use with tank farms logging data.
- Add certain enhancements to the shape-factor log analysis software, such as error bars for SF1 and SF2 values.
- Perform additional measurements with point sources to further characterize the dependence of shape factors on dead time, to benchmark simulated ^{60}Co shape factors, and to determine the dependence of the SF2 signature for ^{90}Sr on source distribution.

- C Measurements should also be done to characterize the SGLS tool response to vertically thin contaminant zones. Of particular interest is the dependence of computed shape factors on tool location relative to the thin zone.
- Resolve the discrepancies between simulated and measured spectra observed for certain source distributions.
 - Examine the negative correlation between shape factor SF1 and contaminant count rate and determine a method to minimize this undesirable effect.

8.0 Acknowledgments

The various experiments to benchmark the simulation software were conducted by James E. Meisner of Waste Management Federal Services and by Dr. David C. Stromswold of Pacific Northwest National Laboratory. I am grateful for their help. Thanks are extended to the DOE Richland Operations Office for supporting this work.

9.0 References

Briesmeister, J.F., editor, 1993. *MCNP—A General Monte Carlo N-Particle Transport Code, Version 4A*, LA-12625 (manual), Los Alamos National Laboratory, Los Alamos, New Mexico.

Brodeur, J.R., 1996. Unpublished letter report “41-12-01 Borehole Log Report,” Rust Geotech, Richland, Washington, September.

Brodeur, J.R., 1997a. *Log Analysis Report for Borehole 41-09-39*, draft report, prepared by MACTEC-ERS for the U.S. Department of Energy Grand Junction Office, Grand Junction, Colorado.

_____, 1997b. Personal communication, MACTEC-ERS, Richland, Washington.

Browne, E., and R.B. Firestone, 1986. *Table of Radioactive Isotopes*, V.S. Shirley (ed.), John Wiley and Sons, New York.

Engelman, R.E., R.E. Lewis, D.C. Stromswold, and J.R. Hearst, 1995. *Calibration Models for Measuring Moisture in Unsaturated Formations by Neutron Logging*, PNL-10801, prepared for the U.S. Department of Energy by Pacific Northwest Laboratory, October.

Knoll, G.F., 1987. *Radiation Detection and Measurement*, John Wiley and Sons, New York, p. 303.

Koizumi, C.J., 1996. Calibration data were processed by Dr. Koizumi and provided as a personal communication, MACTEC-ERS, U.S. Department of Energy Grand Junction Projects Office, Grand Junction, Colorado.

Leino R., D.C. George, B.N. Key, L. Knight, and W.D. Steele, 1994. *Field Calibration Facilities for Environmental Measurement of Radium, Thorium, and Potassium*, DOE/ID/12584-179 GJ/TMC-01 (Third Edition) UC-902, U.S. Department of Energy Grand Junction Projects Office, Grand Junction, Colorado.

Price, R.K., 1997. Personal communication of Radiological Logging System spectrum files for borehole 299-E25-191, Waste Management Federal Services, Richland Washington.

Randall, R., 1996. *Feasibility Tests For Gamma Ray Spectral Shape Information Regarding Formation Distribution of ¹³⁷Cs*, informal report to Westinghouse Hanford Company, Richland, Washington, September 28.

Stromswold, D.C., 1997. Personal communication of ⁹⁰Sr source specifications, Pacific Northwest National Laboratory, Richland, Washington.

U.S. Department of Energy (DOE), 1996a. *Tank Summary Data Report for Tank BY-106*, GJ-HAN-23, prepared by Rust Geotech for the U.S. Department of Energy Grand Junction Projects Office, Grand Junction, Colorado.

_____, 1996b. *Tank Summary Data Report for Tank BY-108*, GJ-HAN-25, prepared by Rust Geotech for the U.S. Department of Energy Grand Junction Projects Office, Grand Junction, Colorado.

_____, 1996c. *Tank Summary Data Report for Tank TX-103*, GJ-HAN-44, prepared by Rust Geotech for the U.S. Department of Energy Grand Junction Projects Office, Grand Junction, Colorado.

_____, 1997a. *TWRS Vadose Zone Contamination Issue Expert Panel Status Report*, DOE/RL-97-49, Rev. 0, U.S. Department of Energy Richland Operations Office, Richland, Washington.

_____, 1997b. *Vadose Zone Characterization Project at the Hanford Tank Farms - Data Analysis Manual*, P-GJPO-1787, Rev. 1, prepared by MACTEC-ERS for the U.S. Department of Energy Grand Junction Projects Office, Grand Junction, Colorado, Appendix A.

Westinghouse Hanford Company, 1993. *Results of Spectral Gamma-Ray Logging of Select Boreholes for the Aggregate Area Management Study*, Appendix A, WHC-SD-EN-TI-021, Rev. 0, Richland, Washington.

Wilson, R.D., 1994. *Pipe Scale Gauge for Use in Oil Field Production Tubing: A Feasibility Study*, internal report, Program Support Research and Development Program, prepared by Rust Geotech for the U.S. Department of Energy Grand Junction Projects Office, Grand Junction, Colorado.

_____, 1997. *Spectrum Shape Analysis Techniques Applied to the Hanford Tank Farms Spectral Gamma Logs*, GJO-96-13-TAR (GJO-HAN-7), prepared by MACTEC-ERS for the U.S. Department of Energy Grand Junction Projects Office, Grand Junction, Colorado.

Wilson, R.D. and J.G. Conaway, 1993. "Simulations of Spectral Gamma-Ray Logging Tool Response to Formation and Borehole Wall Source Distributions," *Nuclear Geophysics*, Vol. 7, No. 1, pp. 35-53.